Alma Mater Studiorum – Università di Bologna

DOTTORATO DI RICERCA IN
Scienze della Terra

Ciclo XXV

Settore Concorsuale di afferenza: 04/A2
Settore Scientifico disciplinare: GEO/02

LOW-TEMPERATURE THERMOCHRONOLOGICAL EVOLUTION OF THE EASTERN PONTIDES, THE EASTERN ANATOLIAN PLATEAU AND NORTHWESTERN LESSER CAUCASUS (TURKEY, GEORGIA, ARMENIA)

Presentata da: Dott.ssa Irene Albino

Coordinatore Dottorato:
Prof. Roberto Barbieri

Relatore:
Prof. William Cavazza

Co-relatori:
Prof. Massimiliano Zattin
Prof. Aral I. Okay

To my parents and Luca,
for their love and support.

LIST OF CONTENTS

LIST OF FIGURES

Chapter One

Chapter Two

Chapter Three

Chapter Four

Appendix A

LIST OF TABLES

ACKNOWLEDGMENTS

Many people have contributed to the realization of this work. Foremost, I would like to express my sincere gratitude to my advisor Prof. William Cavazza for the continuous support of my PhD study and research, for his patience, motivation and enthusiasm. His guidance helped me in all time of research and writing of this thesis. I am deeply grateful to Prof. Massimiliano Zattin for his detailed and constructive comments, for all time spent on my training in the lab and his important support during the writing of this thesis. I thank Prof. Aral Okay for his expert guidance on collecting samples in the Eastern Anatolia. I also express my gratitude to Dr. Claudio Dal Monte who advised me in sample processing. I thanks Prof. Rafael Melkonian and Dr. Ghazar Galoyan from the Armenian Academy of Sciences for the guidance during fieldwork in northern Armenia. Thanks to Prof. Shota Adamia and Dr. Nino Sadradze for guidance on collecting samples from Georgia. Thanks to Prof. Vincenzo Picotti for his useful comments on a earlier version of this dissertation. Funding from MIUR (Italian Ministry of University and Research), the University of Bologna, and TÜBA (The Turkish Academy of Sciences) is gratefully acknowledged. I am grateful to all my "tracker-friends" who contributed fruitful discussions, in particular Benedetta Andreucci and Giorgio Di Fiore. I also express my gratitude to Federico Fanti and Veronica Rossi for their help and support during this last year. Thanks to my "roommate" Francesco and Luigi. I would also like to thank my friends, most of all Alessia, Andrea, Rosanna and Fulvio. Last but not least, special thanks go to Luca and my sister.

ABSTRACT

In this dissertation, the analysis of apatite fission tracks (AFT) is applied to the study of the syn- and post-collisional thermochronological evolution of a vast area that includes the Eastern Pontides, their continuation in the Lesser Caucasus of Georgia (Adjara-Trialeti zone) and northern Armenia, and the eastern Anatolian Plateau. The resulting database is then integrated with the data presented by Okay et al. (2010) for the Bitlis Pütürge Massif, i.e. the western portion of the Bitlis-Zagros collision zone between Arabia and Eurasia.

Despite a significant spectrum of sampled lithologies and the large geographic distribution of collected samples, AFT ages can be grouped in two discrete, space-related clusters: (1) Middle Miocene ages are concentrated along the Bitlis collision zone, along the Black Sea coast, and in the Lesser Caucasus of northern Armenia, (2) Paleogene exhumation ages are concentrated in the Anatolian Plateau and in the Georgian Lesser Caucasus (Adjara-Trialeti zone), with a significant age cluster of samples dated to the Middle-Late Eocene.

The mid-Miocene exhumation episode along the Black Sea coast and Lesser Caucasus of Armenia documented in this dissertation mirrors the age of collision between the Eurasian and Arabian plates along the Bitlis suture zone. We argue that tectonic stresses generated along the Bitlis collision zone were transmitted northward across eastern Anatolia and focused (i) at the rheological boundary between the Anatolian continental lithosphere and the (quasi)oceanic lithosphere of the Black Sea, and (ii) along major pre-existing discontinuities like the Sevan-Akera suture zone.

Although there is abundant evidence for wholesome uplift of the eastern Anatolian Plateau during the Plio-Quaternary, significant exhumation in this region and in the Georgian Lesser Caucasus (Adjara-Trialeti zone) occurred instead in the Paleogene, coevally with the late stage of development of the İzmir-Ankara-Erzincan suture. This implies that successive uplift of the Anatolian Plateau did not exhume a new partial annealing zone and thus is not recorded by the apatite fission-track record.

The integration of both present-day crustal dynamics (GPS-derived kinematics and distribution of seismicity) and thermochronological data presented in this paper provides a comparison between short- and long-term deformation patterns for the entire eastern Anatolia-Transcaucasian region. Two successive stages of Neogene deformation of the northern foreland of the Arabia-Eurasia collision zone can be inferred. (i) Early and Middle Miocene: continental deformation was concentrated along the Arabia-Eurasia (Bitlis) collision zone but tectonic stress was also transferred northward across eastern Anatolia, focusing along the eastern Black Sea continent-ocean rheological transition and along major pre-existing structural discontinuities. (ii) Since Late-Middle Miocene time the westward translation of Anatolia and the activation of the North and Eastern Anatolian Fault systems have reduced efficient northward stress transfer. In this new tectonic regime -still active today - most of the Arabia-Eurasia convergence has been accomodated by the westward motion of Anatolia and the Eastern Pontides have been mechanically decoupled from the foreland of the Bitlis collision zone, as shown by the absence of significant seismicity in the area.

The results of this dissertation elucidate the temporal variations in mechanical coupling between the Bitlis-Zagros collision zone and its foreland and may have wider application. Integration of our dataset with published geodetic, seismologic, and structural data constrains the transition from an orogen dominated by shortening to one dominated by escape tectonics and major strike-slip faults, including the inception of the North Anatolian Fault system and overall “escape” tectonics of the Anatolian Plate.

RIASSUNTO

In questa tesi l'analisi delle tracce di fissione su apatite (AFT) è stata utilizzata per lo studio dell'evoluzione termocronologica sin- e post-collisionale di una vasta area che comprende: (i) le Pontidi orientali, (ii) la loro prosecuzione nel Caucaso Minore in Georgia (zona di Adjara-Trialeti) e in Armenia settentrionale, (iii) il plateau anatolico orientale. I risultati ottenuti sono stati integrati con quelli presentati da Okay et al. (2010) inerenti il Massiccio di Bitlis-Pütürge. Nonostante le differenti litologie campionate e l'ampia distribuzione spaziale, le età di raffreddamento ottenute possono essere distinte in due gruppi temporalmente e spazialmente coerenti: (1) le età medio-mioceniche sono concentrate lungo il fronte collisionale (Massiccio di Bitlis- Pütürge), nel settore armeno del Caucaso Minore e lungo la costa orientale del Mar Nero; (2) le età paleogeniche (con un cluster di età dell'Eocene Medio-Superiore) sono concentrate invece nel Plateau Anatolico e nel settore georgiano del Caucaso Minore (zona di Adjara-Trialeti).

L'episodio esumativo di età medio-miocenica documentato in questo lavoro corrisponde all'età della collisione tra le placche araba ed eurasiatica lungo la zona di sutura di Bitlis. La nostra ipotesi è che lo *stress* tettonico generato lungo il fronte collisionale di Bitlis sia stato trasmesso verso nord attraverso l'Anatolia orientale concentrandosi al confine reologico tra la litosfera continentale anatolica e la litosfera (quasi)oceanica del Mar Nero nonché lungo preesistenti discontinuità come la linea di sutura Sevan-Akera .

Nonostante vi siano molteplici evidenze di un generale sollevamento plio-quaternario del Plateau Anatolico Orientale, l'ultima fase di significativa

esumazione registrata nell'area si verificò invece nel Paleogene, contemporaneamente allo sviluppo della sutura İzmir-Ankara-Erzincan. Il successivo sollevamento del Plateau Anatolico non ha esumato una nuova *partial annealing zone* e per questo non è stato registrato dalle tracce di fissione.

L'integrazione dell'attuale dinamica crostale (velocità dei vettori GPS e distribuzione dei terremoti) e dei dati termocronologici presentati in questa tesi permette di vincolare la storia deformativa a breve e lungo termine dell'intera Anatolia orientale e della regione transcaucasica. Possono essere distinti due stadi di deformazione neogenica per l'avampaese settentrionale della zona di collisione Arabia-Eurasia. (i) Nel Miocene inferiore-medio la deformazione continentale si concentrava lungo la zona di collisione Arabia-Eurasia (Bitlis). In questo periodo però lo stress tettonico fu anche trasferito verso nord attraverso l'Anatolia orientale, concentrandosi lungo la costa orientale del Mar Nero alla transizione reologica continente-oceano e lungo alcune delle maggiori discontinuità strutturali preesistenti come la linea di sutura Sevan-Akera. (ii) Dalla fine del Miocene medio, il movimento verso ovest della placca anatolica e la contemporanea attivazione del sistema trascorrente Nord- ed Est-Anatolico ridusse il trasferimento dello stress verso nord. In questo nuovo regime tettonico -che continua ancora oggi– la maggior parte della convergenza tra Arabia ed Eurasia è accomodata dal movimento verso ovest della placca anatolica e la catena delle Pontidi Orientali è stata separata meccanicamente dall'avampaese della zona di collisione di Bitlis, come dimostrato dall'assenza di terremoti significativi in quest'area, nonché dall'andamento dei vettori GPS.

I risultati di questa tesi forniscono importanti elementi per la comprensione delle variazioni temporali nel grado di accoppiamento meccanico

tra il prisma orogenico di Bitlis-Zagros e il suo avampaese euro-asiatico. Tali risultati possono avere applicazione altrove. L'integrazione del *dataset* qui presentato con dati geodetici, sismologici e strutturali già pubblicati vincola infatti la transizione da un orogene dominato dalla collisione e dalle strutture di ricoprimento ad uno dominato dalla tettonica trascorrente, con importanti implicazioni per la creazione della Faglia Nord-Anatolica e la cosiddetta "estrusione" tettonica della neoformata Placca Anatolica verso ovest.

Chapter One

INTRODUCTION AND GEOLOGICAL SETTING

1.1 INTRODUCTION

The present-day geological setting of the area including easternmost Turkey, northwestern Iran, Armenia, Georgia and Azerbaijan is the result of complex geodynamic processes that involved the Tethyan domain during Palaeozoic, Mesozoic, and Cenozoic times (for an introduction, see Stephenson et al., 2004, and references therein). Such area (Fig. 1.1) consists of several continental fragments that during the evolution of the Paleotethys and the Neotethys rifted off from either sides of the two oceanic domains and eventually collided with the opposite continental margin (e.g., Okay, 2008).

Fig. 1.1 – Tectonic map of Mediterranean region, including the Caucasian area (Okay & Tüysüz, 1999).

This area is geologically divided into several structural sub-domains. From north to south, these are (i) the Greater Caucasus, (ii) the Lesser Caucasus and the equivalent Eastern Pontides, (iii) the Anatolide- Tauride block (which in this

area forms most of the Anatolian Plateau, and (iv) the Arabian Platform (e.g., Okay & Tüysüz, 1999). The Pontides and the Lesser Caucasus exhibit Laurasian affinities and are comparable to the tectonic units in the Balkans and in Central Europe (Okay, 2008). They were all located north of the northern branch of NeoTethys (e.g., Okay, 2008). The complete closure of this ocean resulted in the İzmir-Ankara-Erzincan suture, which marks the boundary between terranes that show Laurasian affinities (to the north) and those showing Gondwanian affinities (to the south). Further south, the Anatolide-Tauride block and the Arabian Platform are separated by the Bitlis (Assyrian)-Zagros suture zone and both show Gondwanian characters but differing degrees of deformation (Okay & Tüysüz, 1999).

The last main tectonic compressive event that interested Anatolia and Trascaucasia was the collision between Arabia and Eurasia (Fig. 1.2). The Arabia-Eurasia collision closed the Neotethyan oceanic gateway by isolating the Mediterranean and Indian Oceans, possibly inducing the mid-Cenozoic global cooling (Allen & Armstrong, 2008). The collision has also been linked to the rifting of the Red Sea, extension in the Aegean, the formation of the North and East Anatolian fault system (Armijio et al., 1999; Jolivet & Faccenna, 2000; Okay et al., 2010) and the structural inversion of the Caucasian basins (Koçyiğit et al., 2001; Saintot et al., 2006). Following post-collisional intracontinental convergence along the Lesser Caucasian and Bitlis-Zagros suture, the southern margin of Eurasia (Fig. 1.2) was squeezed as a 2 km-high plateau (Koçyiğit et al., 2001; Copley & Jackson, 2006; Reilinger et al., 2006), namely the east Anatolian-Iran plateau. Volcanism and plateau uplift have also been interpreted as surface

manifestation of the erosion of the mantle root caused by delamination of mantle lithosphere and/or slab break-off (e.g., Keskin, 2003; Şengör & Yılmaz, 2003).

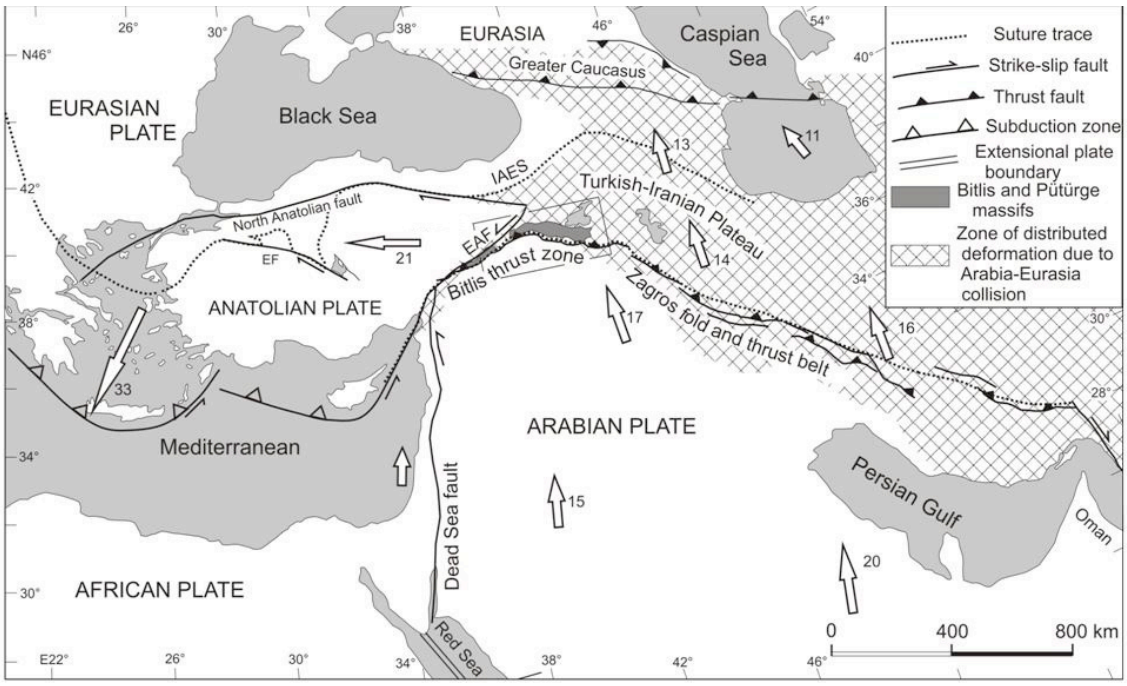

Fig. 1.2 – Tectonic map of the eastern Mediterranean and Middle East (Okay et al., 2010). Arrows and numbers indicate global positioning system (GPS)-derived velocities with respect to Eurasia (modified from Reilinger et al. 2006; Copley & Jackson, 2006). EAF-East Anatolian Fault; EF- Ekişehir fault; İAES – İzmir-Ankara-Erzincan suture.

Faccenna et al. (2006) proposed that the roll-back of the Hellenic trench and the Arabia indentation are produced by a unique mechanism able to explain the major crustal features in the collisional area, such as the uplift of the Turkish-Iranian plateau, the surge of alkaline volcanism, and the pattern of velocity anomaly in the mantle below eastern Anatolia. This model suggests that the deep deformation of the Bitlis-Hellenic slab may have caused the Neogene plate re-organization in the Middle East. In particular, they proposed that the onset of the North Anatolian Fault strike-slip deformation could be triggered by the break-off of the slab under the Bitlis collision zone and by the westward propagation of the rupture edge toward the Rhodes-Cyprus area. In this model, the lateral westward

propagation of the slab break-off at shallower depth could have produced, on the one hand, the acceleration of collisional processes in the Bitlis area and the rapid uplift of the Anatolian Plateau, and on the other hand, the rapid Hellenic trench roll-back due to the extra-pull provided laterally by the detached portion of the slab.

Despite the importance of the event, the areal extent, nature, and timing of collision-related deformation between Arabia and Eurasia is poorly known, with estimate ranging from Late Cretaceous (Hall, 1976; Berberian & King, 1981; Alavi, 1994), to Late Eocene-Oligocene (35-25 Ma; Jolivet & Faccenna, 2000; Agard et al., 2005; Allen & Armstrong, 2008), to Miocene (Şengör et al., 1985; Dewey et al., 1986; Yılmaz, 1993; Robertson et al., 2007). These estimates are generally based on the stratigraphy and age of deformation of the facing margins of the Arabia and Eurasia plates (Okay et al., 2010). The only low-temperature thermochronological data, based on apatite fission-track (FTA), available for the Bitlis-Pütürge massif point to an episode of fast exhumation in the Middle Miocene (Okay et al., 2010) (Fig. 1.5).

The fact that Eocene intrusive rocks crop out extensively in the Eastern Pontides (e.g., Boztuğ et al., 2004; Fig. 1.3) from Samsun in the west to Georgia in the east (Adjara-Trialeti and Artvin-Bolnisi zones) is evidence for significant post-Eocene exhumation and led us to hypothesize preliminarily that indentation of the Arabian plate may have induced widespread tectonism, not only in the Caucasus but also in the Eastern Pontides and possibly over a wide region including the Anatolian-Iranian plateau and Transcaucasia. From this viewpoint, the sharp structural relief between the easternmost Pontides and the bottom of

the eastern Black Sea and the outcrop of Eocene plutonic rock along the Black Sea coast may indicate significant uplift/exhumation.

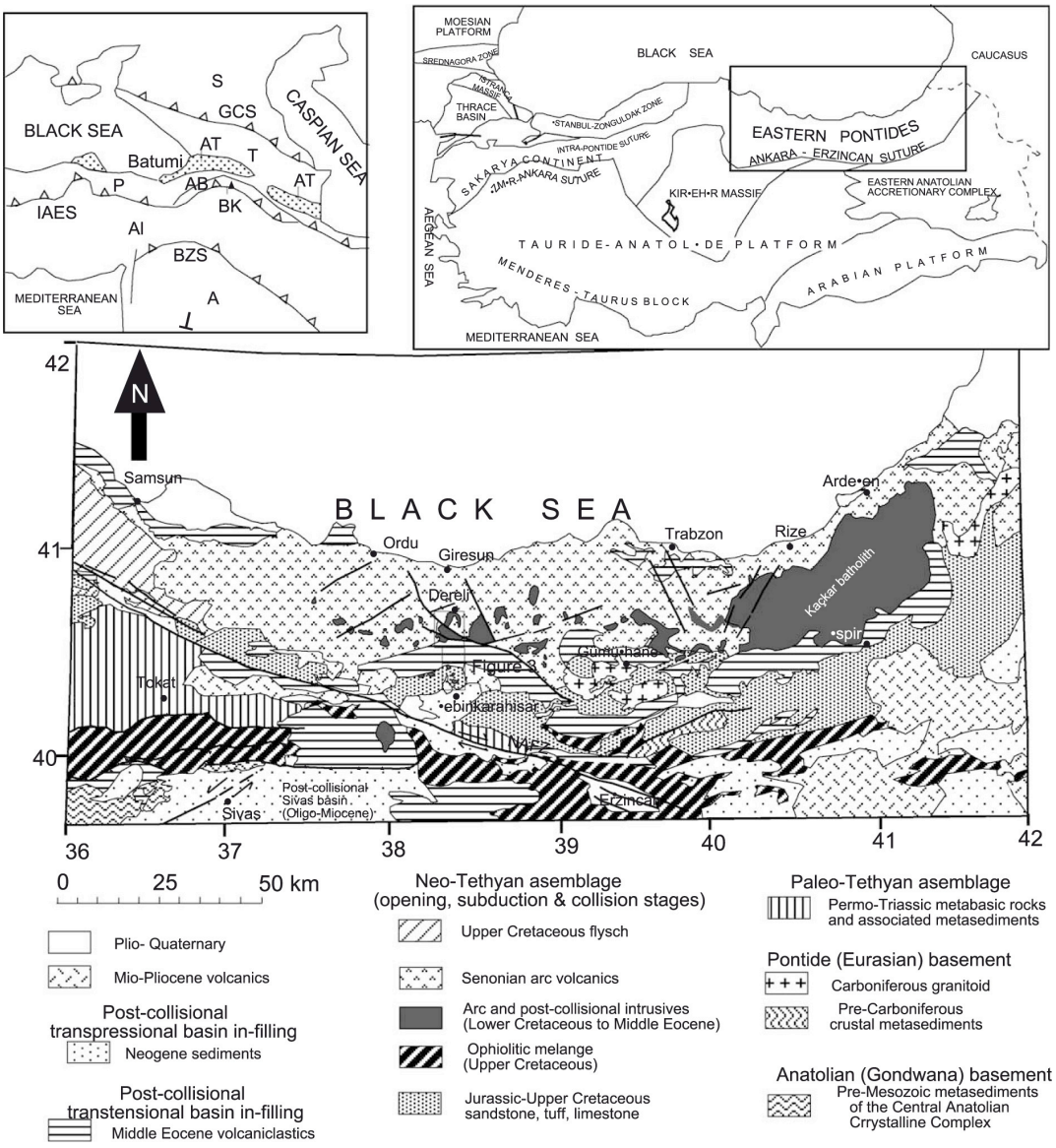

Fig. 1.3 – Simplified geological map of the Eastern Pontide igneous terranes and surrounding area (Boztuğ et al., 2004). Abbreviations in the upper left inset: S, Scythian Platform; GCS, Greater Caucasus suture; AT, Adjara-Trialeti unit; T, Transcaucasus; P, Pontides; AB, Artvin-Bolnisi unit; BK, Bayburt-Karabagh imbricated unit; İAES, İzmir-Ankara-Erzincan suture; AI, Anatolia-Iranian plateau; BSZ, Bitlis-Zagros suture; A, Arabian Platform.

Fission track-analysis (FTA) has been widely used to constrain the thermochronologic evolution of single geological structures or relatively small

area. More rarely, FTA helped in elucitading the geological history of large geological provinces, including large orogens and the surrounding terrains. The latter approach has been already proven useful in other areas of the Middle East (e.g. Okay et al., 2010; Zattin et al., 2011; Cavazza et al., 2012), where it identified large-scale cooling exhumation episodes related to Mesozoic and Cenozoic collisional orogenies inducing widespread deformation/exhumation. In the case of this dissertation, FTA has been employed to test the hypothesis that the most intense phase of mechanical coupling between Arabia and Eurasia during continental collision induced far-field effects and widespread deformation over a wide area of the upper (Eurasian) plate. Our main goal is the study of syn-and post-collisional thermochronological evolution of (a) the Eastern Pontides, (b) the Lesser Caucasus of Georgia (Adjara-Trialeti zone) and northwestern Armenia, (c) the Eastern Anatolian Plateau.

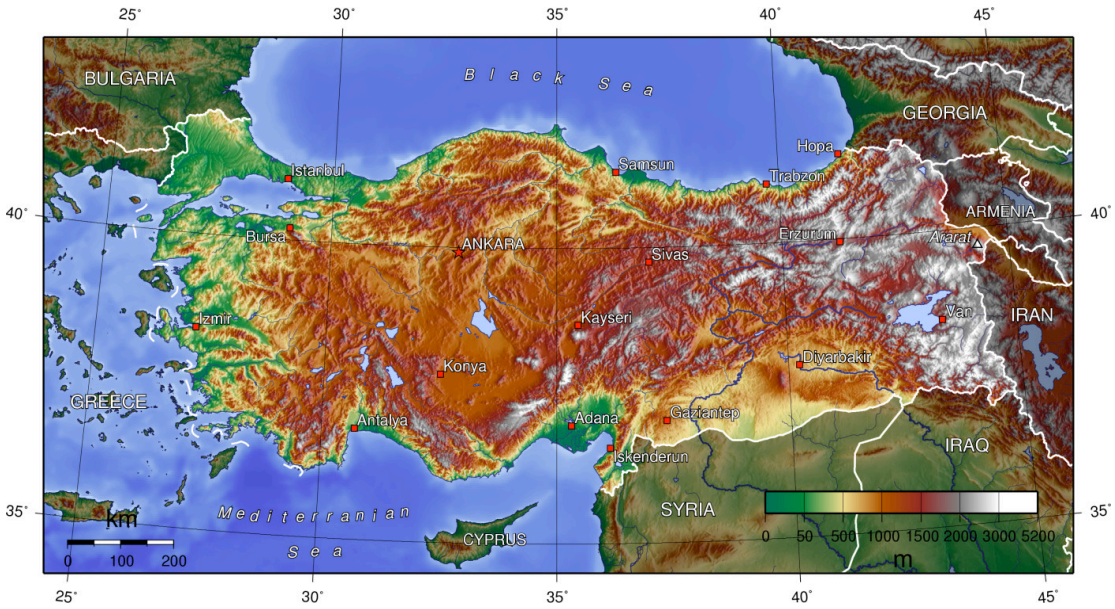

Fig. 1.4 – Relief map of Anatolia (from Google Images).

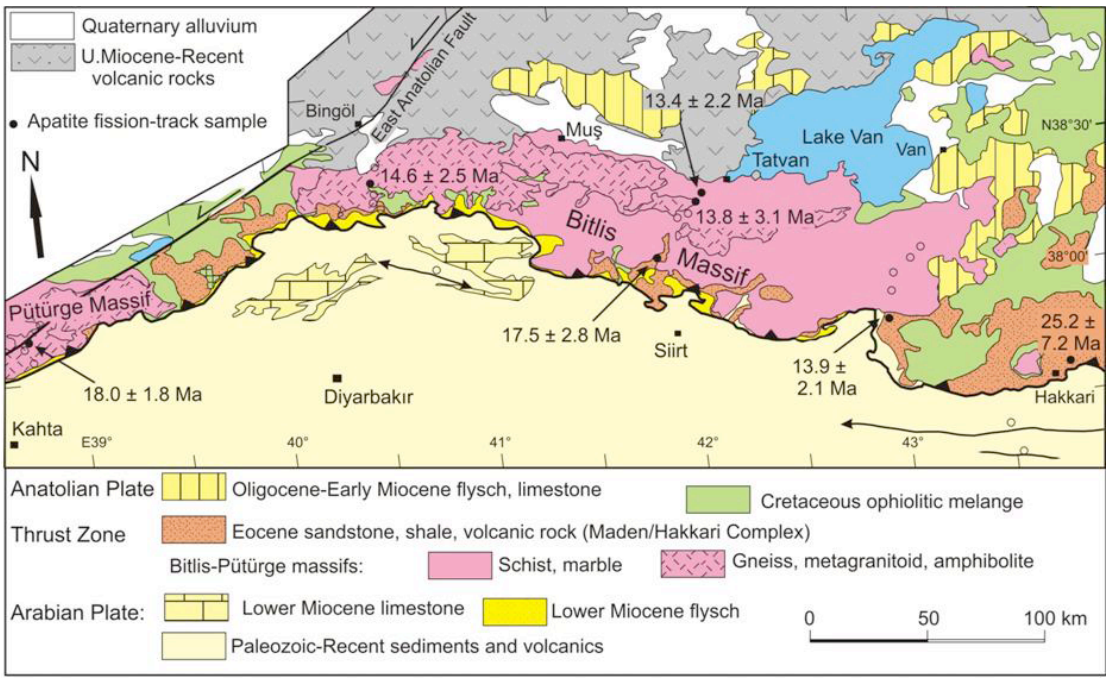

Fig. 1.5 – Tectonic map of the Bitlis thrust zone with apatite fission-track sample localities and age (Okay et al., 2010).

The present thesis is organized as follows:

- Chapter I: describes the geological setting of the investigated area and illustrates the aim of the work.
- Chapter II: comprises a manuscript titled "Far-field tectonic effects of the Arabia-Eurasia collision and the inception of the North Anatolian Fault system" by I. Albino, W. Cavazza, M. Zattin, A.I. Okay, S. Adamia and N Sadradze. The manuscript is currently being reviewed for publication.
- Chapter III: presents additional thermochronological data (AFT) from northern Armenia.
- Chapter IV: discussion and main conclusions.
- Appendix A: illustrates the fission-track dating method and the laboratory procedures utilized during this study.

- Appendix B: is dedicated to the statistics of fission-track dating and thermochronologic modelling employed in this dissertation.

1.2 THE NORTH ANATOLIAN FAULT

The North Anatolian Fault (NAF) has been subject of numerous geological, geomorphological and seismological studies since its recognition as a major strike-slip fault in 1948 by Ketin (Şengör et al., 2005). Ketin noted that during all major earthquakes in northern Turkey since 1939, the surface break always had the character of a generally east-west-striking, right-lateral fault. Ketin further pointed out that because the Anatolian interior south of the fault was largely aseismic, a whole Anatolian block had to be moving westward with respect to the Black Sea along the NAF. Ketin also argued that to accommodate such movement another left-lateral fault had to exist to the south of the Anatolian block; his prediction was confirmed a quarter of a century later when the East Anatolian Fault (EAF) was identified (Seymen & Aydin, 1972).

After the large earthquakes of 1999 (e.g., Barka et al., 2000a, 2002) the NAF has received renewed attention with many new studies from various Earth sciences disciplines, but the age and the current understanding of the origin and displacement history remains somewhat limited and controversial (Bozkurt, 2001).

The NAF is located almost entirely within Anatolia, only its westernmost extremity is located in the Marmara Sea, in the Gallipoli peninsula, and in the northern Aegean Sea (Şengör et al., 2005, Fig. 1.6). The Marmara Sea consists essentially of depressions and ridges aligned along the E-W trend of the NAF

(Zattin et al., 2010; Fig. 1.6). In this region, the NAF widens into a complex fault zone stretching some 100 km in a N-S direction, from Ganos Mt. in southern Thrace (Okay et al., 2004) to Kazdağ in the southern Biga peninsula (Cavazza et al., 2008). Such configuration translates into a high degree of structural complexity, with coexisting deep basins, push-up structures, and block rotations (Zattin et al., 2010). The most important basins related to the activity of the NAF (Fig. 1.7) are well described in Şengör et al. (2005). Based on paleontological data these basins are Middle-Upper Miocene and Pliocene to Quaternary in age (Şengör et al., 2005).

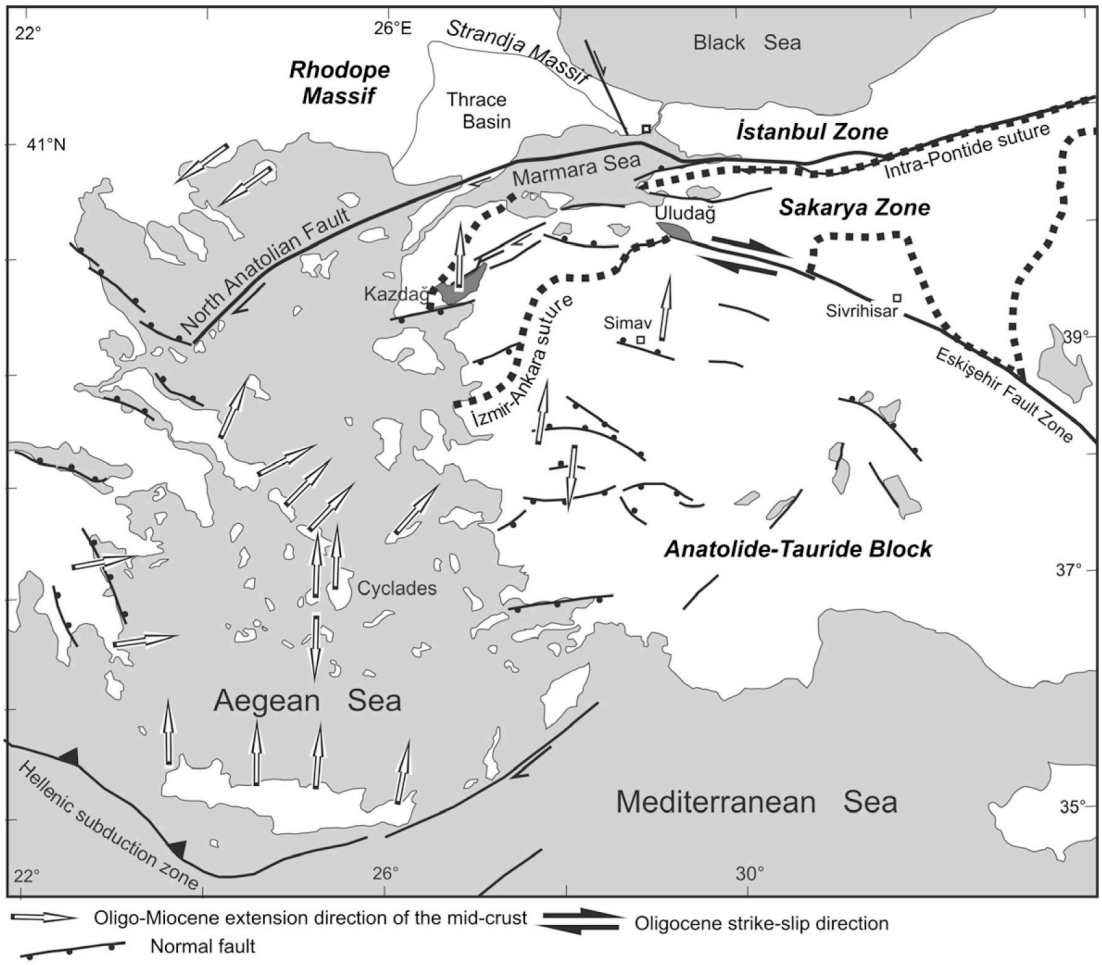

Fig. 1.6 – Simplified tectonic map of the Marmara region showing the major terranes and sutures, as well as the North Anatolian Fault system. The large arrows refer to the direction of shear in the mid-crust during the Oligo-Miocene extension (Zattin et al., 2010).

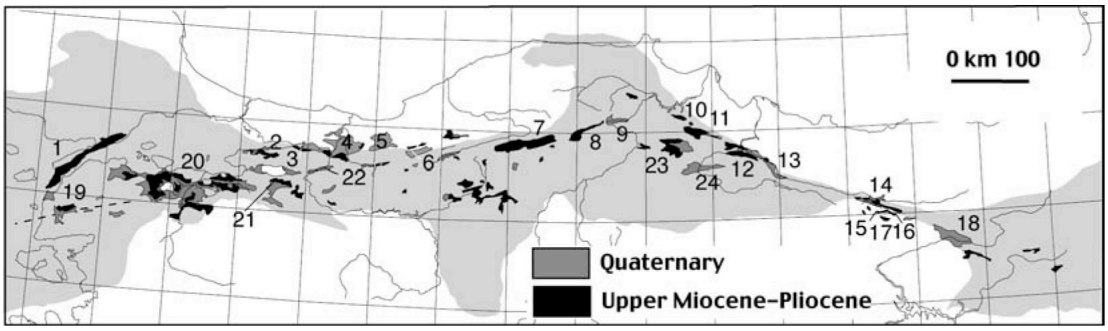

Fig. 1.7– Basins along North Anatolian Fault. Numbers refer to those studied by Şengör et al., 2005.

There is an ongoing debate about whether the NAF was initiated in the Late Miocene- Early Pliocene (Barka, 2000; Bozkurt, 2001) or in the Middle Miocene (McKenzie, 1972; Şengör et al., 2005). In recent times, a mounting body of evidence is suggesting that NAF follows the course of a pre-existing structural discontinuity. For the Ganos segment of the NAF in the Gallipoli peninsula Zattin et al. (2005, 2010) suggested –based on thermochronological evidence- the existence of a pre-existing discontinuity with a significant component of dip slip at least of Late Oligocene age and possibly older. This conclusion is also supported by Usyal et al. (2006) who studied a ca. 500 km long segment of the NAF east of the Marmara Sea by radiometric dating of fault gouges. They found that an early event of significant strike-slip was initiated at about 57 Ma, but further intensified at ca. 26 Ma and later at ca. 8 Ma. Kaymankci et al. (2007), on the basis of paleomagnetic data, proposed that the Ganos fault and other ENE-trending faults experienced dextral strike-slip activity before the Late Pliocene arrival of the NAF in the Marmara region. Another Oligocene major strike-slip shear zone in western Anatolia, with a right-lateral offset of ca. 100 km, was

described by Okay et al. (2008) in the Uludağ area, near the city of Bursa. All these papers support the idea that pre-existing mechanical weakeness zones such as faults and shear zones greatly influenced the locus of subsequent tectonic activity (Holdsworth et al., 1997; Zattin et al., 2010).

According to the common interpretation, the NAF and EAF nucleated in eastern Anatolia following Arabia-Eurasia collision and the southward roll-back of the Hellenic trench. Today the NAF and EAF accomodate most of the convergence between Arabia and Eurasia plate and the lateral trasport westward of the Anatolian Plate (Reilinger et al., 2006). The question if the nucleation of the NAF and EAF is related to (i) the collision between Arabia and Eurasia, (ii) roll-back of the Hellenic trench, or –perhaps more likely- (iii) a combination of both mechanisms is still debated. Several data derived from GPS-velocity and seismicity (Relinger et al., 2006), proprietary seismic stratigraphic data (i.e. Middle to Late Miocene clastic wedges generically prograding northwestward across the eastern Black Sea), Middle Miocene ages derived from apatite fission-track for Bitlif Massif along the collision zone (Okay et al., 2010), and other stratigraphic evidence (i.e. Middle Miocene unconformity between Late Oligocene/Early Miocene and Late Miocene volcanic deposits, Fig.1.8) indicate that a major change in stress regime from contraction to extension or strike-slip occurred in the Middle Miocene. From this viewpoint this dissertation provides evidence to constrain this dramatic change in stress regime using low-temperature thermochronological data. This evidence will be discussed at length in the following chapters.

Fig. 1.8 - Middle Miocene angular unconformity between Oligocene/Early Miocene and Late Miocene volcano-sedimentary deposits of the Eastern Pontides (road to Artvin).

1.3 THE PONTIDES

The Pontides (Fig. 1.1), comprising the region north of the İzmir-Ankara-Erzincan suture, are a composite orogen stretching > 1,500 km from Bulgaria to the Lesser Caucasus. From Late Palaeozoic to recent times, this orogen has suffered the cumulative effects of a complex structural history, including the Variscan (Carboniferous), Cimmerian (Triassic), and Alpine (Late Cretaceous-Palaeocene) orogenies (e.g. Okay, 2008). The Pontides consist of three terranes, which show markedly different geological evolution: (i) the Strandja Massif, (ii) the İstanbul terrane, and (iii) the Sakarya terrane (Fig. 1.1).

The Strandja Massif forms part of the large crystalline terrane in the southern Balkans, which also includes the Rhodopes and the Serbo-Macedonian Massif. It consist of a Variscan crystalline basement overlain by a Triassic–Jurassic continental to shallow-marine sedimentary sequence (Fig. 1.9). The

basement is made predominantly of quartzo-feldspathic gneisses intruded by late Carboniferous and Early Permian (ca. 257 Ma) granitoids (Okay et al., 2001; Sunal et al., 2006). The basement lithologies form a belt about 20 km wide extending from Bulgaria to Çatalca near İstanbul.

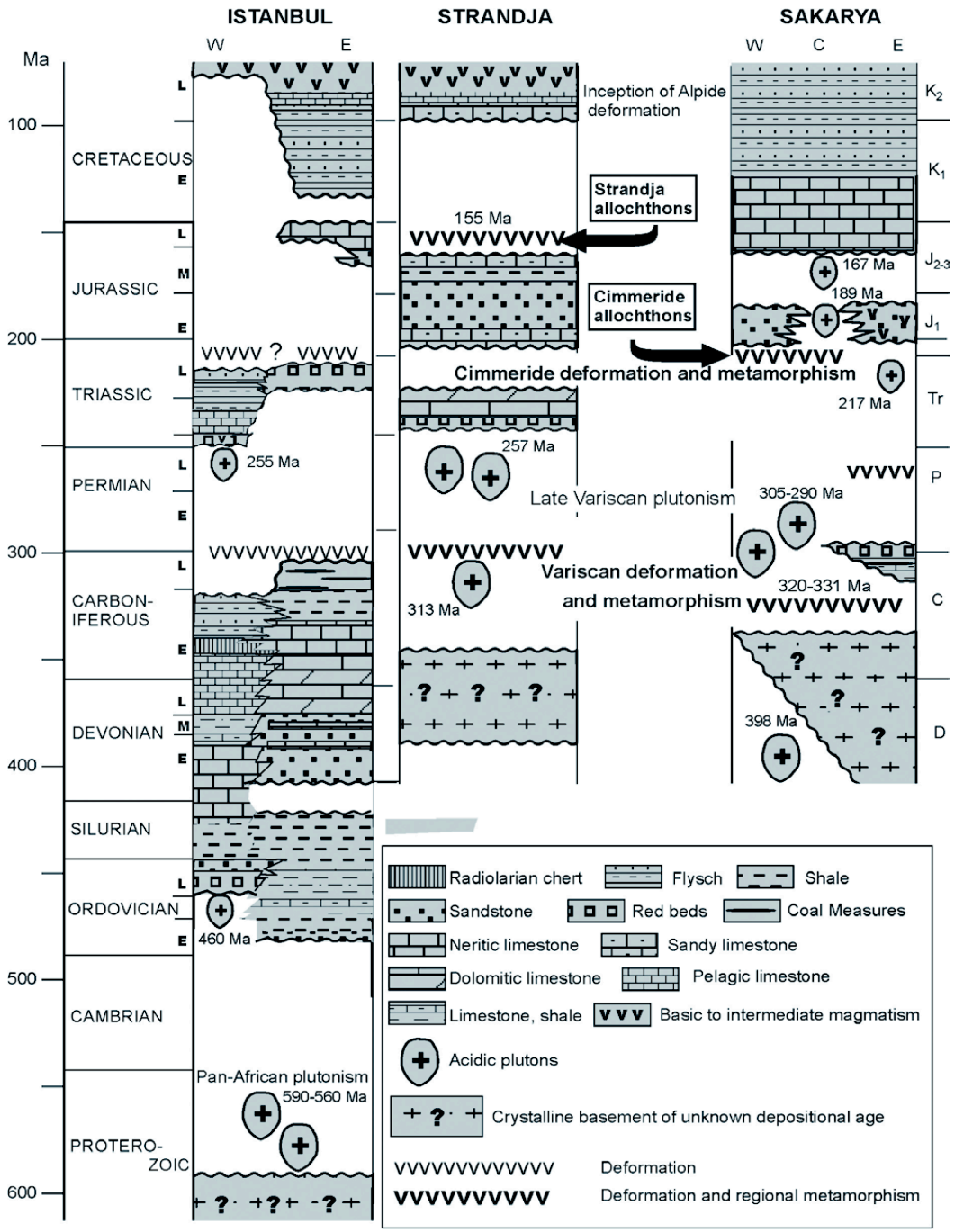

Fig. 1.9 – Synthetic stratigraphic sections of the İstanbul, Strandja and Sakarya terranes (Okay et al., 2008).

The İstanbul Terrane is a continental fragment, approximately 400 km long and 55 wide, located along the southwestern margin of the Black Sea (Fig. 1.1). It has a late Precambrian crystalline basement characterized by gneiss, amphibolite, metavolcanic rocks, metaophiolite and voluminous Late Precambrian granitoids (Fig. 1.9; Chen et al., 2002; Yiğitbaş et al., 2004; Ustaömer et al., 2005). The Istanbul Terrane is separated from the Sakarya terrane by the Intra-Pontide suture marking the trace of the Intra-Pontide ocean (Şengör & Yılmaz, 1981). Cavazza et al., (2012) have recently demonstrated that the amalgamation of the two terranes occurred in pre-Cenozoic times.

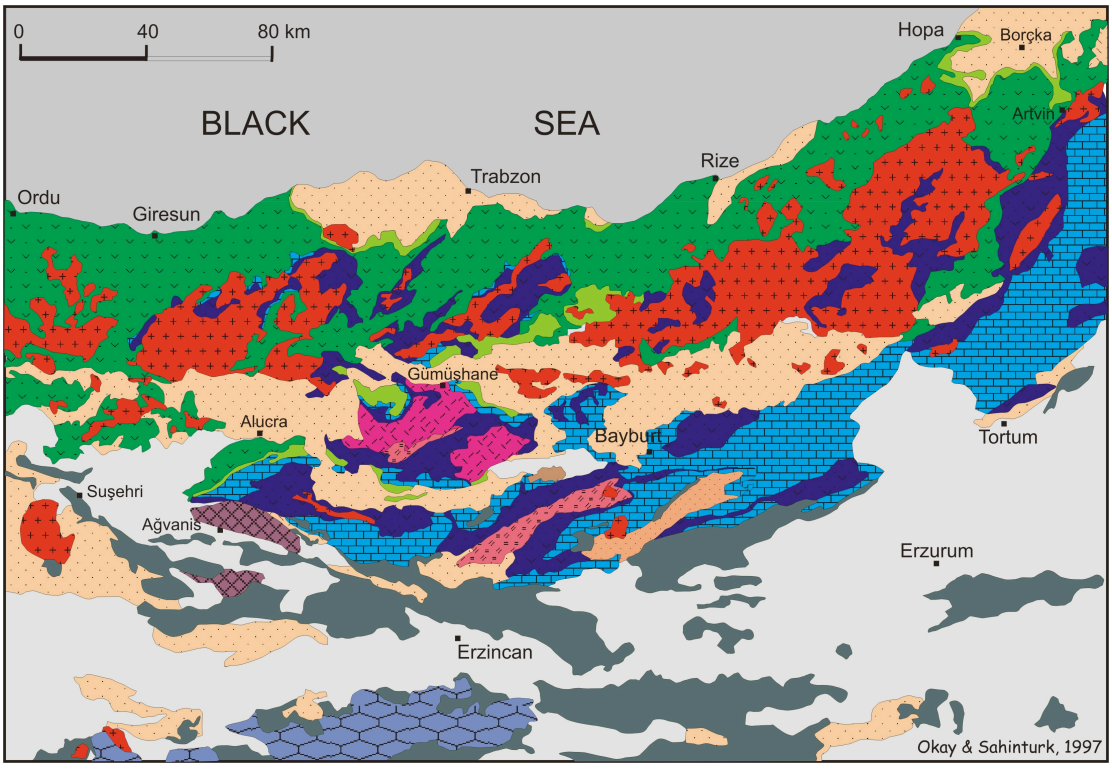

Fig. 1.10 – Simplified geological map of the Eastern Pontides (Konak et al., 2009).

The Sakarya terrane, which includes the Eastern Pontides, is characterized by a general absence of in-situ Paleozoic sedimentary rocks, by the presence of Paleo-Tethyan Permo-Triassic accretion/subduction complexes (the Karakaya

Complex) and by a ubiquitous Liassic transgression (Okay et al., 1996; Federici et al., 2010). In contrast, the Taurides to the south show a well-developed Palaeozoic sedimentary succession and do not comprise Paleo-Tethyan accretion-subduction complexes. The Sakarya and Tauride terranes and paleogeographic realms are separated by the Izmir-Ankara-Erzincan suture zone, which is marked by large bodies of peridotite and ophiolitic mélange (Fig. 1.10). The three Pontic terranes were amalgamated in the Mesozoic following the closure of the Intra-Pontide suture and the opening of the western Black Sea. Isotopic data from eclogites and blueschists in the Central Pontides indicate that the NeoTethys was already subducting under the Pontides in the Early Cretaceous (ca. 105 Ma, Okay et al., 2006). However, the corresponding magmatic arc started to develop only in the Late Cretaceous (ca. 90 Ma, Robinson et al., 1995; Okay & Sahinturk, 1997). The Upper Cretaceous magmatic arc can be traced along the Black Sea coast from the Lesser Caucasus to Sredna Gora in Bulgaria. The magmatic arc switched off in the Maastrichtian, although the collision between Pontides and the Anatolide-Tauride was delayed until the Late Palaeocene – Early Eocene (Okay, 2008). The collision was followed by uplift and extensive erosion. A new cycle of deposition and volcanism started in the Middle Eocene, probably related to extension associated with opening of the eastern Black Sea (e.g., Okay, 1994, 2008). The sea finally left the Pontides by the end of the Eocene and the region has been subaerially exposed since the Oligocene.

The Eastern Pontides form a mountain chain 500 km long and 100 km wide along the southeastern coast of the Black Sea (Fig. 1.10). Geographically, Eastern Pontides is a term used for the region skirting the eastern Black Sea coast of Turkey. Its western boundary is taken arbitrarily either as the Yeşilırmak or

Kızılırmak rivers near Samsun. Geologically, the Eastern Pontides are well known as one of the best preserved examples of paleo-island arc, which was formed above the northward-subducting Tethyan ocean floor during the Senonian (Şengör & Yılmaz, 1981; Akinci, 1984; Okay & Şahintürk 1997). The Eastern Pontides are bounded to the south by the Ankara-Erzincan Neo-Tethyan suture and to the north by the eastern Black Sea basin. Eastward they extend without a break into the Lesser Caucasus of Georgia (Adjara-Trialeti and Artvin-Bolnisi tectonic zones) (e.g., Khain, 1975; Yılmaz et al., 1999). Their western geological boundary with the Central Pontides is stratigraphic and corresponds to a facies change in the Cretaceous sequence.

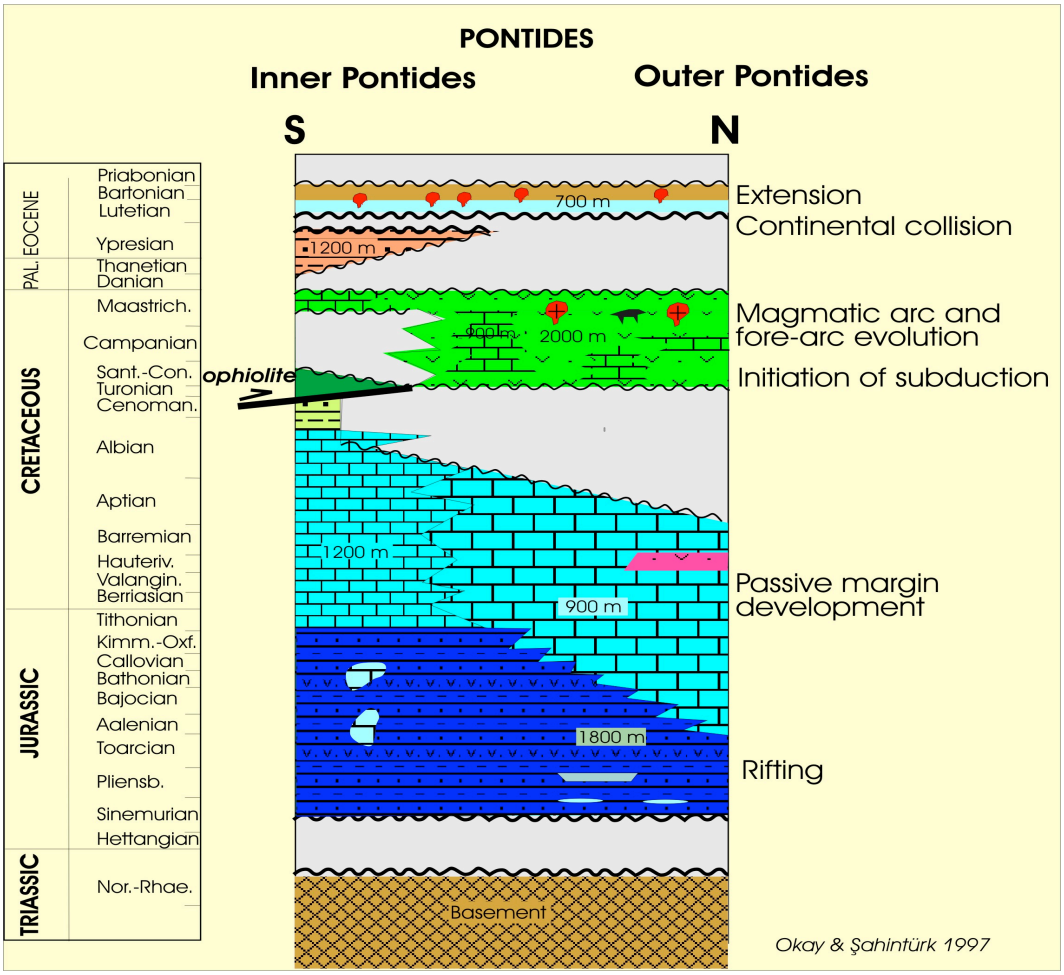

Fig. 1.11 – Jurassic-Tertiary stratigraphy of the Eastern Pontides (Okay & Şahintürk, 1997).

The Eastern Pontides are commonly divided into an inner/southern and an outer/northern part (Fig. 1.8; Konak & Hakyemez, 2001; Konak et al., 2009). The outer Eastern Pontides are dominated by Senonian and Middle Eocene volcanic and volcanoclastic rocks, which hide much of the pre-Senonian geology (Fig. 1.8). Pre-Senonian rocks are instead exposed in the inner Eastern Pontides, which occupied a fore-arc position during the Senonian and underwent more intense deformation than the outer Eastern Pontides during the early Tertiary continental collision. The transitional boundary between these two parts follows approximately the Niksar-Gümüşhane-Artvin line.

According to some authors Okay et al. (2008) the major stratigraphic and tectonic features of the Eastern Pontides can be summarized as follows. Heterogeneous pre-Jurassic basement was consolidated during the Hercynian and Cimmeride orogenic events (Fig. 1.11). Triassic sedimentary rocks are absent possibly due to metamorphism during the Cimmeride orogeny. The Mesozoic sequence starts with a widespread Liassic transgression – a common feature of the entire Sakarya Terrane- and continues essentially uninterrupted until the mid-Cretaceous, when a major break in sedimentation with uplift and erosion of the entire Eastern Pontides occurred (Okay & Tüysüz, 1999). This was followed by a flip in the subduction polarity and consequently a volcanic arc developed during the Turonian to Campanian in the outer Eastern Pontides above the northward subducting Tethyan ocean floor (Konak et al., 2009). The inner parts of the Eastern Pontides were in a forearc position during the Senonian. Major thrust imbrication of the southern continental margin of the Eastern Pontides occurred during the Late Palaeocene/Early Eocene (Konak & Hakyemez, 2001). Thrusting involved the pre-Jurassic basement; thick foreland

flysch basins developed in front of the northward moving nappes. In the outer Eastern Pontides the Late Palaeocene/Early Eocene is characterized by folding, uplift and erosion. This orogenic event, the strongest in the Eastern Pontides during Mesozoic and Tertiary times, marks the continental collision between the Eastern Pontide arc and the Anatolide-Tauride Block to the south. Essentially undeformed basaltic and andesitic volcanic rocks and shallow marine sedimentary rocks of Middle Eocene age occur throughout the Eastern Pontides and cover nonconformably a folded and thrust-faulted basement (Konak et al., 2009; Konak & Hakyemez 2001). They mark regional extension probably related to an accelerated phase of opening of the eastern Black Sea basin. Minor plutonic occurrences (i.e. Kackar batholith) are associated with the mid-Eocene volcanic phase). From the end of the Middle Eocene the Eastern Pontides stayed above sea level with minor volcanism and continental sedimentation.

1.4 THE LESSER CAUCASUS

The structure and geological evolution of the Caucasian segment of the Black Sea-Caspian region (Fig. 1.12) are largely determined by its position between the still converging Eurasia and Africa-Arabia lithosphere plates within a wide zone of continent-continent collision (e.g., Adamia et al., 1987). According to some authors (Khain, 1975; Adamia et al., 1981, 2008; Zakariadze et al., 2007), the region in the Late Proterozoic, Palaeozoic, and Mesozoic until the Early Cretaceous belonged to the now-vanished branches of the Tethys Ocean and to its Eurasian and Gondwanan/Africa-Arabian margins. Within this ocean-continent convergence zone, there existed a system of island arcs, intra-arc rifts,

and back-arc basins characteristic of the early Cenozoic pre-collisional stage of evolution of the region. During the syn-collisional (Oligocene-Middle Miocene) and post collisional (Late Miocene-Quaternary) stages of the convergence between Africa-Arabia and Eurasia, back-arc basins were inverted to form fold-thrust belts in the Greater and Lesser Caucasus and, in between, the Transcaucasian intermontane depressions (Rioni and Kura basins; Fig. 1.13).

Fig. 1.12 – Physical map of the Caucasus and adjacent areas of the Black Sea-Caspian region (Adamia et al., 2010).

The Caucasus is located at the junction of the Turkish and Iranian segments of the Alpine-Himalayan fold-and-thrust belt (Fig. 1.13). It is bordered by the Scythian Platform to the north and the southern Armenian-Nakhichevan sub-

platform to the south. The Scythian Platform consists of an Hercynian basement overlain by late Hercynian molasse and calc-alkaline volcanic rocks, in turn overlain by Mesozoic-Cenozoic epicontinental, marine, lagoonal and, continental deposits (Adamia et al., 2010, 2011). The southern Armenian-Nakhichevan sub-platform is similar to the Taurus-south Anatolian zone, and characterized by a pre-Campanian basement complex overlain nonconformably by monotonous shelf carbonates of Palaeozoic-Triassic age.

The Caucasus is divided into several main tectonic units or terranes (Fig.1.13). From north to south these are (i) the Scythian (Pre-Caucasus) platform; (ii) the fold-and-thrust mountain belt of the Greater Caucasus, comprising the so-called Fore-Range, Main Range, and Southern Slope zones; (iii) the Transcaucasian intermontane depression superimposed mainly on a rigid platform zone (Georgian Massif); (iv) the Adjara-Trialeti (Georgia) and the Talysh (Azerbaijan) fold-thrust mountains belts; (v) the Artvin-Bolnisi rigid massif; (vi) the Loki-Bayburt-Karabagh-Kaphan fold-thrust mountain belt; (vii) the Sevan-Akera ophiolitic suture; (vii) the Lesser Caucasian part of the Taurus-Anatolian-Central Iran platform; (viii) the Aras intermontane depression (Koçyiğit et al., 2001; Adamia et al., 2010, 2011). The youngest tectonostratigraphic unit is composed of Neogene-Quaternary continental volcanic formations of the Armenian and Javakheti plateaux and extinct volcanoes of the Greater Caucasus-Elbrus, Cheghem, Keli and Kazbegi. Existing data allow the division of the Caucasian region *sensu lato* into two large-scale geological provinces: southern Tethyan and northern Tethyan, respectively located to the south and to the north of the Lesser Caucasian ophiolite suture. The southern and northern provinces differ one from the other throughout the

Mesozoic and Early Cenozoic. The boundary between them runs along the complex North Anatolian (İzmir-Ankara-Erzincan) – Lesser Caucasian (Sevan-Akera) – Iranian Karadagh ophiolitic suture belt.

The Lesser Caucasus, including Armenia, is an area of common ophiolite occurrences. Small ophiolite bodies include the Aparan-Arzacan Massif of late Precambrian age and Upper Jurassic-Lower Cretaceous outcrops in the Terter river basin (Rolland et al., 2009). The largest outcrops of ophiolitic rocks are invariably dated to the Jurassic. From S to N across Armenia ophiolites are present in the following areas:

- the Vedi ophiolite area, within the Armenian (Haikakan) Par Range, the Ararat Valley and the basins of the Azat, Vedi, Kuyusuz and Nakhichevan rivers;
- the Zangezur areas, within the Shirak and Bargushat ranges;
- the Amasia-Sevan-Akera area within the Shirak and Bargushat ranges (the basins of the Dzoraget, Akhurian and Akera rives and Lake Sevan).

The rocks cropping out in the areas listed above include a full ophiolite belt which can be considered as the easternmost part of the İzmir-Ankara-Erzincan ophiolite suture belt, interpreted by many authors as the main suture of the NeoTethys (e.g., Adamia et al. 1981, 1987, 2011).

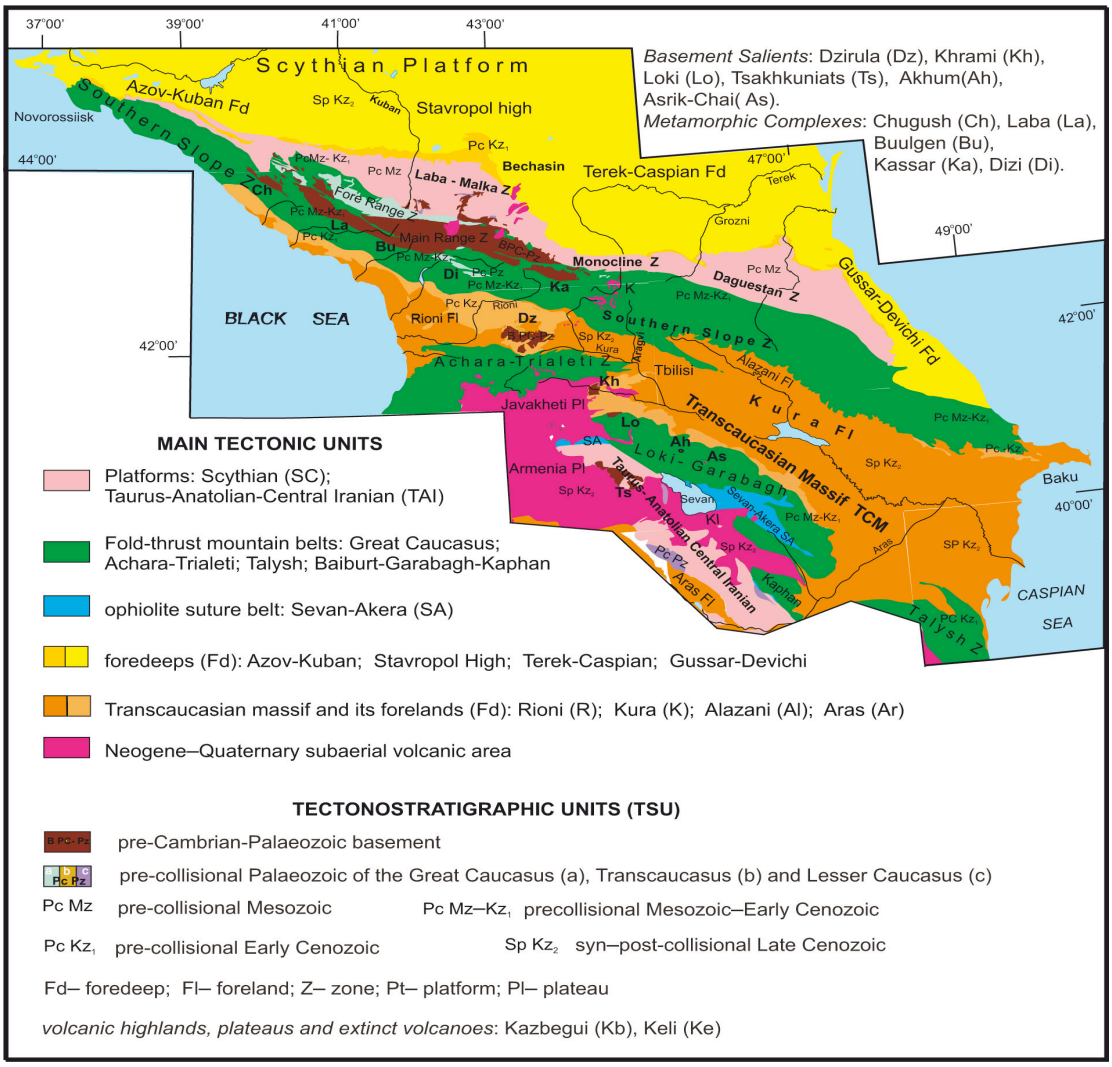

Fig. 1.13 – Tectonic sketch map of the Caucasus (Adamia et al., 2010).

The stratigraphy of the Lesser Caucasus is similar to the classic sections of other areas of the Mediterranean region (southern Europe, Balkan peninsula, Asia Minor and the Middle East). Rocks range in age from Precambrian to Pleistocene and volcanogenic rocks alternating with normal sedimentary deposits are widespread throughout the stratigraphic sequence (e.g., Aslanian, 1977, 1982). Volcanogenic deposits are predominantly andesite-basalt and andesite in composition. Along the Turkish-Georgian border area three volcano-sedimentary sequences occur (Fig. 1.14B). The oldest of these is 5.5 km thick and

coal-bearing volcano-sedimentary sequence of Late Eocene-early Miocene age (Koçyiğit et al., 2001). This sequence consists of andesitic-basaltic volcanic rocks, shallow-marine sedimentary clastic and fluvio-lacustrine magmatic rocks.

This first sequence is overlain with angular unconformity by a second volcano-sedimentary sequence consisting of various volcanic rocks alternating with fluvio-lacustrine deposits of Late Miocene-Early Pliocene age. The mid-Miocene angular unconformity described above is typical of the region and marks a rather fast episode of deformation, uplift and erosion. Such tectonic event –discussed at length in Chapters 2 and 4- is marked not only by the unconformity but also by clastic wedges prograding in the eastern Black Sea and by a distinctive cooling/exhumation episode documented by the thermochronologic data presented in this dissertation. The second sequence is > 500 m thick and overlain with angular unconformity by the third volcano-sedimentary sequence of Late Pliocene-Quaternary age. The first two sequences are folded and thrust-to-reverse faulted. Plutonic magmatism is also present as differentiated tholeiitic intrusions and as widespread Mesozoic Tethyan ophiolite.

In the Caucasian region Precambrian rocks of Panafrican affinity form part of the structure of the metamorphic basement lying at the depth of 0 to 6-8 km to the south of the İzmir-Ankara-Erzincan-Sevan-Akera ophiolitic suture. They include gneissic granites, amphibolites, and gabbro-peridotite. North of the suture intrusive rocks are represented by Palaeozoic, Hercynian-related gabbroids, diorites, and quartz-diorites, Late Palaeozoic plagiogranites, granitoids, granodiorites, granites and quartz diorites. Late Jurassic granitoids and Late Cretaceous gabbro diorites and diorites are associated with northward

subduction beneath the Eurasian continental margin. Eocene plagiogranites, gabbros, gabbros monzonite syenite and syenite diorite mark the late- to post-collisional phase related to the definitive closure of the eastern portion of the İzmir-Ankara-Erzincan-Sevan-Akera oceanic domain (Koçyiğit et al., 2001). The plutonics listed above were of primary interest for this study as they represented primary targets for apatite fission-track analysis.

Three major elements characterize the Neogene fabric of the Lesser Caucasus: (1) NW- and NE-trending dextral to sinistral active strike-slip faults, (2) N-S to NNW-trending fissures and/or Plio-Quaternary volcanoes, and (3) a 5 km thick, hardly deformed Plio-Quaternary continental volcano-sedimentary succession

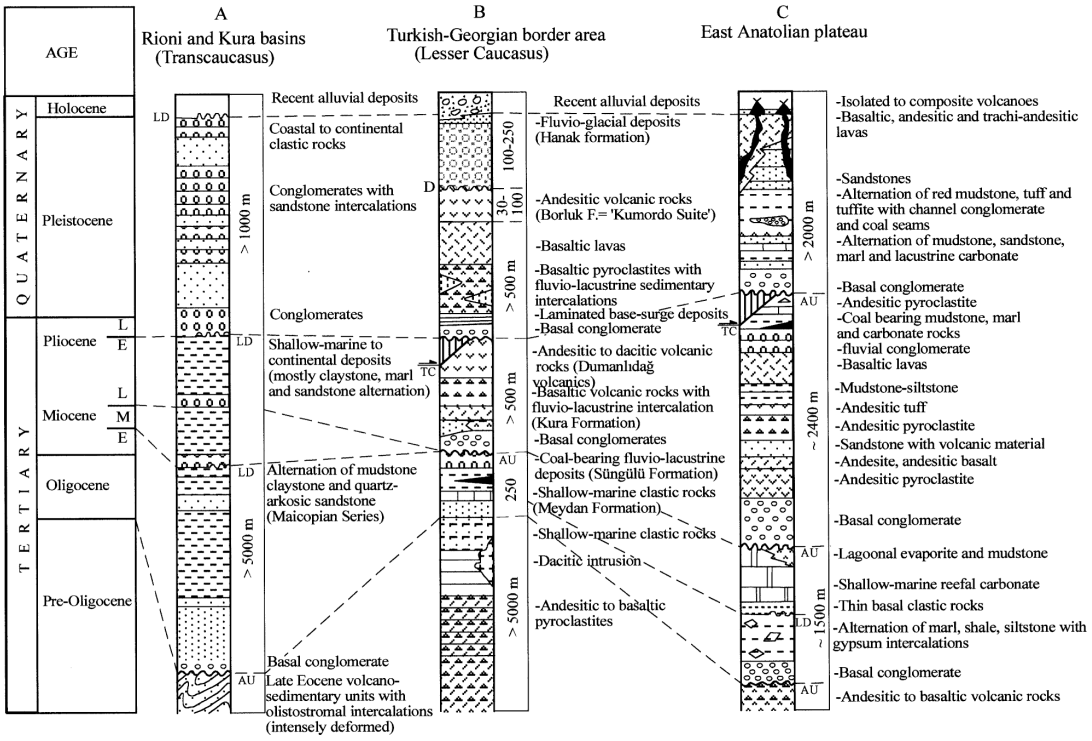

Fig. 1.14 – Simplified stratigraphic columns of Oligocene-Quaternary neotectonic fill in the Rioni and Kura basins, Turkish-Georgia border area and East Anatolian basins. AU, angular unconformity; D, disconformity; E, early; L, late; LD, local disconformity; M, middle; TC, thrust-to-reverse fault contact (Koçyiğit et al., 2001).

accumulated in various strike-slip basins (Koçyiğit et al., 2001). Starting from the southern foot of the Transcaucasus southward the nature of both the tectonic

regime and geological structures vary gradationally (Fig. 1.15). The N-S-directed compressional-contractional structures (folds, thrust to high-angle reverse fault, and ramp basins) are prominent to the north (Greater Caucasus and Transcaucasus), whereas the transtensional structures (both the sinistral and dextral strike-slip faults, various strike-slip basins, and N-S trending fissures become prominent to the south (the Lesser Caucasus and the East Anatolian Plateau). This is clearly an oversimplification, as significant shortening is evident in several parts of the otherwise strike-slip-dominated southern area. According to Koçyiğit et al. (2001) the strike-slip faults cut and displace dykes and other

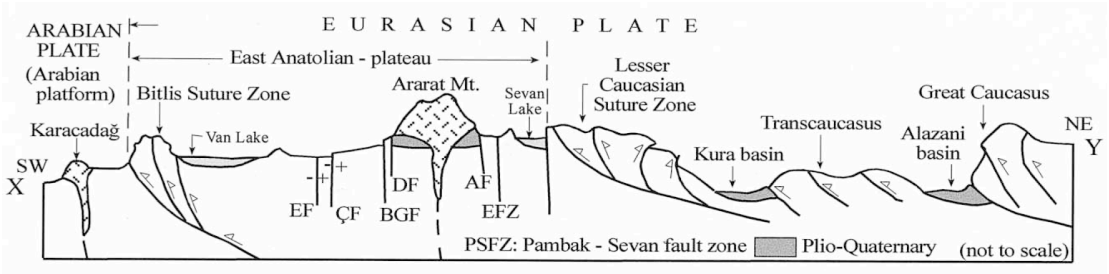

Fig. 1.15 – Simplified geological cross-section across eastern Anatolia and Transcaucasia, showing major compressional and extensional structures. AF, Aras Fault, BGF, Balıkgölü fault, ÇF, Çaldıran fault, DF, Doğubeyazıt fault; EF, Erciş fault; EFZ, Yerevan fault zone (Koçyiğit et al., 2001).

structures of Late Miocene age hence they are younger than Late Miocene. Therefore, they conclude that the time period between the Serravallian and the Late Early Pliocene is characterized by inversion in tectonic regime, basin type, and deformation pattern (from folding/thrusting to strike-slip faulting). The results of this dissertation provide more detailed constraints on this important transition in structural style (see Chapters 2 and 4).

The collision stage in the Lesser Caucasus still needs to be thoroughly elucidated. For the Armenian sector, Sosson et al. (2010) proposed a new geodynamic evolutionary model since the Late Jurassic (Fig. 1.16). This model

envisions the presence of two main subduction zones and the South Armenian Block (SAB). According to this model, the onset of collision is dated as Palaeocene. This process occurred around 20 Ma later than the obduction (Late Coniacian-Santonian, 88-83 Ma) of the marginal basin over the SAB. From the Coniacian to the Palaeocene the intra-oceanic subduction (SSZ) evolved to a continental subduction of the SAB beneath the intra-oceanic arc and the marginal basin. This event is supported by HP-LT metamorphism at 94-90 Ma of oceanic formations identified within the accretionary prism in the Stepanavan area (Rolland et al., 2007; Galoyan et al., 2007). From Palaeocene to Early Miocene time the occurrence of a foreland basin in front of the orogenic belt and the folding and erosion of the Sevan-Akera ophiolitic zone suggest the entrance of the SAB in the subduction zone beneath the Eurasia margin, pulled by the dense eclogitized oceanic slab to which it was still attached. The Early to Middle Eocene magmatism in the Sevan-Akera suture zone could correspond to the first stage of a slab retreat triggered by the continental subduction and to the slab break-off (Lordkipanidze et al., 1988). Slab retreat and break-off lead to astenospheric upwelling below the suture zone, producing significant weakening of the SAB contintental lithospheric mantle and the beginning of its delamination

The recent geodynamics of the Caucasus and the adjacent territories is determined by its position between the still converging Eurasia and Arabia plates (Jackson & McKenzie, 1988; DeMets et al., 1990; Jackson & Ambraseys, 1997; Reilinger et al., 1997, 2006; Allen et al., 2004; Podgorosky et al., 2007; Forte et al., 2010). According to geodetic data, the overall rate of convergence is ca. 20-30 mm/y. The present-day geodynamic pattern and its bearing on the

reconstruction of the structural evolution of the area will be discussed in Chapters 2 and 4.

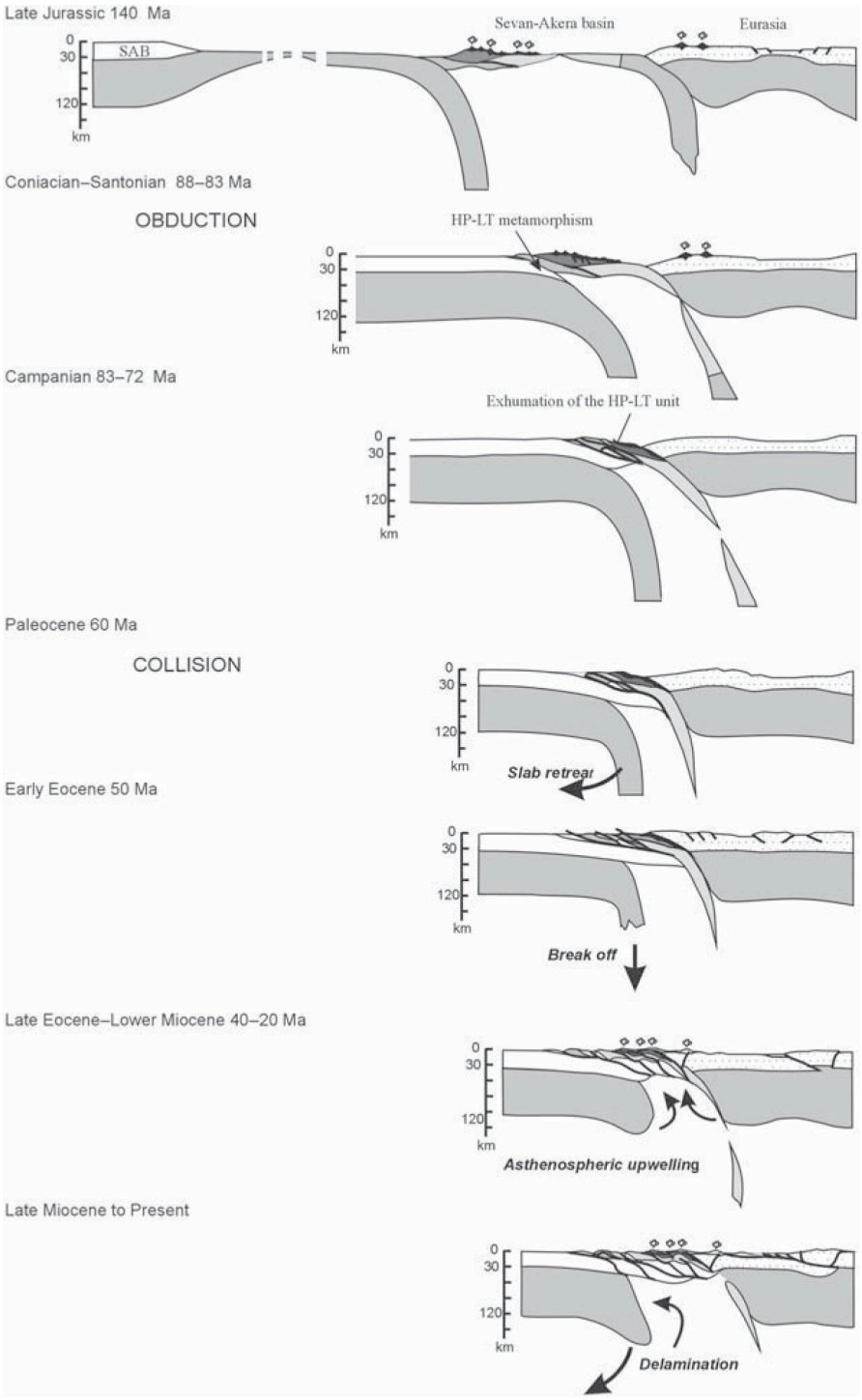

Fig. 1.16 – Geodynamic model of the evolution of the Lesser Caucasus from the Late Jurassic to the present (Sosson et al., 2010).

1.5 THE ANATOLIAN PLATEAU

The hinterland of the Arabia collision zone is a high-standing plateau (the Turkish-Iranian plateau, Fig.1.17) with an average elevation of ca. 2 km above sea level. A large portion of the plateau is covered by Late Miocene-Quaternary calc-alkaline to alkaline volcanic rocks (Yılmaz et al., 1987; Pearce et al., 1990; Yılmaz, 1990). The plateau displays structural evidence for active diffuse north-south shortening and broad east-west extension thru a conjugate system of strike-slip faults (Şengör et al., 2008; Fig. 1.18) displacing crustal fragments toward Iran and the Caspian Sea (Jackson & McKenzie, 1988; Dilek, 2006).

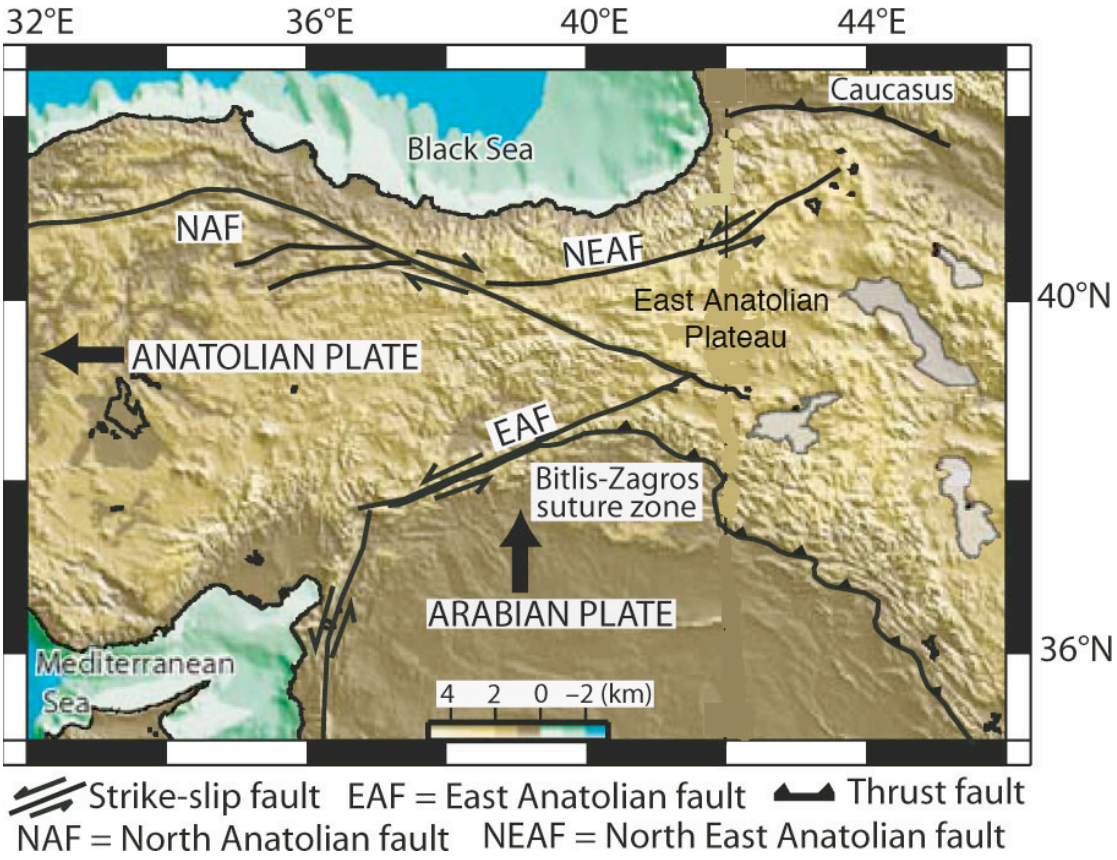

Fig. 1.17 – Topographic map of the eastern Anatolia showing major tectonic boundaries (Göğüş & Pysklywec, 2008).

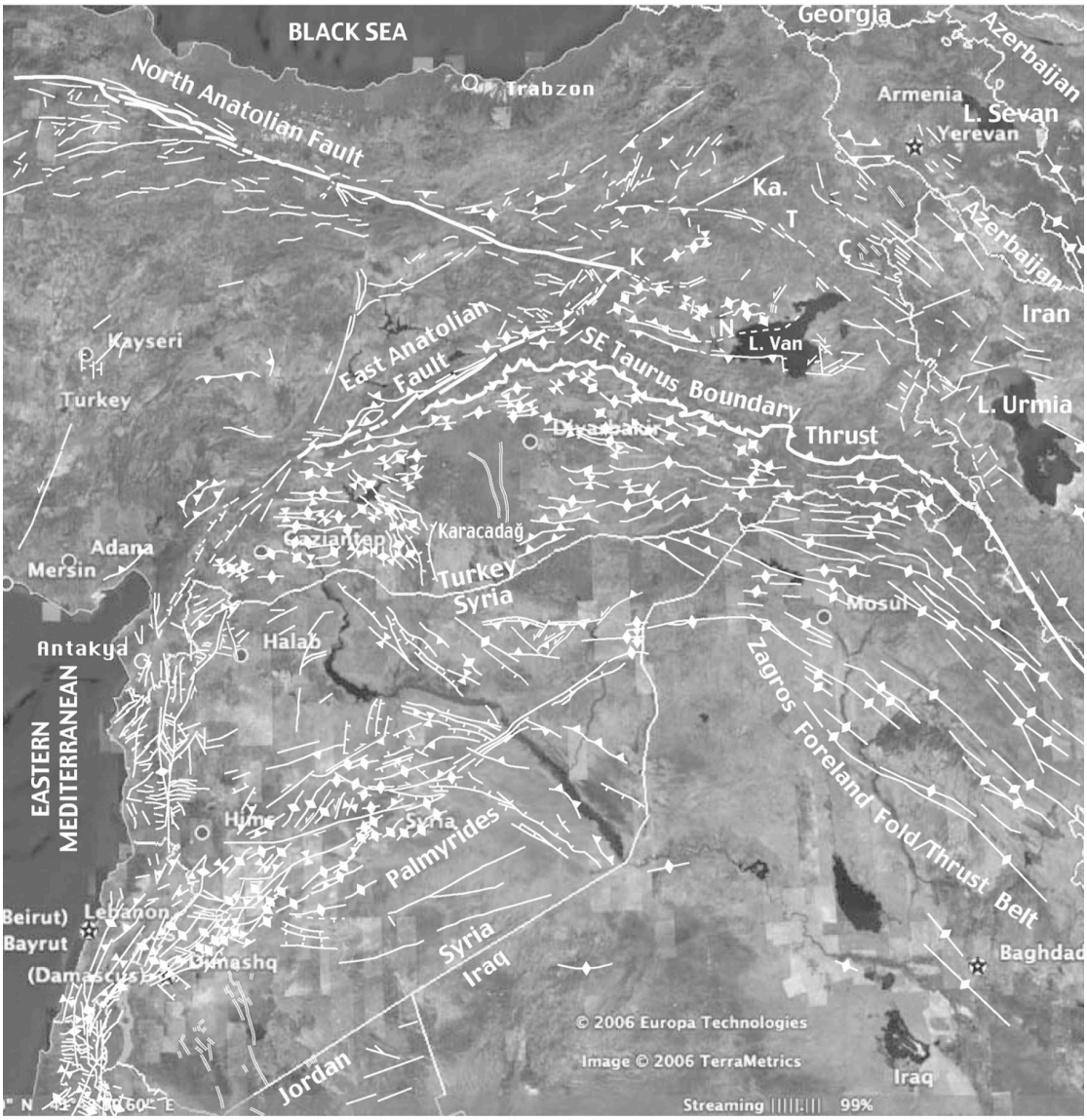

Fig. 1.18 – Neotectonic map of the Middle East showing the tectonic environment of the East Anatolian Plateau (Şengör et al., 2008).

The plateau is divided into two high depressions surrounded by mountains. The bottom of each depression is commonly at elevations > 1,500 m. To the north, the triangular Erzurum-Kars plateau is separated from the larger and more trapezoidal Murat region in the south by the Central Range, where elevations of the crests are consistently above 3,000 m above sea level. The city of Erzurum itself has an elevation of 1,950 m whereas the Araxes river flows in a

valley that descends from 1,670 m just northeast of Erzurum to < 1,000 m in the Yerevan Plain, close to the Turkish-Armenian border (Şengör & Yılmaz, 2003).

The Murat region in entirely surrounded by higher mountains and is an endorheic area centred around Lake Van. Lake Van lies mainly in a major contractional structure, a sort of "ramp valley" (Şengör et al., 1985). However, the rise of the topography is not due to the ramping, as it also rises where the ramp faults do not exist, especially to the east (Şengör & Yılmaz, 2003). This is a common situation across eastern Anatolia, where the plateau seems to have attained its characteristic elevation by wholesome uplift rather than by cumulative structural relief along discrete structures.

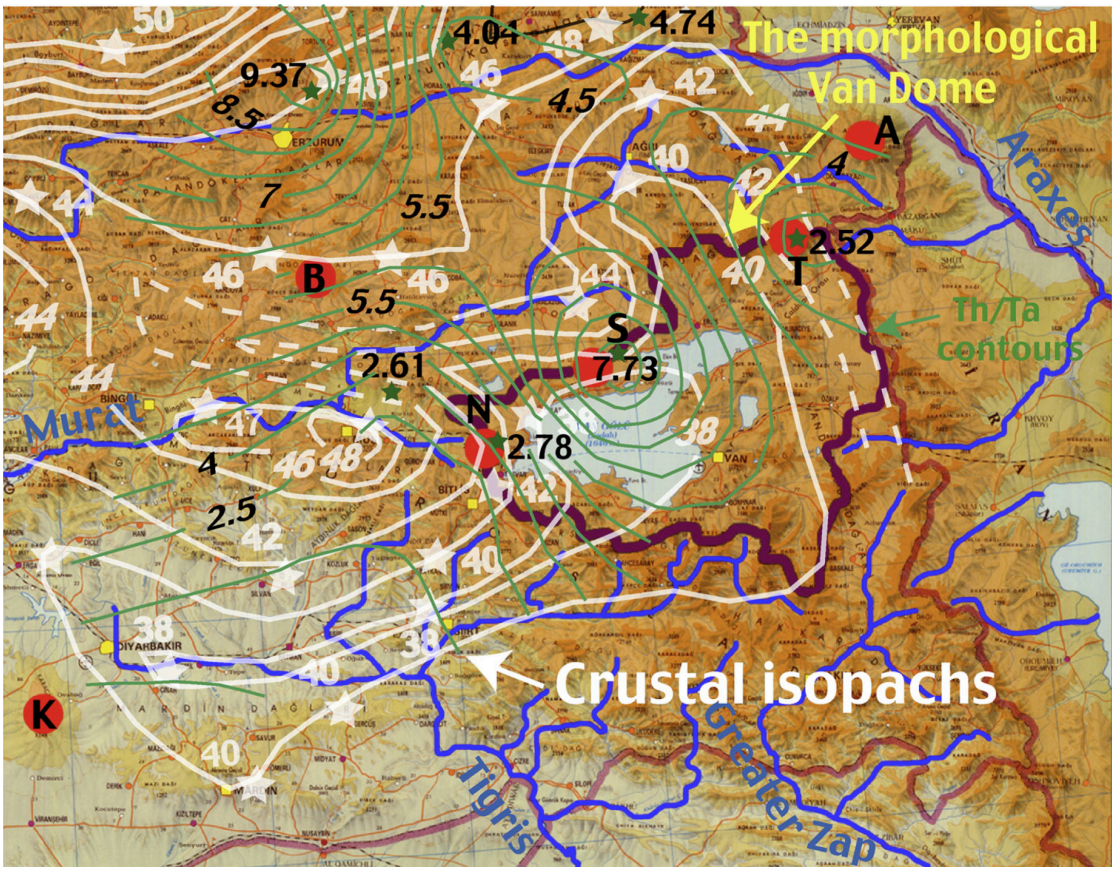

Fig. 1.19 – The Lake Van Dome showing topography, drainage and crustal thickness (Şengör et al., 2008).

The Lake Van region coincides with the thinnest crust in eastern Turkey at the acme of an asthenospheric dome. As seen in Fig.1.19 such dome contains three of the five sub-active volcanic centres in eastern Turkey (Şengör et al., 2008). With the exception of the Mt. Süphan volcano (Fig. 1.19), the Th/Ta ratios indicate that the volcanoes within the dome have been fed by an enriched asthenosphere. Güleç et al. (2002) found in the water samples from the Nemrut caldera lake and Lake Van, the highest R/R_A values (R= sample $^3He/^4He$ and R_A= air $^3He/^4He$) in Turkey (6.15 - 7.54), clearly indicating more than 75% mantle He. All of this would have been expected in a extensional region, but Lake Van lies mainly in a major shortening structure (Şengör et al., 1985, 2008), with significant strike-slip faulting along its northern and southern sides and some as yet unspecified amount of east-west extension.

The Arabia-Eurasia collision induced deformation in the Erzurum-Kars plateau and the Caucasian region. Such deformation is taken up by both strike-slip and thrust faulting (Dilek, 2006; Fig. 1.18). Lateral eastward displacements of crustal material along some major strike-slip fault systems (e.g., Pompak-Sevan fault and Van-Tebriz fault zone) have resulted in east-directed shortening, roughly perpendicular to the northwest-southeast regional strike of the fold-and-thrust belt in this region and show that the collision-induced strain is partitioned across a nearly 1,000-km-wide-zone encompassing eastern Anatolia, northern Iran, and the Caucasus (Dilek, 2006). Large scale plate deformation in the region is dominated by plate convergence with shortening and contraction, but normal fault-controlled extensional basins such as the Kagizman-Tuzluca, Hinis, Karliova, and Muş basin are well documented within the plateau (Göğüş & Pysklywec, 2008). Global Positioning System measurement (Fig. 1.20) slightly to

the west of this region also indicate local extension, but directed N-NW (Reilinger et al., 2006).

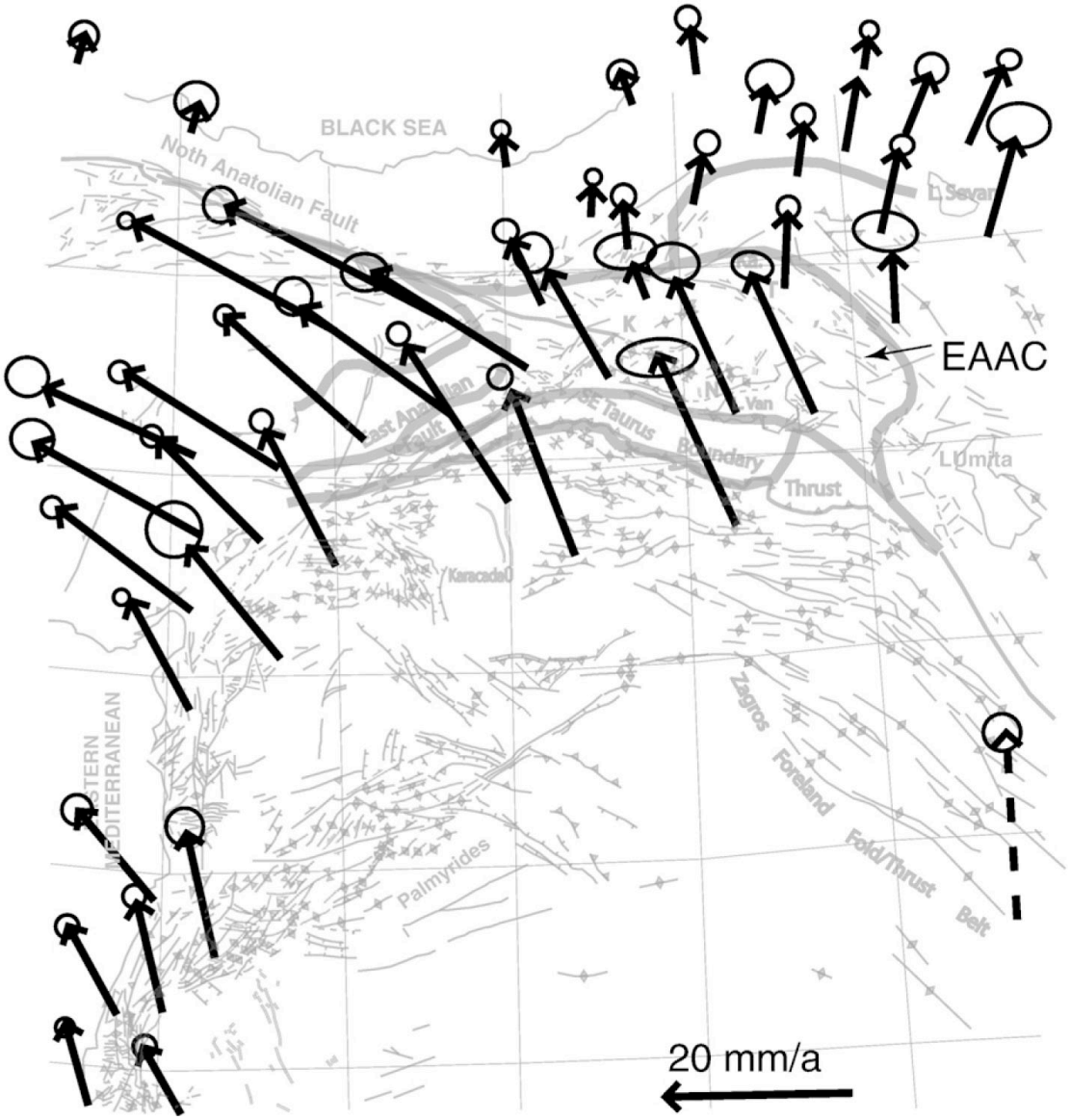

Fig. 1.20 – GPS velocities plotted relative to Eurasia with 1σ velocity uncertainties (after Reilinger et al., 2006).

Overall, GPS measurements indicate coherent W-ward motion vectors in the western Anatolian Plateau and NE- and E-ward vectors in its eastern portion. The structural implications of this change in the orientation of motion vectors wil be discussed in detailed in Chapter II. North-south shortening on thrust faults clearly also contributes to the motion of the points as represented by the

relavitive velocity vectors. The velocities do not abruptly diminish but gradually decrease so that the southern parts of the Murat region move almost as fast as Arabia, whereas its northernmost part move almost slowly as the Erzurum-Kars plateau (Şengör et al., 2008). As seen in Fig.1.21 the distribution of earthquakes is in complete agreement with this inference.

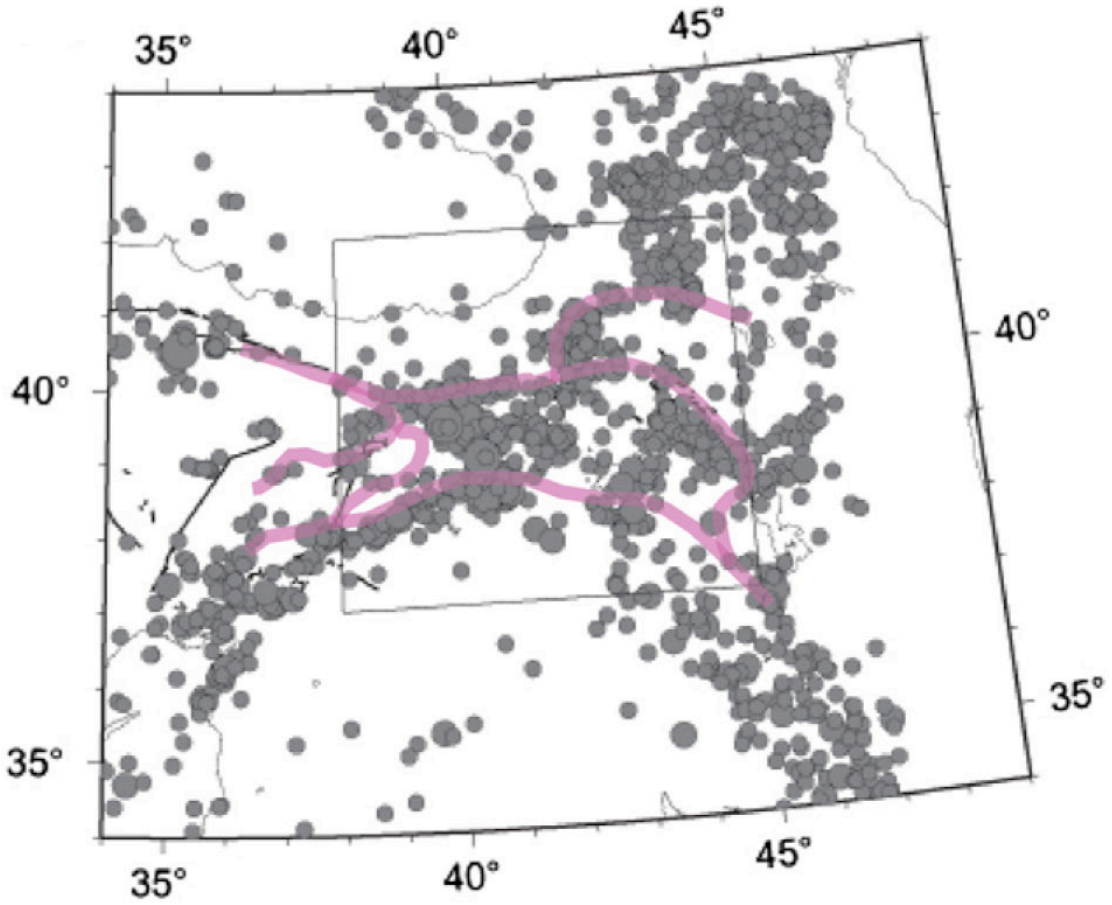

Fig. 1.21 – Earthquake epicentres in eastern Turkey follow closely the block boundaries. All earthquakes are intracrustal and no earthquake is know from mantle depths (Şengör et al., 2008).

Like the Lesser Caucasus, the East Anatolian Plateau is also characterized and shaped by three major groups of structures: (1) dextral to sinistral strike-slip faults, (2) strike-slip basins, and (3) N-S trending fissures and lines of Plio-Quaternary volcanoes. Again these structures cut across and displace fold axes, reverse faults, dykes and sills of Late Miocene age and hence are younger than

Late Miocene (Koçyiğit et al., 2001). The total offset measured on drainage systems, formation boundaries, and fold axes cut and displaced by strike-slip faults range from a minimum of 100 m to a maximum of 7 km. In more detail, two systems of strike-slip faults occur in the East Anatolian Plateau: (a) NW-SE trending dextral strike slip faults parallel to the North Anatolian Fault, (b) NE-SW trending sinistral strike-slip fault parallel to the East Anatolian Fault (Koçyiğit et al., 2001). The two fault systems have mostly the same Pliocene age, and are generically connected with a stress field linked to the N-S directed intracontinental convergence between the Eurasian and the Arabian plates.

The geology of the East Anatolian Plateau is best described in terms of its neotectonic and paleotectonic rock packages and structures (Fig. 1.22). According to Şengör & Yılmaz (2003), the paleotectonic structures of the plateau occur in three major tectonic units described below from north to south:

- the East Rhodope-Pontide arc was an ensialic, south-facing magmatic arc of Albian to Oligocene age, as previously discussed. It formed by north-dipping subduction beneath the Eurasian continental margin (Yılmaz, 1993). An extensive zone of backthrusting brings ophiolitic mélange nappes of Cretaceous age onto its southern margin. These are the innermost parts of the East Anatolian Accretionary Complex (Şengör & Yılmaz, 1981);
- the East Anatolian Accretionary Complex basement consists of ?Late Cretaceous ophiolitic mélange and Paleocene-to-Late Oligocene flysch sequences. The mélange occurs in imbricate, mainly north-dipping, slices commonly incorporating younger flysch (e.g., Şengör & Yılmaz, 1981). The flysch becomes younger from north to south and it represents

progressively shallower environments from the Cretaceous to the Oligocene (Şengör & Yılmaz, 1981);

- the Bitlis-Pütürge Massif is a highly deformed metamorphic massif formed by the collision between the eastern end of the Menderes-Taurus block (Anatolide-Tauride Block of Okay & Tüysüz, 1999) and the northern margin of the Arabian Platform (Yılmaz, 1993).

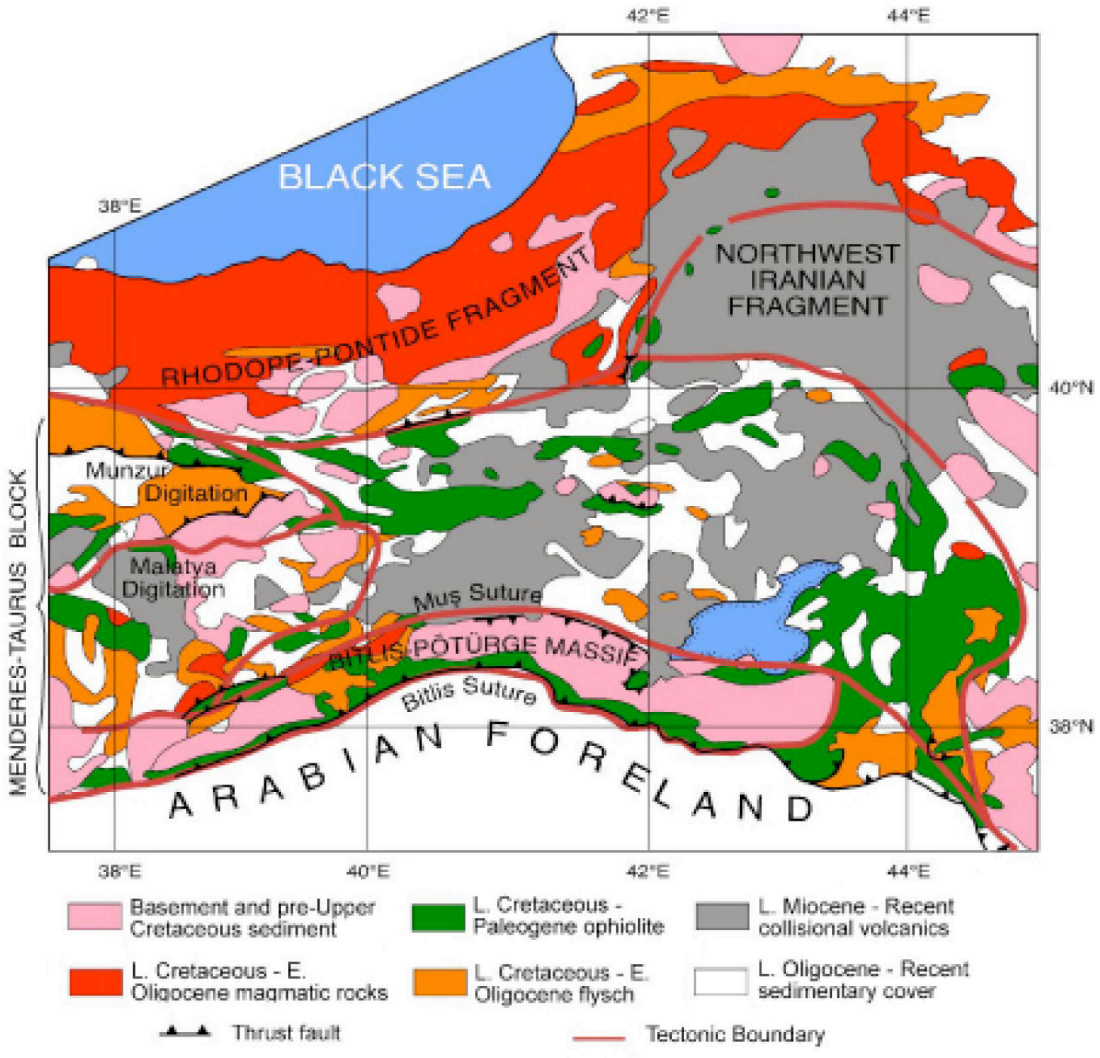

Fig. 1.22 – Simplified geological map and tectonic units of the Eastern Anatolian Plateau (Şengör et al., 2003).

In the Anatolian Plateau folding is widely distributed north and northwest of Lake Van, whereas thrusting is more confined to the Muş-Van depression, along

the northern and the southern sections of the mountainous frame of the Murat region (Şengör et al., 2008) (Fig. 1.18). This is in a agreement with a generic decrease in the amount of shortening from the Bitlis orogen towards the north into the foreland. There are exceptions to this general rule like, for example, in the area west of Yerevan in Armenia, where some thrusting is evident.

Except for the north-south striking Nemrut fissure (Şengör et al., 1985; Dewey et al., 1986) there are no notable north-south trending extensional features, although small-scale ones have been mapped following earthquakes (Koçyiğit, 2001; Şengör et al., 1985) and seismic reflection profiling has discovered a number of north-south trending normal faults in Lake Van (Şengör et al., 1985).

As previously pointed out, the eastern Anatolian Plateau is dominated by strike-slip fault that form two main sets: a sinistral northeast–southwest striking set and a dextral northwest-southeast striking set (Şengör et al., 1985; Bozkurt, 2001; Koçyiğit et al., 2001; Philip et al., 2001). The first set is more dominant in the Erzurum-Kars plateau, whereas the latter set predominates to the south. GPS velocities (Fig. 1.20) corroborate the observation that in the Murat region the northwest-southwest striking right-lateral strike-slip fault set must be dominant, as the points in this region move NNW-ward with respect to Eurasia (Şengör et al., 2008). The velocity field indicate that north-south-directed shortening on thrusts and folds continues to provide a significant contribution to overall shortening in the region (Şengör et al., 2008).

Four successions overlie the tectonic edifice of the east Anatolian Plateau. One of them is sedimentary, the remaining three are volcano-sedimentary successions separated from each other by angular unconformities (Koçyiğit et al.,

2001; Fig. 1.14C). The oldest succession consists of shallow-marine-to-continental conglomerate, siltstone, shale, gypsum, reefal limestone, and evaporite of Oligocene – Early Miocene age (Koçyiğit et al., 2001). This sedimentary succession -ca. 1,500 m thick- is unconformably overlain by a 2,400 m thick succession consisting of coal-bearing fluvio-lacustrine deposits and andesitic to basaltic rocks alternation of late Miocene – early Pliocene age (Koçyiğit et al., 2001). The transition from the shallow marine and transitional deposits of the first succession to the continental deposits of the second succession marks the acme of Arabia-Eurasia collision and the definitive closure of the Mediterranean-Indian Ocean seaway. The second succession is overlain with angular unconformity by a 2,000 m thick continental volcano-sedimentary succession dominated by Plio-Quaternary volcanics. These first three successions of East Anatolian Plateau are somewhat folded and reverse faulted, whereas the last Plio-Quaternary volcano-sedimentary succession is undeformed, confirming the transition from an earlier compressional-contractional paleotectonic regime to a strike-slip extensional neotectonic regime (Koçyiğit et al., 2001). The thermochronological results of this dissertation refine further this important transition in the tectonic evolution of the Bitlis foreland (see Chapters 2 and 4).

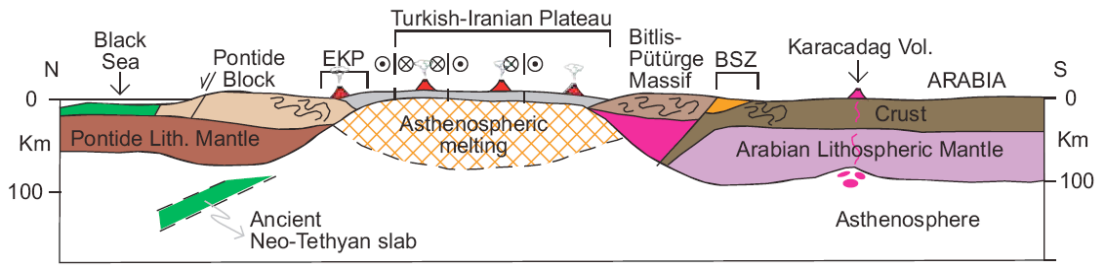

Fig. 1.23 – Crustal and lithospheric thickness across the Turkish-Iranian Plateau and the surrounding regions (Dilek, 2006).

According to Zor et al. (2003), the crust beneath the plateau is 38-50 km thick, hence it has been suggested that the high topography is not isostatically supported by a thick crustal root (Şengör & Yılmaz, 2003; Keskin, 2003). Furthermore, seismic data for eastern Anatolia are interpreted as evidence for the complete absence of mantle lithosphere beneath the Plateau (Dilek, 2006; Gok et al., 2007; Fig. 1.23) and are consistend with high heat flow and volcanic activity (e.g., Nemrut, Suphan, and Agri-Arat volcanoes) across eastern Anatolia.

Several interpretations have been proposed for the genesis of the genesis of the East Anatolian Plateau. The evolutionary model by Şengör & Yılmaz (2003) (Fig. 1.24), explains well the geochemical characteristics and temporal-evolution of the widespread volcanics of the East Anatolian Plateau. Nevertheless, it must be pointed out that the model of Şengör & Yılmaz (2003) does not envision the presence of any continental block between the Pontide arc to the north and the Arabian platform to the south. In other words, the model implies that the Anatolide-Tauride terrane of western and central Turkey does not continue into eastern Anatolia. According to these authors, in the Early Eocene the Rhodope-Pontide arc was still active and associated with a large subduction-accretion complex. By Late Eocene time, the toe of this accretionary complex may, in some points, have touched the northern margin of the Bitlis-Pütürge Massif. Throughout the Oligocene, the East Anatolian Accretionary Complex was shortened and thickened above an oceanic lithosphere sliding beneath it (Şengör & Yılmaz, 2003). This “hidden subduction” (Şengör et al., 1984) may have created the last, Oligocene intrusions in the Rhodope-Pontide arc and extrusives to its immediate south (38.5 Ma; Keskin et al., 1998). After the East Anatolian Accretionary Complex thickened to normal continental crustal thickness,

subduction was arrested and Arabia-Eurasia convergence began to be accommodated by intracontinental convergence and crustal shortening from the Greater Caucasus to northern Arabian Plate at the beginning of the Miocene (ca. 24 Ma ago).

Şengör & Yılmaz (2003) proposed that slab break-off commenced at 11 Ma, when the first collisional-related magmatism began about 200 km north of the present-day suture line and when the plateau surface entirely cleared out of water (Keskin et al., 1998). By 8 Ma ago slab break-off was probably complete and post collisional volcanism became plateau wide by spreading mainly southward. The falling off of the slab exposed the underbelly of the East Anatolia Accretionary Complex to at least asthenospheric temperatures, which resulted in it widespread partial melting, (Şengör et al., 2003). The volcanism of Eastern Turkey, exhibiting a complex composition and geochemistry ranging from andesitic-rhyolitic melts to alkali olivine basalts, probably reflects the rise of the asthenosphere, its adiabatic melting and heating of the overlying crust (Keskin, 2003). It should be noted that according to Şengör & Yılmaz (2003) the scattered outcrops of metamorphic rocks locally cropping out in the volcanic and volcano-sedimentary series of the East Anatolian Plateau are the result of the progressive incorporation and methamorphism of older sediments in a large south-verging accretionary complex underlying much of eastern Anatolia. From this viewpoint, no Anatolide-Tauride terrane can be traced to the east of the eastern Taurus Mountains, in disagreement with much of the pre-existing literature.

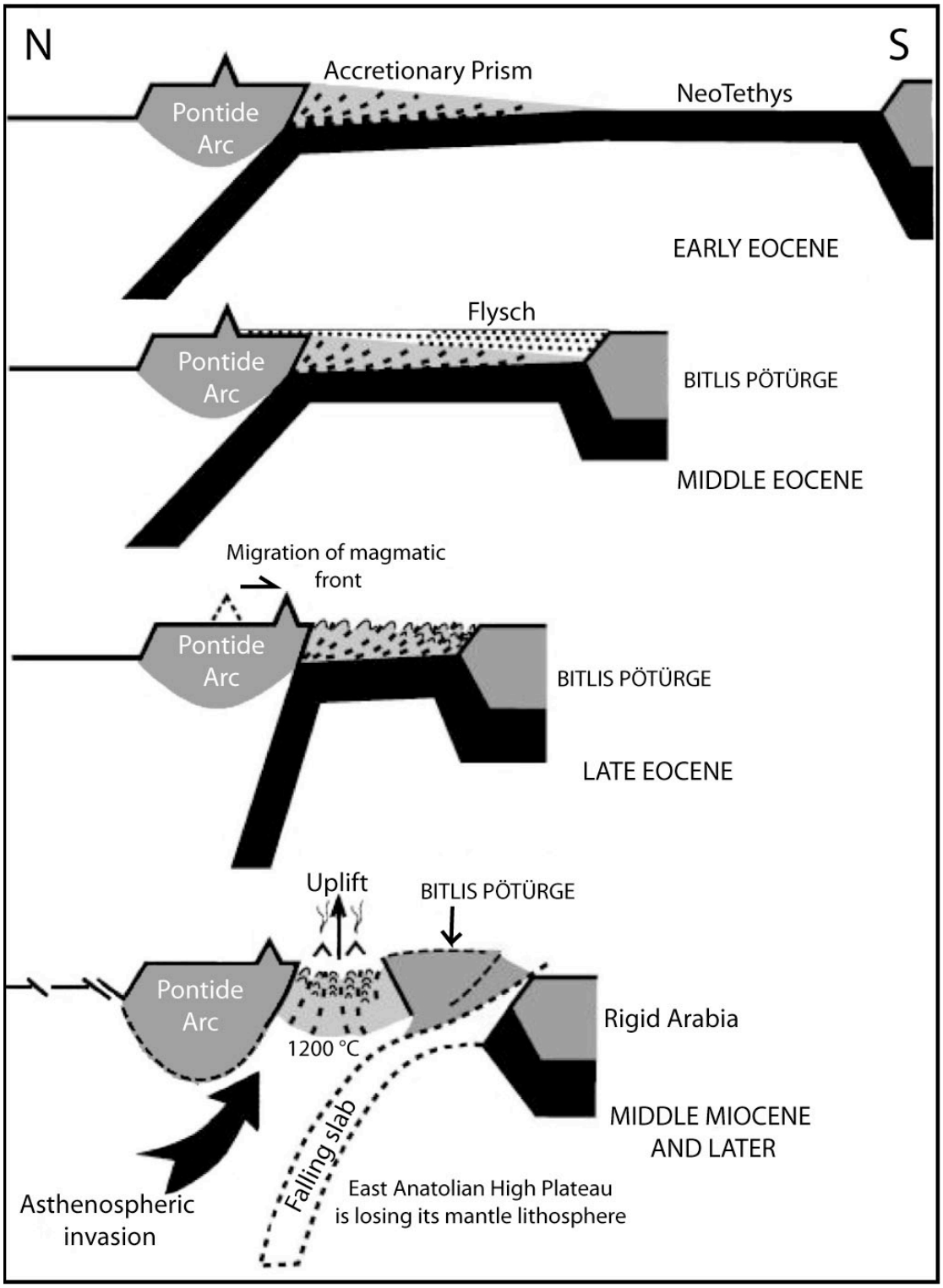

Fig. 1.24 – Schematic cross-sectional tectonic evolution of the East Anatolian Plateau from early Eocene to present days (Şengör & Yılmaz, 2003).

Keskin (2003) proposed that break-off of the northward-subducting oceanic Arabian plate in the past 7-8 my has caused domal uplift and volcanic activity in

the eastern Anatolia through rising mantle. In this model is implicity assumed a delamination-style separation of the mantle lithosphere from crust prior to its detachment. Alternatively, Ershov & Nikishin (2004), proposed a mantle plume scenario for eastern Anatolia. However, petrological and geophysical evidence, the migration of volcanism from north to south, its geochemical variation from change calc-alcaline to alkaline (Keskin, 2003), and seismic tomographic interpretations of the detached slab beneath the plateau (Lei & Zao, 2007) - do not favour the plume model. Anderson (2005, 2007) suggested that topographic uplift with widespread volcanism in eastern Anatolia may be related to lithosperic delamination in the manner defined by Bird (1979): mantle lithosphere is removed as a coherent slice by peeling away along the crust-mantle boundary or at the upper margin of anomalously dense lower crust (Anderson, 2007). Faccenna et al., 2006 proposed a model (Fig. 1.25) to explain the possibility that the formation of North Anatolian Fault (NAF) was accompanied by (i) uplift of the Turkish-Iranian Plateau, (ii) a surge of volcanism in the eastern Anatolian collisional area, and (iii) acceleration of the Aegean trench retreat. In this model, uplift of Anatolian Plateau is interpreted as a surface manifestation of the slab rupture in the Middle-Late Miocene.

The result of recent seismic experiments across the eastern Anatolia plateau and the northernmost Arabian plate, combined with tomographic models of regional seismic velocity and attenuation, have definitively shown that most of the plateau is lacking mantle lithosphere and that it is supported by hot asthenospheric mantle (Dilek, 2006). According to Dilek (2006), the absence of lithospheric mantle is interpreted to have resulted from break-off of northward-subducted slab beneath the east Anatolian accretionary prism. The extensive

Pliocene-Quaternary volcanism in the region may be a consequence of melting of the lower crust above hot asthenosphere. Göğüş & Pysklywec (2008), using a computational geodynamic model, tested whether the geological and geophysical data are consistent with delamination of the mantle lithosphere.

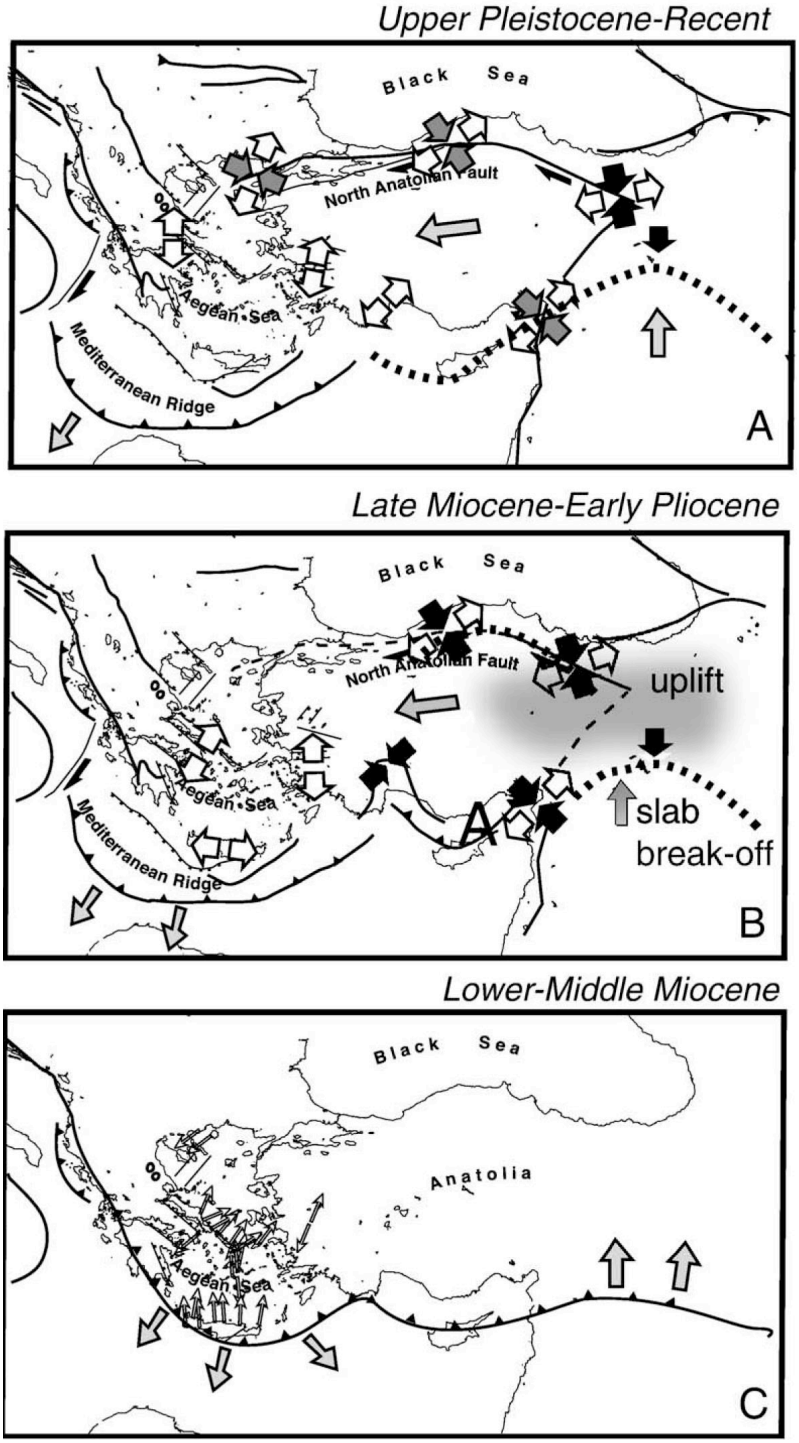

Fig. 1.25 – Tectonic evolution of the Anatolia-Aegean region after to the formation of the NAF. Shadow area represents the uplifted region of the Anatolian Plateau. Dashed line indicates the broken slab (Faccenna et al., 2006).

They proposed that all the primary tectonic anomalies for eastern Anatolian plateau uplift and heating, but also the presence of synconvergent crustal extension, may be interpreted as the coupled response of the crust to active underlying mantle dynamics during plate collision. They conducted a series of experiments with variable rates of imposed convergence of delaminated slab and with a higher yield strength of the mantle lithosphere. Fig. 1.26 shows the evolution of this model. The model shows that first the mantle lithosphere is delaminating from the crust, exposing a Moho width of 300 km ca. The detachment and/or break-off of this mantle lithosphere slab follows. In the latest stage the Eurasian mantle lithosphere undergoes a much more subducted delamination as it is eroded by the mantle flow. This geodynamic experiment demonstrates that the delamination causes surface uplift as a result of the isostatic and dynamic effects of lithospheric removal and possibly renconciles the high heat flow and volcanism that occur across eastern Anatolia.

The exact dynamics of uplift in the eastern Anatolian plateau are still debated, but it is fairly obviously that both crustal evolution and mantle dynamics played a significant role in the eastern Mediterranean region during the Late Tertiary (Dilek & Whitney, 2000). It is commonly accepted that the plateau that the plateau was formed some time in the Middle Miocene, following the terminal collision between Arabia-Eurasia and slab break-off. Subsequent removal of the lithospheric mantle (lithospheric delamination) beneath eastern Anatolia caused asthenospheric upwelling and extensive melting, leading to regional uplift and the ensuing high mean elevation of the Turkish-Iranian plateau.

A Miocene uplift for the plateau is also supported by Cosentino et al. (2012), this work-based on nannofossil, ostracod, and planktic foraminifera

biostratigraphy of the Başyayla section within the Mut and Köselerli Formations in the central Anatolian Plateau indicates a Tortonian age for marine sediments unconformably capping basement rocks at ca. 2 km elevation.

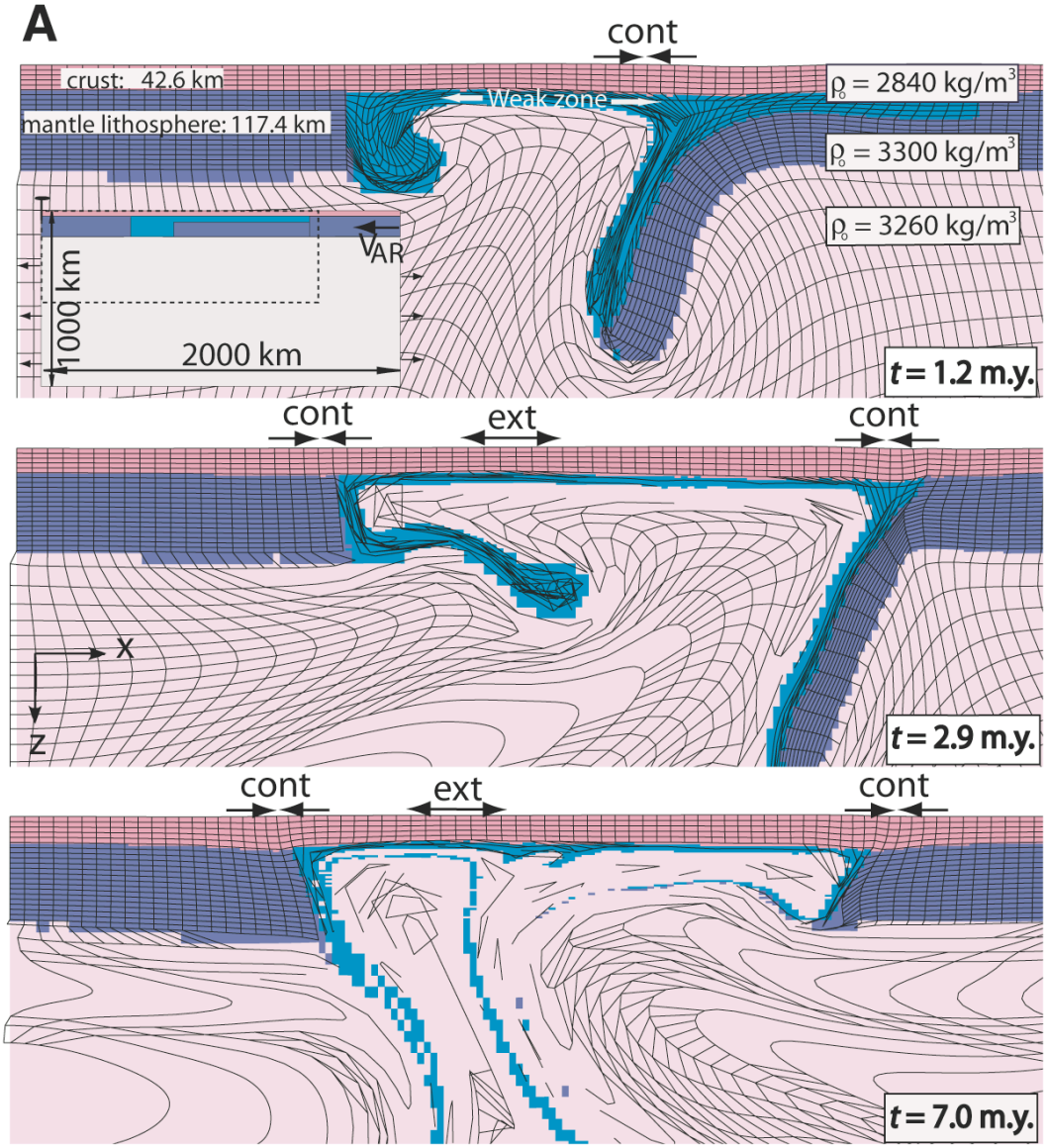

Fig. 1.26 – Progressive evolution of mantle lithosphere delamination for eastern Anatolia (Göğüş & Pysklywec, 2008).

The Anatolian Plateau-Caucasus-Caspian region is an area of complex structure accompanied by large variations in seismic wave velocities (Gök et al., 2009). Such region shows considerable spatial variability in travel times and phase propagation. Regional phase variations have been documented by a

number of a studies (e.g., Kadinsky-Cade et al., 1981; Rodgers et al., 1997; Gök et al., 2003) showing that Lg waves is blocked by both the Black Sea and south Caspian basins, and Sn does propagate through the cold and stable lithosphere of the south Caspian and Black Sea basins (Rodgers et al., 1997, Sandvol et al., 2001, Gök et al., 2003). Recentely Gök et al. (2009), to better constrain shear wave velocity model for the region, conducted a study based on the combination surface waves (SW) with receiver functions (RF). They used all available broad-band stations in the vast region showing in Fig. 1.27.

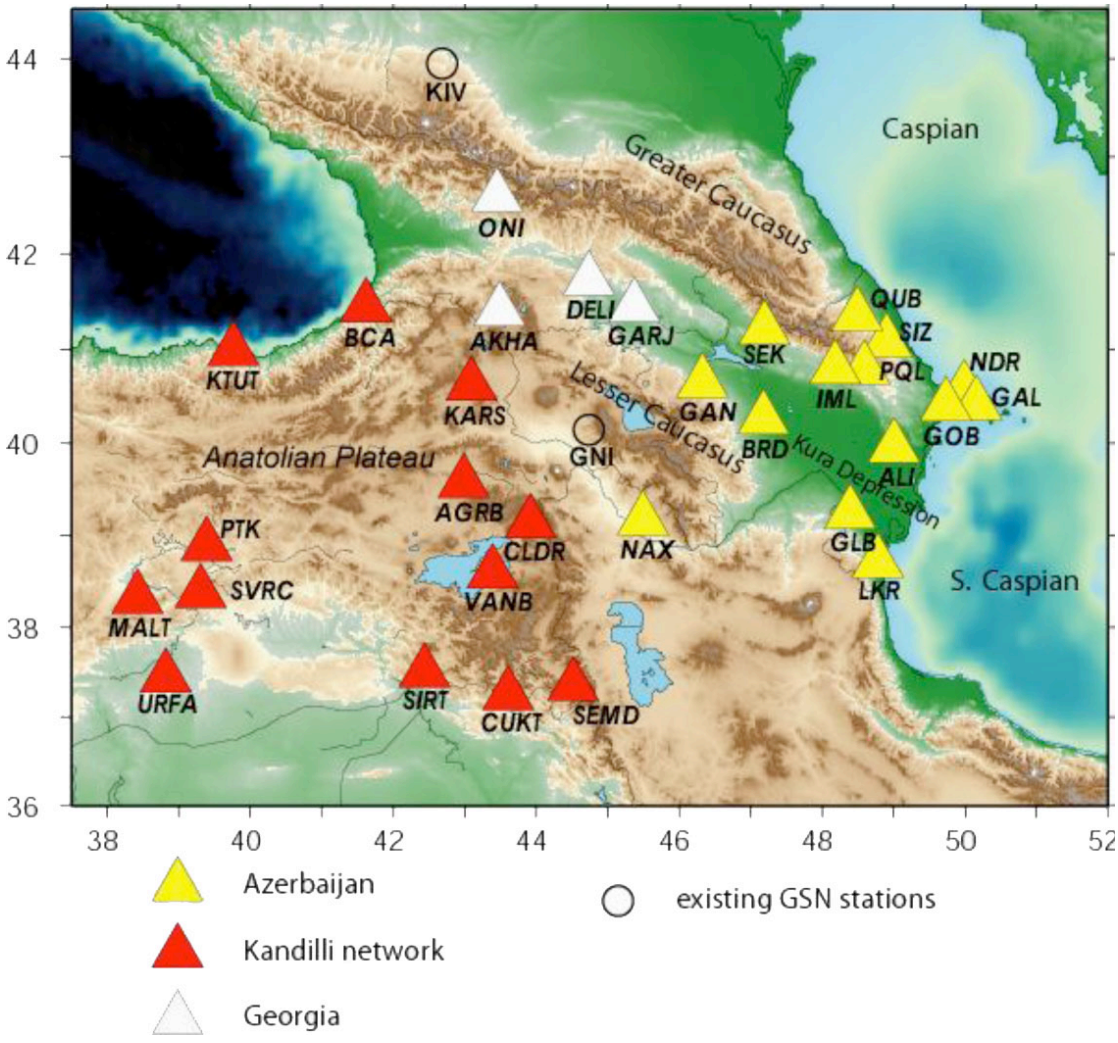

Fig. 1.27 – Station used for study conducted by Gök et al., 2009. Station are color-coled with their belonging countries (Gök et al., 2009).

The most important result of this study can be summarized as follows: the Moho map (Fig. 1.28) shows that the Moho is deepest in the Lesser Caucasus region and shallowest in the Arabian Plate. The resulting crustal thickness is at odds with several simplistic renditions (see, for example, Fig. 1.23). Average crustal thickness in the Anatolian Plateau is 42 km. The Lesser Caucasus in the border region between Turkey, Georgia and Armenia has the thickest crust in the region (ca. 52 km). Crustal thickness of the Arabian plate is around 35 km and the Greater Caucasus is similar to the Anatolian Plateau (ca. 42 km).

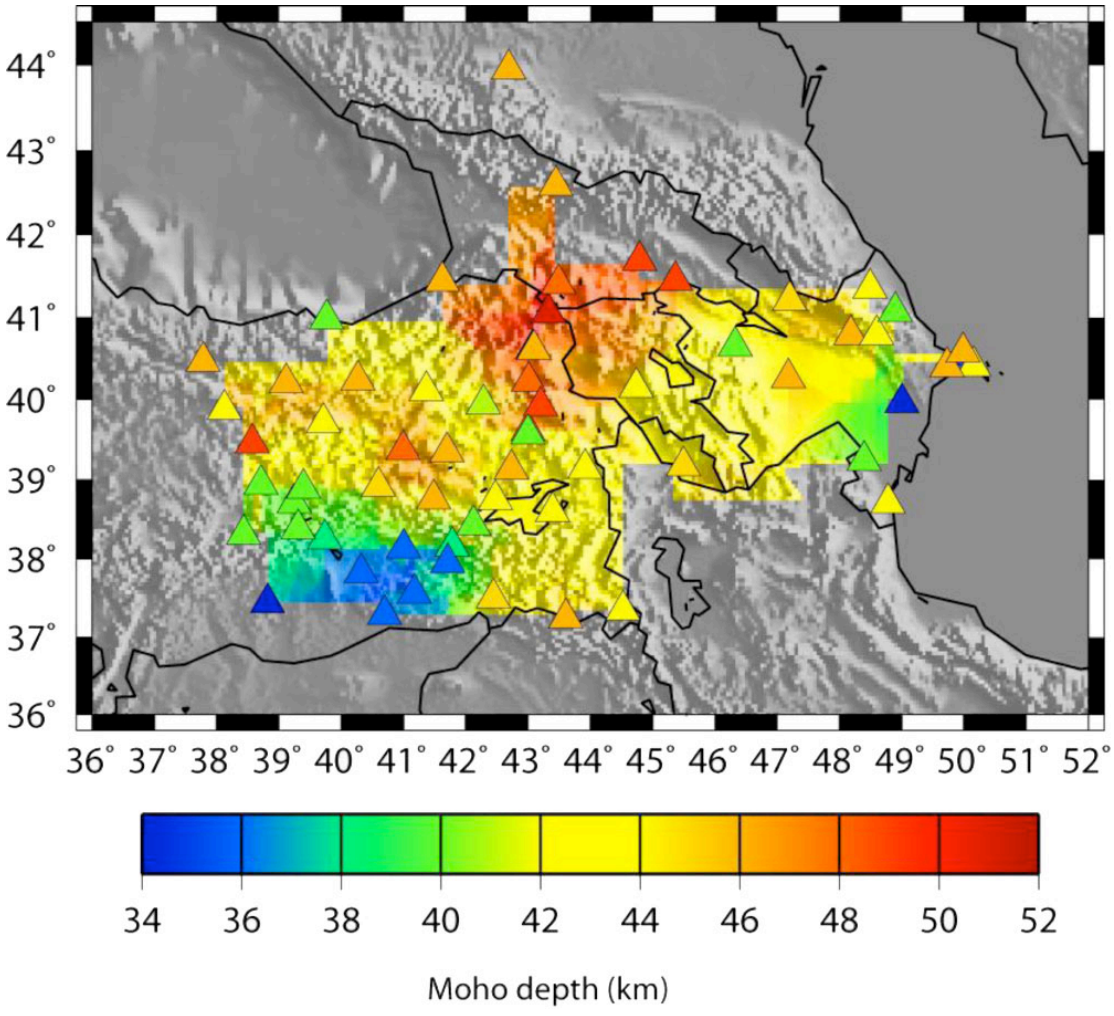

Fig. 1.28 – Moho depth in the Anatolian Plateau-Caucasus-Caspian region (Gök et al., 2009).

Chapter Two

FAR-FIELD TECTONIC EFFECTS OF THE ARABIA-EURASIA COLLISION AND THE INCEPTION OF THE NORTH ANATOLIAN FAULT SYSTEMS*

*manuscript currently under review

Far-field tectonic effects of the Arabia-Eurasia collision and the inception of the North Anatolian Fault system

Irene Albino[1], William Cavazza[1], Massimiliano Zattin[2], Aral I. Okay[3], Shota Adamia[4], and Nino Sadradze[5]

[1]*Department of Biological, Geological and Environmental Sciences, University of Bologna, Piazza di Porta San Donato 1, 40126 Bologna, Italy (E-mail: william.cavazza@unibo.it)*
[2]*Department of Geosciences, University of Padua, Via Gradenigo 6, 35131 Padua, Italy (massimiliano.zattin@unipd.it)*
[3]*Istanbul Technical University, Eurasia Institute of Earth Sciences, Maslak 34469, İstanbul, Turkey (okay@itu.edu.tr)*
[4]*Institute of Geophysics, 1 M. Alexidze str., 0193 Tbilisi, Georgia (sh_adamia@hotmail.com)*
[5]*Geological Institute, 1/9 M. Alexidze str., 0193 Tbilisi, Georgia (nino.sadradze@gmail.com)*

2.1 ABSTRACT

During the Middle Miocene a discrete episode of rapid exhumation occurred synchronously along the Bitlis suture zone between Arabia and Eurasia (SE Anatolia) and along the southern coast of the eastern Black Sea (NE Turkey, E Georgia), ca. 200 km to the north. Based on thermochronological, stratigraphic, geophysical, and geodetic data, we argue that such exhumation occurred as a far-field effect of the Arabia-Eurasia indentation, when collision-related strain focused preferentially along the rheological boundary between the multideformed continental lithosphere of NE Anatolia and the strong (quasi) oceanic lithosphere of the eastern Black Sea.

Rapid mid-Miocene exhumation along the southern coast of the eastern Black Sea conflicts with the absence of a significant level of seismicity in the area, thus pointing to a change of tectonic regime. A two-stage Neogene evolution for the eastern Anatolian and Transcaucasian regions is thus proposed: (1) initially, tectonic stresses related to the Arabia-Eurasia collision were transmitted over a wide area and concentrated along the coast of the eastern Black Sea and in the Greater Caucasus, inducing significant shortening and exhumation; (2) since late Middle Miocene time coherent westward motion of Anatolia and the corresponding activation of the North and Eastern Anatolian Fault systems have partitioned tectonic stresses differently, decoupling the eastern Black Sea from the stress field related to the Arabia-Eurasia collision.

2.2 INTRODUCTION

The Bitlis-Zagros orogenic belt of western Asia and the related wide area of deformation within the European foreland to the north (Fig. 2.1) are regarded as one of the best examples of ongoing continental collision in the world. Present-day reduction of surface area within the collision zone is estimated at 31 x 10^3 km^2/My (Reilinger et al., 2006). Most of the decrease in surface area is being accommodated by coherent lateral transport of Anatolia out of the collision zone (ca. 70%) and by shortening along the Bitlis-Zagros and Greater Caucasus orogenic wedges (ca. 15%). The remaining decrease in surface area is distributed across the Anatolian-Iranian plateau and the Lesser Caucasus (Fig. 2.2).

The age of the initial collision between Arabia and Eurasia has been the topic of much debate, with estimates of Late Cretaceous (Hall, 1976; Berberian and King, 1981; Alavi, 1994), Late Eocene-Oligocene (35–25 Ma, Jolivet and Faccenna, 2000; Agard et al., 2005; Allen and Armstrong, 2008), and Miocene (Şengör et al., 1985; Dewey et al., 1989; Yılmaz, 1993; Robertson et al., 2007). The only available low-temperature thermochronological dataset for the Bitlis collision front points to an episode of fast exhumation in the Middle Miocene (Okay et al., 2010).

In this paper, the first low-temperature thermochronological dataset for the Eurasian foreland north of the Bitlis collision zone suggests that the tectonic stresses related to the Arabian indentation were transmitted efficiently over large distances, focusing preferentially at rheological discontinuities along the eastern Black Sea coast and in the Caucasus. Since the late Middle Miocene a new tectonic regime is active as the westward translation of Anatolia is accommodating most of the Arabia-Eurasia convergence, thus precluding efficient northward stress transfer.

2.3 GEOLOGICAL SETTING

The study area represents the region of maximum indentation between Arabia and Eurasia (Fig. 1). From north to south, four major geological provinces are present: (i) the eastern Black Sea (EBS), (ii) the eastern Pontides (EP), (iii) the Anatolide-Tauride block (ATB), and (iv) the Arabian platform (AP).

(i) The more than 2,000 m deep EBS is partly floored by quasi-oceanic crust and represents the remnant of a composite Paleocene-Middle Eocene back-arc basin which developed on the Eurasian upper plate during north-dipping subduction of the Neotethys (e.g., Spadini et al., 1997; Stampfli and Borel, 2004).

(ii) The EP are the easternmost segment of a west-east-trending composite mountain belt traceable for more than 1,200 km from Thrace to the Adjara-Trialeti region of the Lesser Caucasus of Georgia (Fig. 2.1). The EP are part of the Sakarya Zone, a continental fragment of Laurasian affinity (Okay and Tüysüz, 1999; Cavazza et al., 2011).

(iii) The ATB forms the bulk of southern Turkey and can be traced to the east in Transcaucasia and Iran (Fig. 1). In contrast to the Pontides, the ATB shows a stratigraphy similar to the Arabian platform (Okay and Tüysüz, 1999). The Paleogene İzmir-Ankara-Erzincan suture marks the boundary between the ATB and the Pontides to the north.

(iv) The southern portion of the study area is characterized by the Gondwanian terrains of the AP flexurally bent towards the Bitlis-Zagros orogenic front to the north.

2.4 APATITE FISSION-TRACK DATA AND THERMAL MODELING

We collected samples for apatite fission-track (AFT) analysis across a wide swath of territory from the eastern Pontides and Adjara-Trialeti region to the north to the Bitlis collision zone to the south. The samples were taken from a variety or rock types, comprising Cretaceous and Paleogene granitoids, gneisses and metasandstone of the Bitlis and Pütürge massifs, and deeply buried Paleogene sandstones (Table 2.1, data repository). Very few localities were suitable for sampling in the eastern Anatolian Plateau since most of this region is covered by a thick pile of Plio-Quaternary volcanics and volcaniclastics. Procedures for sample preparation and analysis are those described in Zattin et al. (2000). Apatite grains from sixty samples were sent for irradiation. However, only twenty-six samples yielded apatite grains suitable for fission-track analysis.

Despite the lithological and age diversity, AFT results have a consistent geographic distribution, with younger ages (18-12 Ma; early-middle Miocene) in the Bitlis orogen and in the eastermost Pontides along the Black Sea, and Paleogene ages in the Anatolian plateau and Adjara-Trialeti region (Table 1, Fig. 3). There is no relationship between AFT ages and sample elevations.

Modeling on samples containing a statistically significant number of confined tracks constrained further the thermochronological evolution of the study area (Fig. 2.4). Sample TU274 (Late Cretaceous granodioritic body of the eastern Pontides magmatic arc) shows a phase of fast cooling (average cooling rate ca. 22°C/My) between ca. 16 and 14 Ma. Considering a geothermal gradient of 25-30°C/km, based on heat flow (Tezcan, 1995) and the depth of the Curie point in eastern Anatolia (Aydın et al., 2005), the average exhumation rate in the eastermost Pontides during this period of cooling is 0.7-0.9 km/My. Cooling/exhumation in the eastern Pontides

mirrors the evolution of the Bitlis-Pütürge massif along the Arabia-Eurasia collision zone where sample TU149 (Pan-African augen gneiss) shows a rapid increase in exhumation at ca. 12 Ma (Fig. 2.4; see also Okay et al., 2010, p. 37).

Sample TU255 is an early Oligocene sandstone turbidite at the base of the Muş basin, a foreland basin located north of the Bitlis suture and associated with northward subduction of the Arabian plate (Hüsing et al., 2009). Following deposition, this sample was progressively buried and entered the PAZ at about 23 Ma. A rapid phase of cooling/exhumation began at 19 Ma (late early Miocene), likely the result of the progressive incorporation of the basin southern margin into the growing Bitlis orogenic wedge. Post-depositional burial of sample TU255 was not deep enough to completely erase the thermochronological record of the sediment source rocks, showing a Late Cretaceous-Paleogene episode of cooling/exhumation correlatable with widespread deformation in the area related to the closure of the İzmir-Ankara-Erzincan ocean (Okay and Tüysüz, 1999).

Sample TU279 (Eocene granodiorite intruding volcanics/volcaniclastics in the Adjara-Trialeti zone of western Georgia) shows very rapid cooling at 36-35 Ma (latest Eocene), in line with thermochronologic data from the western Greater Caucasus (Vincent et al., 2011). The sample then underwent progressive heating during most of the Miocene and cooled definitively outside the apatite partial annealing zone (PAZ; 120-60°C) in the Late Miocene, likely the result of orogenic-wedge dynamics in the Adjara-Trialeti northward-verging nappe stack facing the flexural Rioni foreland basin to the north.

2.5 DISCUSSION AND CONCLUSIONS

Our thermochronologic dataset shows that exhumation of Cretaceous and Eocene granitoids along the easternmost Pontides occurred in the Middle Miocene. Other independent evidence supports the notion of a discrete and relatively rapid mid-Miocene episode of exhumation/erosion in the region: (i) fission-track data from the composite Kackar batholith (Cretaceous-Late Eocene) immediately west of our study area also indicate significant Miocene cooling (R. Jonckheere, pers. comm., 2012); (ii) a marked angular unconformity between Early Miocene continental deposits and the flat-lying Late Miocene volcanics of the Erzurum-Kars plateau (Akdeniz, 2002; Konak and Hakyemez, 2008); (iii) proprietary seismic stratigraphic data show middle-late Miocene clastic wedges generically prograding northwestward across the eastern Black Sea (e.g. Menlikli et al., 2009).

The previously unrecognized exhumation/erosion episode along the Black Sea coast documented here mirrors the age of maximum tectonic coupling between the Eurasian and Arabian plates along the 2,400 km long Bitlis-Zagros suture zone, ca. 250 km to the south: exhumation ages along the easternmost Pontides are virtually identical to those obtained by Okay et al. (2010) along the Bitlis suture. We argue that tectonic stresses generated along the Bitlis collision zone were transmitted northward across eastern Anatolia and focused at the rheological boundary between the Anatolian continental lithosphere and the (quasi)oceanic lithosphere of the Black Sea. Mechanical coupling of a collisional orogen and its forelands can induce far-field tectonic stresses and significant compressional structures at distances > 1,500 km from a collision front (e.g. Ziegler et al., 1995; Dickerson, 2003). Localization of compressional deformations far from the collision zone is controlled by spatial and temporal strength variations of the lithosphere (Ziegler et al., 1998; Cloetingh et al.,

2010). Passive continental margins -like the Black Sea coast of the study area- mark the largest compositional and rheological contrast within the lithosphere (Niu et al., 2003) and are, therefore, preferential loci of deformation.

Cooling at temperatures below the apatite PAZ in the Anatolian Plateau and in the Lesser Caucasus (Adjara-Trialeti region of western Georgia) occurred instead in the Paleogene (with a cluster of ages in the Middle-Late Eocene; Fig. 3; Table 1), coevally with the development of the İzmir-Ankara-Erzincan suture (e.g., Okay and Tüysüz, 1999). The successive uplift of the Anatolian Plateau did not exhume a new partial annealing zone and thus is not recorded by the apatite fission-track record.

The GPS-derived velocity field for eastern Turkey, Transcaucasia, and NW Iran (Fig. 2.2) shows that continental material north of the Bitlis suture appears to move around the oceanic lithosphere of the eastern Black Sea. Vectors in eastern Anatolia point coherently to the west, defining the apparent "extrusion" of the Anatolian plate, whereas east of the Karliova triple junction (KTJ) they show a progressive rotation to the east (McClusky et al., 2000; Reilinger et al., 2006). Similarly, the two areas are characterized by different deformations patterns. West of the KTJ the Anatolian plate is moving as a single entity bounded by the North and East Anatolian Fault systems, whereas east of it deformation is distributed along a complex system of strike-slip and thrust faults (Adamia et al., 2011). The different deformation patterns can be explained by the different boundary conditions imposed on these two regions: westward motion of the Anatolian plate is favored by slab retreat along the Hellenic trench (Jolivet, 2001) whereas eastern Turkey and Transcaucasia are caught between the Bitlis collision zone and the rheologically stronger (quasi)oceanic crust of the Black Sea to the northwest and the Eurasian continental crust to the northeast.

The analysis of present-day crustal dynamics and the thermochronological data presented in this paper provide a comparison between short- and long-term deformation patterns for the entire eastern Anatolian-Transcaucasian region. Two successive stages of Neogene deformation of the northwestern foreland of the Arabia-Eurasia collision zone can be inferred. (i) During the Early and Middle Miocene continental deformation was concentrated along the Arabia-Eurasia (Bitlis) collision zone but tectonic stress was transferred northward across eastern Anatolia, focusing along the eastern Black Sea continent-ocean rheological transition. The Black Sea (quasi)oceanic lithosphere is fundamentally stronger than the polydeformed continental lithosphere to the south and therefore represented a "backstop" resisting deformation and deviating the impinging continental lithosphere (McClusky et al., 2000). (ii) Since late Middle Miocene time the westward translation of Anatolia and the activation of the North and Eastern Anatolian Fault systems have reduced efficient northward stress transfer. In this new tectonic regime –still active today- most of the Arabia-Eurasia convergence has been accomodated by the westward motion of Anatolia whereas the eastern Pontides have been mechanically decoupled from the foreland of the Bitlis collision zone, as shown by the absence of significant seismicity in the area (Fig. 2.2). The following wholesome topographic uplift of the Anatolian Plateau has not exhumed a new PAZ and thus is not recorded by the apatite fission tracks.

2.6 ACKNOWLEDGMENTS

W. Cavazza and I. Albino were supported by a grant from MIUR (Italian Ministry of University and Research). A. I. Okay was supported by a grant from TÜBA (The Turkish Academy of Sciences).

2.7 REFERENCES CITED (Chapter Two)

Adamia, S., Zakariadze, G., Chkhotua, T., Sadradze, N., Tsereteli, N., Chabukian, A., Gventsadze, A., 2011, Geology of the Caucasus: a review: Turkish Journal of Earth Sciences, v. 20, p. 489-544.

Agard, P., Omrani, J., Jolivet, L., and Mouthereau, F., 2005, Convergence history across Zagros (Iran): Constraints from collisional an earlier deformation: International Journal of Earth Sciences, v. 94, p. 401–419.

Akdeniz, N., 2002, Kars sheet - 1:500,000 Geological Map of Turkey: General Directorate of Mineral Research and Exploration, Ankara (Turkey).

Alavi, M., 1994, Tectonics of the Zagros orogenic belt of Iran - New data and interpretations: Tectonophysics, v. 229, p. 211-238.

Allen, M.B., and Armstrong, H.A., 2008, Arabia–Eurasia collision and the forcing of mid-Cenozoic global cooling: Palaeogeography Palaeoclimatology Palaeoecology, v. 265, 52–58.

Aydın, İ., Karat, H.İ., and Koçak, A., 2005, Curie-point depth map of Turkey: Geophysical Journal International, v. 162, p. 633–640.

Berberian, M., and King, G., 1981, Toward a paleogeography and tectonic evolution of Iran: Canadian Journal of Earth Sciences, v. 18, p. 210-265.

Cavazza, W., Federici, I., Okay, A.I., and Zattin, M., 2011, Pre-Cenozoic amalgamation of the İstanbul and Sakarya terranes (NW Turkey) – evidence

from low-temperature thermochronology: Geological Magazine, v. 149, p. 133-140.

Cloetingh, S.A.P.L., et al. (18 authors), 2010, Lithosphere tectonics and thermo-mechanical properties: An integrated modelling approach for Enhanced Geothermal Systems exploration in Europe: Earth-Science Reviews, v. 102, p. 159-206.

Copley, A., and Jackson, J., 2006, Active tectonics of the Turkish-Iranian Plateau: Tectonics, v. 25, TC6006.

Dewey, J.F., Helman, M.L., Turco, E., Hutton, D.H.W., and Knott, S.D., 1989, Kinematics of the western Mediterranean. In: Coward, M.P., Dietrich, D., Park, R.G. (Eds.), Alpine Tectonics. Geological Society, London, Special Publication, pp. 265–283.

Dickerson, P.W., 2003, Intraplate mountain building in response to continent-continent collision - the Ancestral Rocky Mountains (North America) and inferences drawn from the Tien Shan (Central Asia): Tectonophysics, v. 365, p. 129-142.

Donelick, R.A., Ketcham, R.A., and Carlson,W.D., 1999, Variability of apatite fission-track annealing kinetics: II. Crystallographic orientation effects: American Mineralogist, v. 84, p. 1224-1234.

Ehlers, T.A., Chaudhri, T., Kumar, S., Fuller, C.W., Willett, S.D., Ketcham, R.A., Brandon, M.T., Belton, D.X., Kohn, B.P., Gleadow, A.J.W., Dunai, T.J., Fu, F.Q., 2005, Computational tools for low-temperature thermochronometer interpretation: Reviews in Mineralogy & Geochemistry, v. 58, p. 589-622.

Hall, R., 1976, Ophiolite emplacement and the evolution of the Taurus suture zone, southeastern Turkey: Geological Society America Bulletin, v. 87, p. 1078-1088.

Hüsing, S.K., Zachariasse, W.J., Van Hinsbergen, D.J.J., Krijgsman, W., Inceöz, M., Harzhauser, M., Mandic, O. and Kroh, A. (2009). Oligo-Miocene foreland basin evolution in SE Anatolia: implications for the closure of the eastern Tethys gateway: Geological Society of London Special Publication, v. 311, p. 107-132.

Jolivet, L., 2001, A comparison of geodetic and finite strain pattern in the Aegean, geodynamic implications: Earth and Planetary Science Letters, v. 187, p. 95-104.

Jolivet, L., and Faccenna, C., 2000, Mediterranean extension and the Africa-Eurasia collision: Tectonics, v. 19, p. 1095-1106.

Ketcham, R.A., Donelick, R.A., and Carlson, W.D., 1999, Variability of apatite fission-track annealing kinetics: III. Extrapolation to geological time scales: American Mineralogist, v. 84, p. 1235-1255.

Konak, N., and Hakyemez, H.Y., 2008, Tortum G-48 sheet - 1:100,000 Geological Map of Turkey: General Directorate of Mineral Research and Exploration, Ankara (Turkey).

McClusky, S., et al., 2000, Global Positioning System constraints on plate kinematics and dynamics in the eastern Mediterranean and Caucasus: Journal of Geophysical Research, v. 105, p. 5695– 5719.

Menlikli, C.T., İspir, H., Apaydin, B., and Bengü, E., 2009, Western Black Sea basin petroleum systems and play concepts: 2nd International Symposium on the Geology of the Black Sea Region Abstract Book, p. 129.

Niu, Y., O'Hara, M.J., and Pearce, J.A., 2003, Initiation of subduction zones as a consequence of lateral compositional buoyancy contrast within the lithosphere: a petrological perspective: Journal of Petrology, v. 44, p. 851-866.

Okay, A.I., Tansel, I., and Tüysüz, O., 2001, Obduction, subduction and collision as reflected in the Upper Cretaceous-Lower Eocene sedimentary record of western Turkey: Geological Magazine, v. 138, p. 117-142.

Okay, A.I. & Tüysüz, O., 1999, Tethyan sutures of northern Turkey: *in* Durand, B., Jolivet, L., Horváth, F., and Séranne, M., eds., The Mediterranean Basins: Tertiary extension within the Alpine orogen: Geological Society of London Special Publication 156, p. 475-515.

Okay, A.I., Zattin, M., and Cavazza, W., 2010, Apatite fission-track data for the Miocene Arabia-Eurasia collision: Geology, v. 38, p. 35–38.

Reilinger, R., McClusky, S., Vernant, P., Lawrence, S., Ergintav, S., Cakmak, R., Ozener, H., Kadirov, F., Guliev, I., Stepanyan, R., Nadariya, M., Hahubia, G., Mahmoud, S., Sakr, K., ArRajehi, A., Paradissis, D., Al-Aydrus, A., Prilepin, M., Guseva, T., Evren, E., Dmitrotsa, A., Filikov, S. V., Gomez, F., Al-Ghazzi, R., and Karam, G., 2006, GPS constraints on continental deformation in the Africa-Arabia-Eurasia continental collision zone and implications for the dynamics of plate interactions: Journal of Geophysical Research, v. 111, No. B5, B05411.

Robertson, A.H.F., Parlak, O., Rızaoğlu, T., Ünlügenç, Ü., İnan, N., Taslı, K., and Ustaömer, T., 2007, Tectonic evolution of the South Tethyan ocean: evidence from the Eastern Taurus Mountains (Elazığ region, SE Turkey), *in* Ries, A.C., Butler, R.W.H., and Graham, R.H., eds., Deformation of continental crust: Geological Society of London Special Publication 272, p. 231-270.

Şengör, A.M.C., Görür, N., and Şaroğlu, F., 1985, Strike-slip faulting and related basin formation in zones of tectonic escape: Turkey as a case study, *in* Biddle, K.D., and Christie-Blick, N., eds., Strike-slip deformation, basin formation and

sedimentation: Special Publication, Society of Economic Paleontologists and Mineralogists 17, p. 227-264 .

Sosson, M., Rolland, Y., Müller, C., Danelian, T., Melkonyan, R., Kekelia, S., Adamia, S., Babazadeh, V., Kangarli, T., Avagyan, A., Galoyan, G., and Mosar., J., 2010, Subductions, obduction and collision in the Lesser Caucasus (Armenia, Azerbaijan, Georgia), new insights: Geological Society of London Special Publications, v. 340, p. 329-352.

Spadini, G., Robinson, A., and Cloetingh, S., 1997. Thermo-mechanical modelling of Black Sea Basin formation, subsidence and sedimentation. In: Robinson, A. (Ed.), Regional and petroleum geology of the Black Sea and surrounding areas. Am. Assoc. Pet. Geol., Mem. 68, pp. 19– 38.

Stampfli, G.M. and Borel, G.D. 2004, The TRANSMED transects in space and time: constrains on the paleotectonic evolution of the Mediterranean domain. In: Cavazza, W., Roure F., Spakman, W., Stampfli, G.M. and Ziegler, P.A. (eds), The TRANSMED Atlas – The Mediterranean Region from Crust to Mantle. Springer, Berlin Heidelberg, 53–80 (see also Appendix 3).

Tezcan, A.K., 1995, Geothermal explorations and heat flow in Turkey, *in* Gupta, M.L., and Yamano, M., eds., Terrestrial Heat Flow and Geothermal Energy in Asia: Balkema Publishers, Rotterdam, p. 23–42.

Vincent, S.J., Carter, A., Lavrishchev, V.A., Rice, S.P., Barabadze, T.G., Hovius, N., 2011, The exhumation of the western Greater Caucasus: a thermochronometric study: Geological Magazine, v. 148, p. 1–21.

Yılmaz, Y., 1993, New evidence and model on the evolution of the southeast Anatolian orogen: Geological Society America Bulletin, v. 105, p. 252-271.

Zattin, M., Landuzzi, A., Picotti, V., and Zuffa, G.G., 2000, Discriminating between tectonic and sedimentary burial in a foredeep succession, Northern Apennines: Journal of the Geological Society London, v. 157, p. 629–633.

Ziegler, P.A., Cloetingh, S., van Wees, J.-D., 1995. Dynamics of intra-plate compressional deformation: the Alpine foreland and other examples. Tectonophysics 252, 7–59.

Ziegler, P.A., van Wees, J.-D., and Cloetingh, S., 1998, Mechanical controls on collision-related compressional intraplate deformation: Tectonophysics, v. 300, p. 103-129.

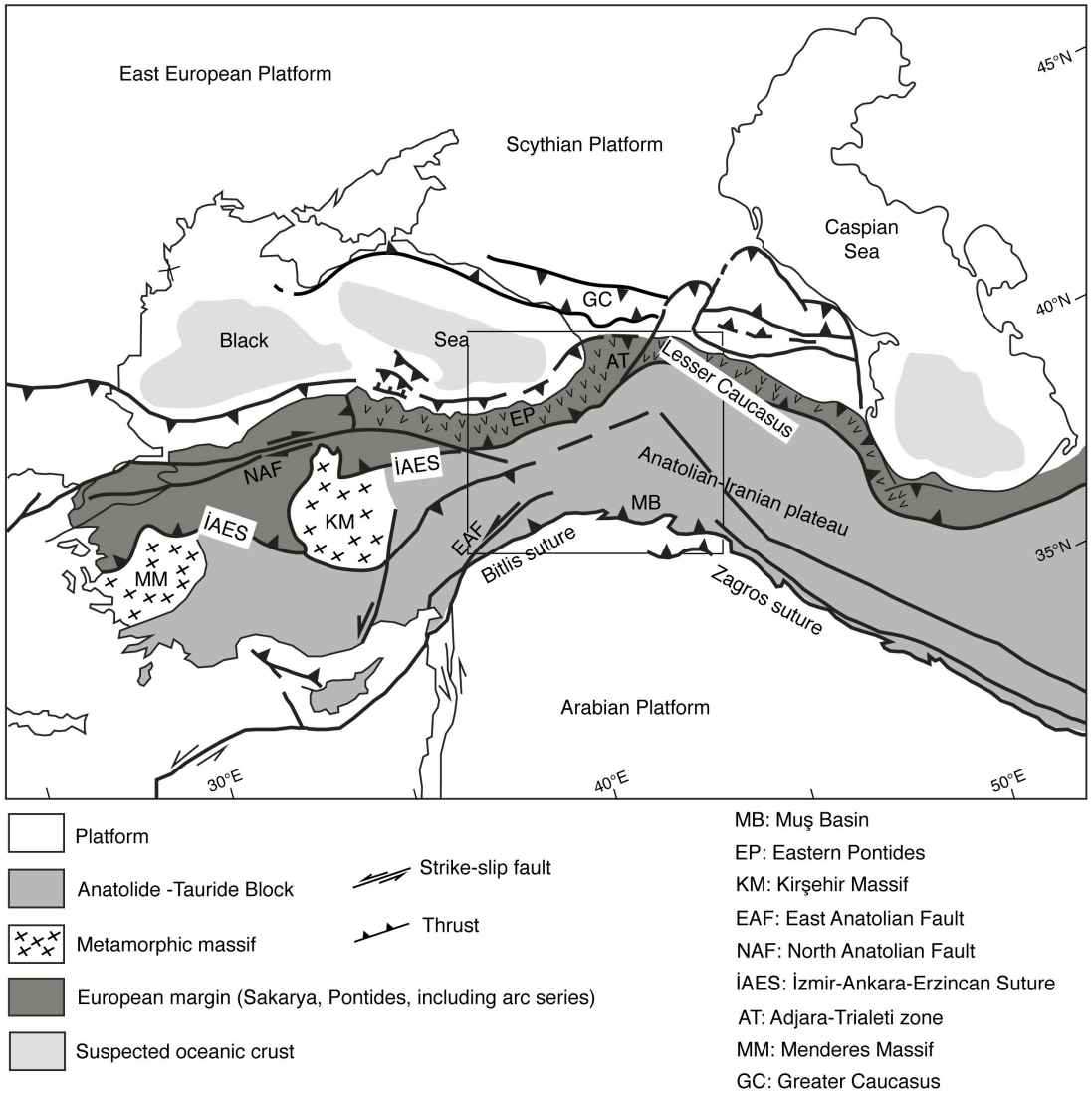

Figure 2.1 - Tectonic map of Asia Minor and Transcaucasia (modified from Sosson et al., 2010).

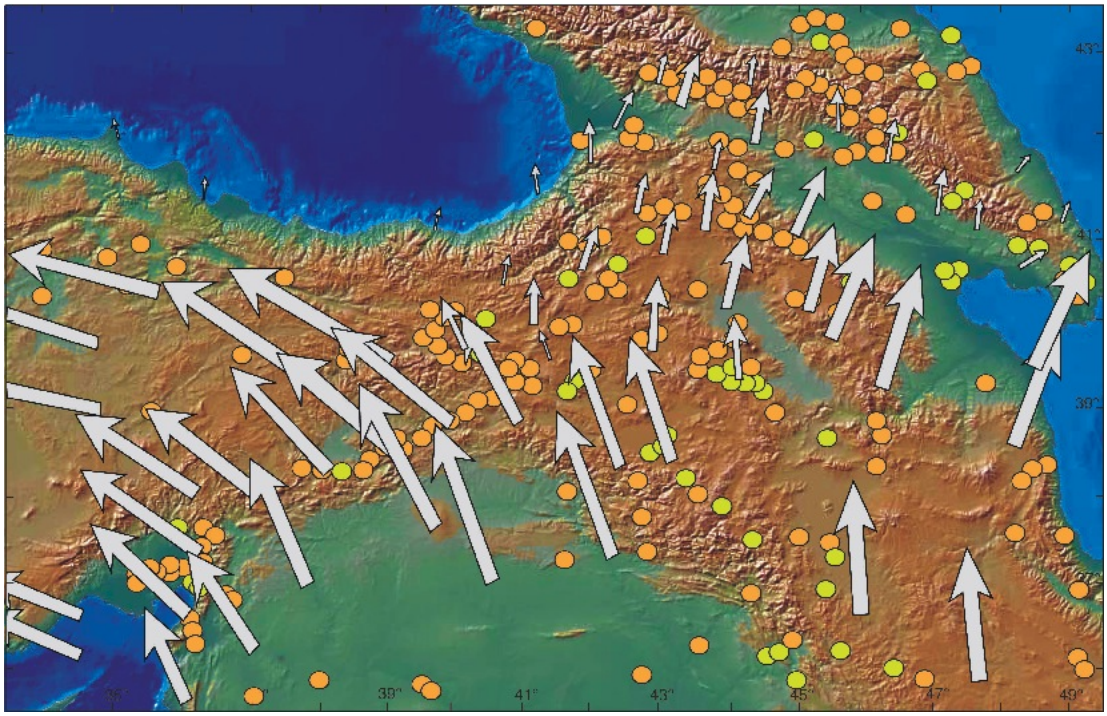

Figure 2.2 - Digital elevation model of the Eastern Mediterranean and the Middle East. The arrows indicate the GPS-derived velocities with respect to a stationary Eurasia (modified from Reilinger et al., 2006; Copley and Jackson, 2006); the dots indicate the epicenters of earthquakes M>4.8 (depth of hypocenters: orange dots 0-33 km; yellow dots: 33-70 km) (1973-2012 data from USGS/NEIC PDE on-line catalog).

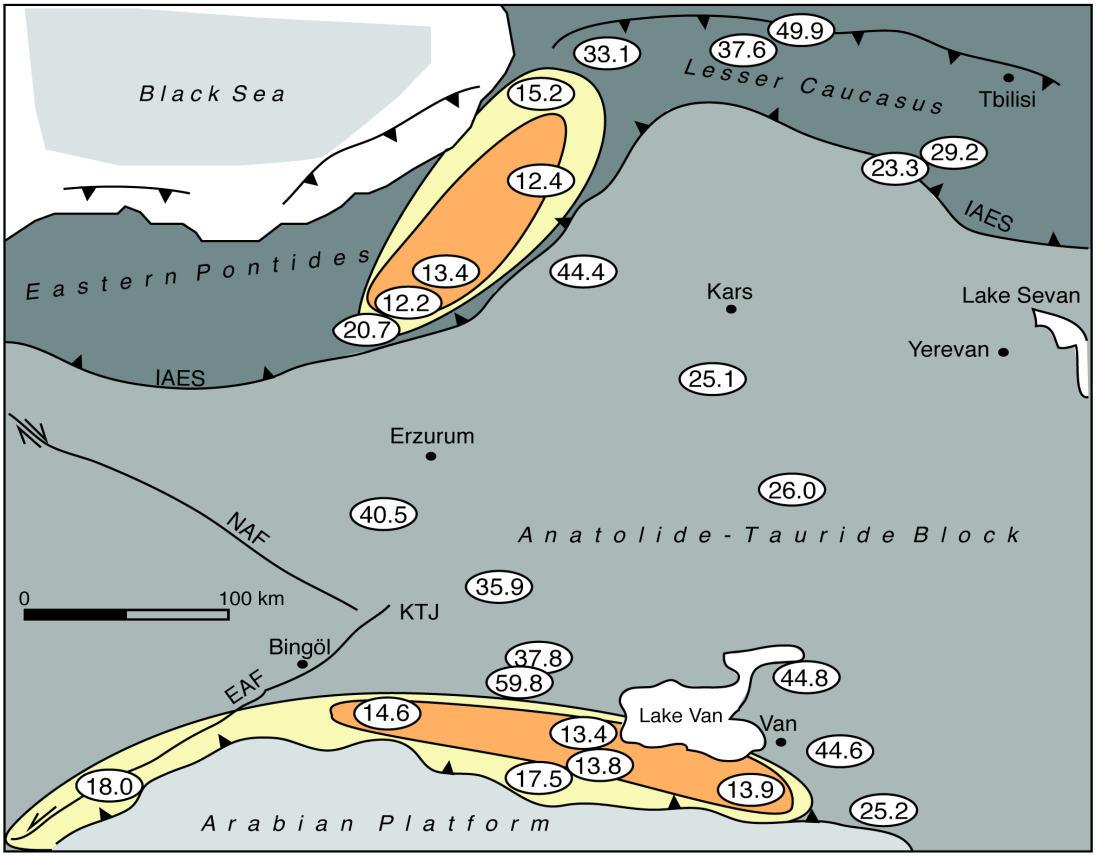

Figure 2.3 - Geographic distribution of apatite fission-track age. See Table 1 for complete dataset. Orange areas includes all FT ages between ca. 12 and 15 Ma; yellow areas those between ca. 15 and 20 Ma. NAF, North Anatolian Fault; EAF, East Anatolian Fault; IAES, Izmir-Ankara-Erzincan suture; KTJ, Karliova triple junction.

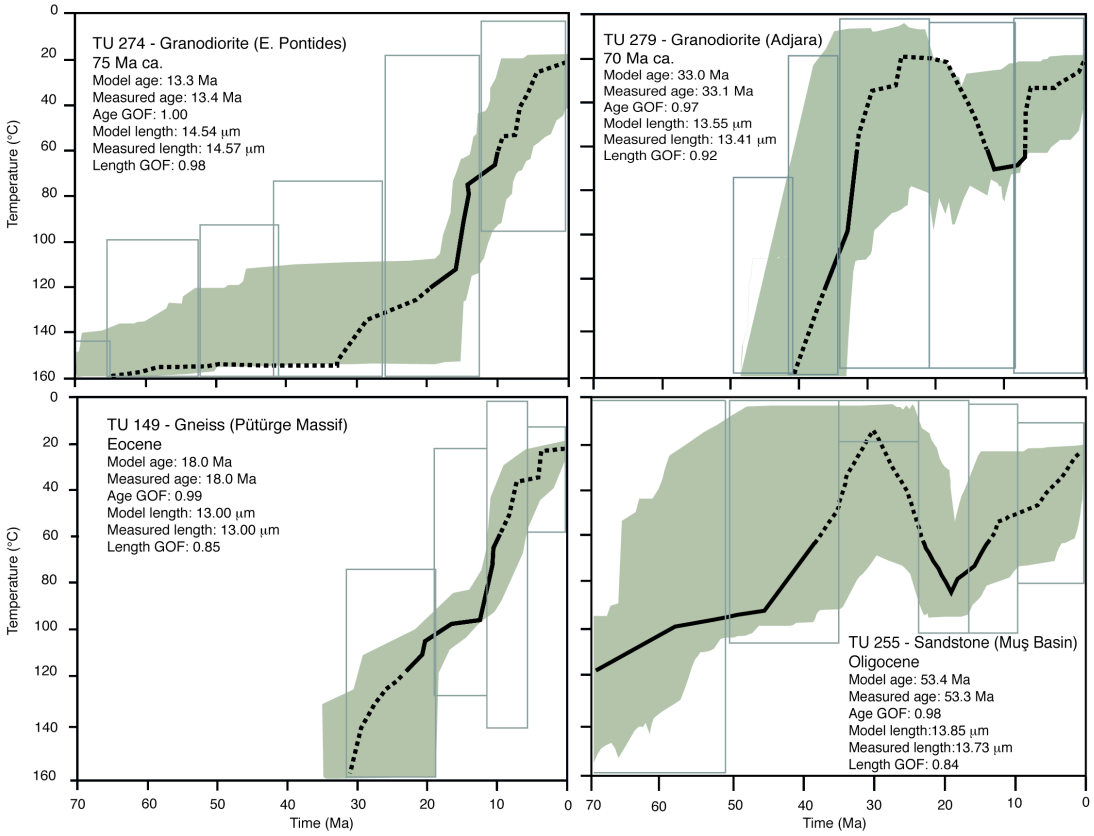

Figure 2.4 - Time-temperature paths obtained from inverse modelling of AFT data using the HeFTy program (Ehlers et al. 2005), which generates the possible T-t paths by a Monte Carlo algorithm. Predicted AFT data were calculated according to the Ketcham et al. (1999) annealing model and the Donelick et al. (1999) c-axis projection. Parameters (model and measured age, model and measured mean length) related to inverse modelling are reported. GOF (goodness-of-fit) values give an indication about the fit between observed and predicted data (values close to 1 are best). Shaded areas mark envelopes of statistically acceptable fit (GOF > 0.5) and the thick lines correspond to the most probable thermal histories. Thermal paths out of the partial annealing zone (dotted) are largely inferential as fission-track data cannot give reliable information out of this temperature range. Range and scale of X and Y axes are identical in all diagrams to facilitate comparison.

Table 1 - Apatite fission-track data.

Sample number	Coordinates (UTM)	Elevation (m)	Rock type	Age	No. of crystals	Spontaneous		Induced		$P(\chi)^2$	Dosimeter		Age (Ma) ± 1σ	MCTL (μm) ± std. err.	Std. dev.	Tracks measured
						ρ_s	N_s	ρ_i	N_i		ρ_d	N_d				
TU250	37S 0676940 4368287	1933	Sandstone	Eocene	20	2,10	107	12,60	640	52,30	14,1	4679	40.5±5.2	-	-	-
TU253	37S 0732079 4344155	1652	Sandstone	Paleocene	9	1,36	33	9,37	227	70,39	14,20	4237	35.9±6.9	12.72	1,84	13
TU254	37S 0754492 4344155	1458	Sandstone	Oligocene	6	1,31	35	7,30	194	59,76	14,00	4798	37.8±10.7	-	-	-
TU255	37S 0750864 4293994	1339	Sandstone	Oligocene	17	1,98	122	6,49	481	87,12	14,30	4679	59.8±2.1	13.85	1,29	35
TU256	38S 0382766 4246434	1948	Sandstone	Oligocene	17	1,23	25	4,27	141	53,02	15,00	4376	44.6±10.0	-	-	-
TU260	38S 0361398 4337228	1743	Sandstone	Oligocene	22	2,28	39	11,96	204	95,57	14,00	4659	44.8±8.1	-	-	-
TU264	38S 0370895 4384757	1862	Granite	Late Cretaceous	15	3,74	134	36,20	1295	100,00	15,00	4736	26.0±2.7	14.48	1,04	50
TU266	38T 0330734 4454167	1401	Sandstone	Eocene	20	2,21	129	34,30	1196	80,32	15,01	4568	25.0±2.8	13.60	0,70	8
TU267	38T 0662375 4513739	1086	Metadiorite	Hercynian basement	20	2,80	189	14,56	982	57,37	14,00	4978	44.4±3.0	-	-	-
TU273	37T 0743625 4761028	842	Granite	Late Cretaceous	18	2,26	179	16,30	1134	98,10	14,00	4823	12.4±2.6	11.91	0,93	5
TU274	37T 0743625 4761028	952	Granodiorite	Late Eocene	20	2,17	137	35,32	2226	86,66	13,30	4536	13.4±1.4	14.57	1,38	37
TU275	37T 0681167 4494619	1055	Granite	Eocene	20	1,65	51	14,25	662	80,24	14,00	4890	12.6±2.7	12.61	1,97	11
TU276	37T 0665263 4481103	1256	Granite	Eocene (?)	15	1,79	62	20,29	702	98,38	14,00	4653	20.7±2.9	11.36	1,39	5
TU278	38T 0374158 4658977	867	Granite	Paleocene	14	2,17	36	10,34	879	50,30	14,00	4459	46.9±5.2	-	-	-
TU279	38T 0260294 4641212	334	Granodiorite	Paleocene	17	4,99	262	32,72	1716	95,52	13,00	4438	33.1±2.7	13.41	1,43	50
TU281	37T 0747431 4607962	376	Diorite	Late Eocene (?)	8	1,73	37	19,14	409	99,19	10,01	4298	15.2±2.7	-	-	-
TU282	38T 0368846 4636796	813	Flysch	Paleocene	14	1,34	76	6,96	197	58,30	14,00	4432	37.5±5.6	-	-	-
TU284	38T 0444177 4570059	1047	Granite	Late Cretaceous	16	3,02	151	18,66	933	99,24	11,00	4765	29.2±4.0	12.23	0,48	21
TU285	38T 0445889 4568770	1187	Granite	Eocene (?)	20	4,82	375	34,77	2696	80,81	12,00	4678	23.3±1.7	11.70	1,29	6
TU136*	38S0251160 4260508	1642	Metasandstone	Paleozoic	20	0,72	40	0,89	496	100,00	0,90	4293	13.4±2.2	-	-	-
TU138*	38S0241967 4249698	1285	Gneiss	Precambrian	16	0,46	22	0,55	264	100,00	0,90	4281	13.8±3.1	-	-	-
TU140*	37S0753971 4234870	871	Sandstone	Paleocene/Eocene	4	5,14	43	4,84	405	91,10	0,90	4256	17.5±2.8	-	-	-
TU145*	37S0630748 4277901	1175	Metagranite	Precambrian	20	0,55	38	0,62	425	82,50	0,89	4219	14.6±2.5	-	-	-
TU149*	37S0476619 4240707	1395	Gneiss	Eocene	20	1,60	112	1,44	1006	87,00	0,88	4181	18.0±1.8	-	-	-
TU155*	38S0321648 4195176	1607	Sandstone	Eocene	20	0,88	53	1,18	711	65,10	1,01	4818	13.9±2.1	-	-	-
TU159*	38S0396240 4162747	1342	Sandstone	Eocene	6	0,53	14	0,39	102	75,40	1,00	4771	25.2±7.2	-	-	-

MCTL: mean confined track length. Central ages calculated using dosimeter glass CN5 and ζ-CN5=336.34±16.24 (analyst Irene Albino). ρ_s: spontaneous track densities (x 10^5 cm^{-2}) measured in internal mineral surfaces; N_s: total number of spontaneous tracks; ρi and ρ_d: induced and dosimeter track densities (x 10^6 cm^{-2}) on external mica detectors (g=0.5); N_i and N_d: total numbers of tracks; $P(\chi^2)$: probability of obtaining χ^2-value for ν degrees of freedom (where ν=number of crystals-1); a probability >5% is indicative of an homogenous population. Samples with a probability <5% have been analyzed with the binomial peak-fitting method. (*) Ages from Okay et al. (2010).

Chapter Three

PRELIMINARY DATA ON THE THERMOCHRONOLOGICAL EVOLUTION OF NORTHERN ARMENIA

3.1 INTRODUCTION

The Caucasian region and eastern Anatolia have been investigated by many authors who have established different stratigraphies and tectonic units. Complex political vicissitudes in the area have made geological comparison and streamlining virtually impossible. Nevertheless, at least from the 27th Session of the International Geological Congress in Moscow (1984), it was generally recognized that the eastern Pontides of Turkey are equivalent to the similarly much deformed magmatic arc of Transcaucasia. On a broader scale, the Pontic geologic structures extend continuously from Bulgaria in the west to the Lesser Caucasus region in the east (e.g., Okay, 2008). A Mesozoic magmatic arc, which originated during northward subduction of the Tethyan ocean floor (see Chapter 1), can be traced confidently to northern Armenia and western Azerbaijan where equivalent volcanic, subvolcanic, and intrusive units crop out extensively (e.g., Rolland et al., 2009; Sosson et al., 2010).

Furthermore, the İzmir-Ankara-Erzincan (IAES) suture can be traced without break to the east of Lake Sevan. However, the identification of the exact continuation (Figs., 3.1, 3.2) of the Mesozoic magmatic arc and the IAES are problematic in Iran due to the thick pile of volcano-sedimentary rocks Plio-Quaternary age that cover these regions (Adamia et al., 1981).

In this chapter data from apatite fission-track of samples collected in northwestern Armenia are presented. Such data will be eventually integrated with other fission-tracks data being gathered in the area and in northwestern Azerbaijan. The results presented in this chapter can be discussed from the perspective of the framework interpretation outlined in Chapter 2 -where the data collected from the Anatolian Plateau, the Eastern Pontides and Georgia are

presented- but they are presented separately because of a different timing of field sampling/data acquisition and the ensuing different degree of confidence in data interpretation. Overall, the database will provide a more complete framework on which more accurate constraints on the syn-post collisional thermochronological evolution of the Mid-Caucasian area will be placed. Finally, this research project will continue in southern Armenia and Nagorno-Karabagh, where field and sampling activities are being planned.

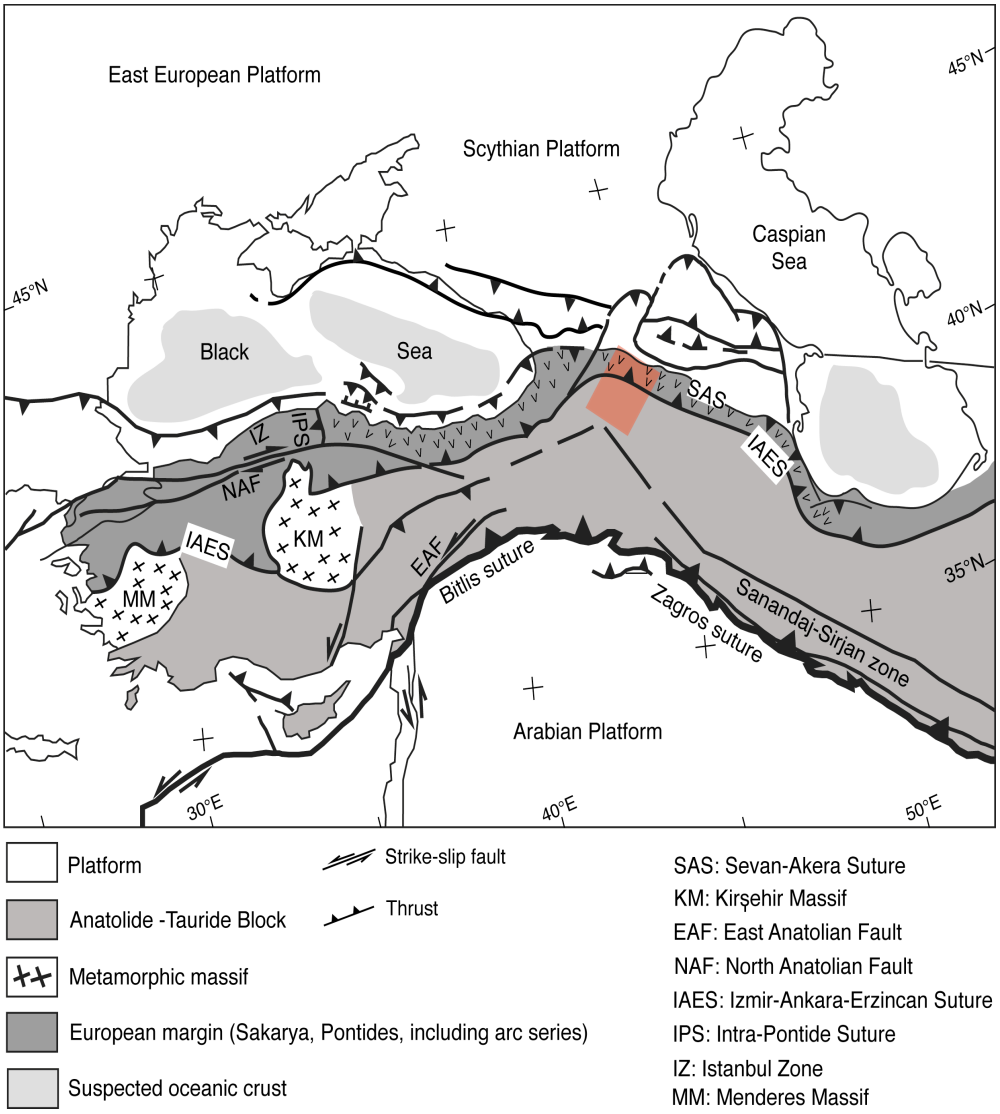

Fig. 3.1 – Structural map of Anatolia and the Caucasian area, red square shows study area (Rolland et al., 2009, mod.).

3.2 GEOLOGICAL SETTING

According to Sosson et al. (2010) in the Lesser Caucasus belt of Armenia three main domains are distinguished from SW to NE (Fig. 3.2): (i) the autochthonous South Armenian Block (SAB), (ii) the ophiolitic Sevan-Akera suture zone, and (iii) the Eurasian plate. The SAB is a possible eastward extension of the eastern Anatolide-Tauride Block. It is made of metamorphic rocks characterized by gneisses, micaschists and leucogranite intrusions (Sosson et al., 2010). It is well exposed NE of Yerevan in the Dzarkuniaz massif (Aghamalyan, 2004; Fig. 2.1). The Sevan-Akera suture zone (e.g., Aslanyan, 1982) is the eastward extension of the Izmir-Ankara-Erzincan suture in Anatolia (Fig. 3.1). It has been interpreted as a suture zone since the work of Milanovski (1968). This suture is the tectonic boundary between the South Armenian Block, which is presumed of Gondwanian origin (Knipper, 1975Rolland et al., 2009;), and Eurasia to the north. The geographic proximity and similarity in the geological units suggests a parallel evolution between northeastern Anatolia and Armenia (Knipper, 1975; Adamia, 1975).

The stratigraphic section of Armenia (Fig. 3.3) is similar to the classic sections of the other areas of the eastern Mediterranean region (Moores & Fairbridge, 1992). Rocks range in age from Precambrian to Pleistocene, volcanogenic rocks alternating with normal sedimentary deposits are widespread throughout the stratigraphic sequences, whose total thickness is as much as 5,000 m (Aslanyan, 1977, 1982).

Volcanogenic deposits are predominantly andesite-basalt and andesite in composition. In addition, Upper Pliocene and Pleistocene liparite and dacite deposits are widespread near Aragats mountain (4,095 m). Plutonic magmatism

is also present as differentiated tholeiitic intrusions and as widespread Mesozoic Tethyan ophiolites.

Precambrian rocks form part of the structure of the metamorphic basement lying at the depth of 0 to 6-8 km. They include gneissic granites, amphibolites, quartz-micaschists and, other metamorphics intruded by granitoid and gabbro-peridotite intrusive rocks.

Palaeozoic sedimentary rocks crop out along the valleys of the Araks, Argichy and Meghrighet rivers. The thick Devonian and Lower Carboniferous section is made of schists, limestones, metaquartzites, and marble. In the basin of the Araks River the Middle and Upper Palaeozoic stratigraphic section is composed of terrigenous limestone rock mass. Triassic sediments are made of bituminous shales, limestones and dolomites with some arkosic and volcanic sandstones. The series thickness is 1,500 m thick. Jurassic sedimentary rocks make up the greater part of the Lesser Caucasus and are represented by the volcanogenic (and subordinately terrigenous) series spread throughout Armenia.

Cretaceous sedimentary deposits are widespread in Armenia. They are exposed in the basins of the Kura, Araks and Agstev rivers and around Lake Sevan. Volcanogenic sedimentary rocks include andesites and keratophyres, Diorite, diorite porphyries, granite porphyries and granites are associated with Early Cretaceous magmatism.

The Upper Cretaceous section includes olistostrome limestones. The section has a thickness of about 1,000 m and includes in the lower part widespread spilites, manganesiferous radiolarites and serpentinites in the volcanogenic

sedimentary complex (mélange), and flysch, clay shales and marls with rich bathyal facies fauna in the upper parts.

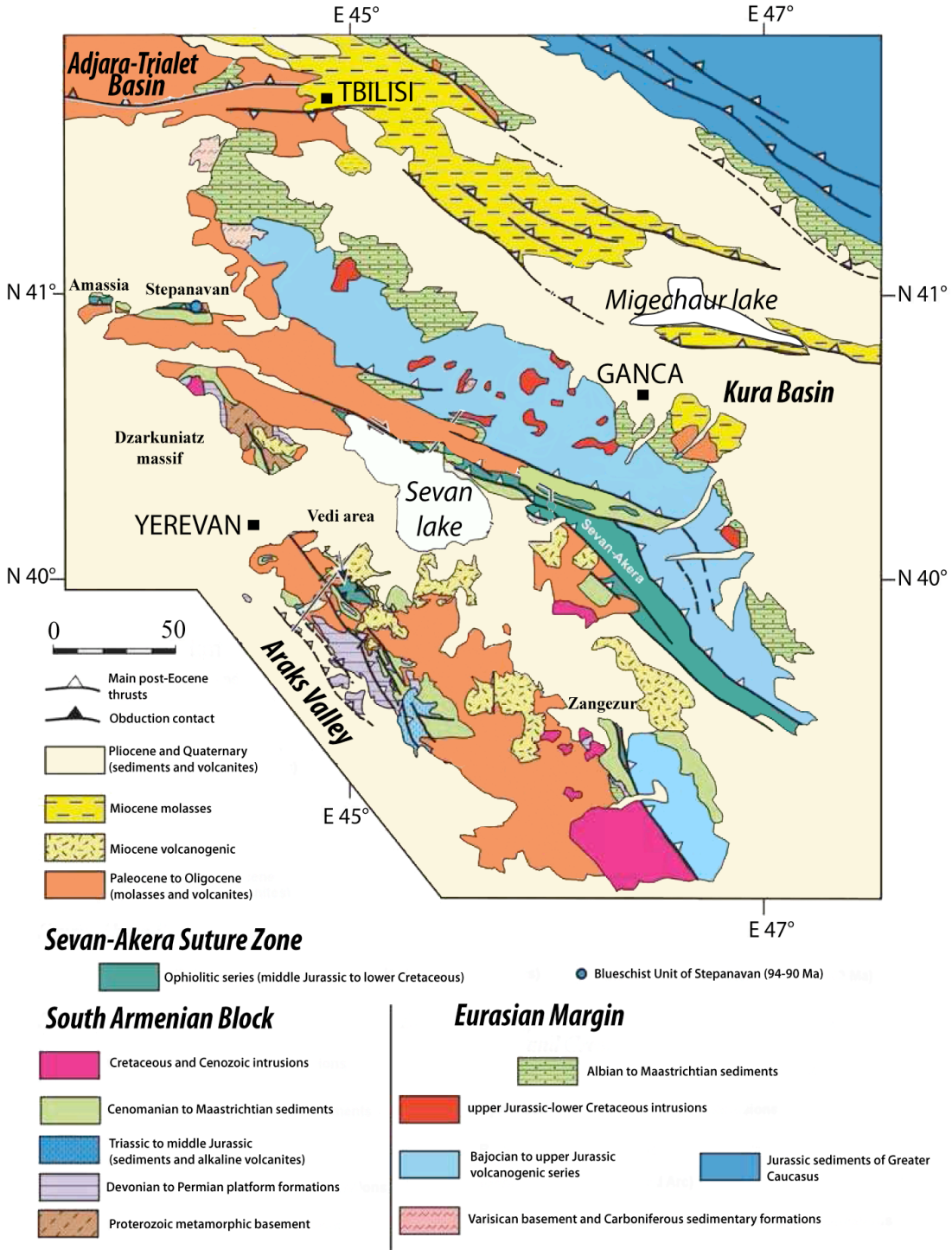

Fig. 3.2 – Structural map of the Lesser Caucasus belt of Armenia and western Azerbaijan (Sosson et al., 2010, mod).

A widespread hiatus and large unconformities mark the closure of the Izmir-Ankara Ocean. The Early Palaeocene is represented by limestone and conglomerates. The Middle-Upper Eocene is represented by volcanogenic deposits. The Upper Oligocene-Miocene is represented by organic-rich continental sediments cropping discontinuously all over Armenia. Miocene sedimentary deposits are represented by molasses and evaporites having a wide distribution and a large thickness (up to 3,000 m). The Upper Miocene is characterized by a gypsum-halite-bearing section.

Extensive Late Tertiary subvolcanic and extrusive bodies of dolerite basalts, andesites, diorites, liparites are also present. Multiphase intrusions of gabbroids, monzonitoids, alkaline syenites, granitoids, granodiorites, granite porphyries occurred simultaneously.

The Pliocene and Pleistocene series is characterized by widespread volcanics. The Lower and Middle Pliocene is represented by thick sheets of andesite-dacite lavas and their pyroclastic equivalents. These deposits are followed by andesite-basalts, andesite and dacite lavas of Ararat, Aragats and Arai-Ler, by subalkaline and alkaline lavas of Ishkhansar and Tskuk, (S Armenia).

Armenia is a classic area for ophiolites. In the Amassia-Stepanavan area (NW Armenia) ophiolites have been long described in association with blueschist and amphibolites facies metamorphic rock (Melikian 1966; Knipper, 1975; Rolland et al., 2009).

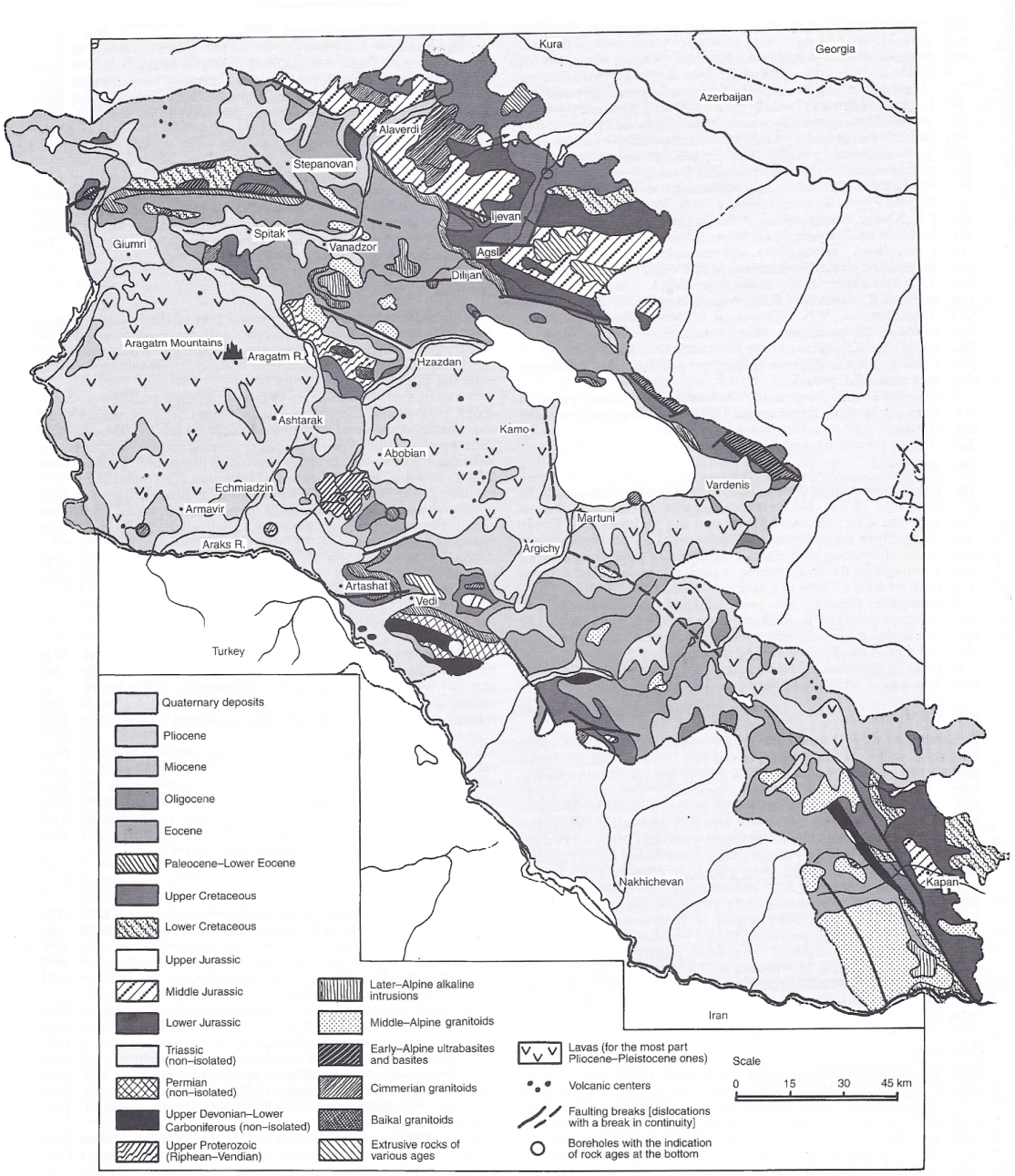

Fig. 3.3 – Geological map of Republic of Armenia (Moores & Fairbridge, 1992).

Armenia is a classic area for ophiolites. In the Amassia-Stepanavan area (NW Armenia) ophiolites have been long described in association with blueschist facies rock (Melikian 1966; Knipper, 1975; Rolland et al., 2009).

The Amassia-Stepanavan blueschist-ophiolite complex is a part of a Late Cretaceous-Early Palaeogene suture zone, which presents similar features as other suture zones from Turkey to Iran. The blueschist *mélange* in the

Stepanavan area (Fig. 3.4) shows the following structural succession (e.g., Aghamalyan 2004; Rolland et al., 2009):

1) a basal part comprising pelites interstratified with dacitic lavas flows, and hydrothermalized and silicified serpentinites;
2) a glaucophane-schist unit including blocks of garnet amphibolites thrust over (1);
3) ophiolitic mélanges comprising ultramafics, volcanic rocks and radiolarites:
4) a conglomeratic and limestone unit overlying uncomformably unit (3);
5) Palaeocene-Eocene series thrust by (1-4). The series (1-4) is attributed an Early to Late Cretaceous age by analogy with the neighbouring Amassia massif where brachiopods have been described in limestones interstratified within lava flows (Rolland et al., 2009).

In the Vedi area (Figs. 3.2, 3.5) an ophiolitic sequence crops out within a folded *klippe*. According to paleontological data (radiolarians), the Vedi ophiolites are mainly Middle-Late Jurassic and probably reach the Early Cretaceous (Danelian et al., 2008, 2010). The whole ophiolitic sequences was interpreted as an ophiolitic mélange (Danelian, 2010). An upper Coniacian to Santonian transgressive series disconformably overlies the ophiolitic Vedi unit. This transgressive series is characterized upwards by breccias and conglomerates, which rework ophiolitic rocks and the Cenomanian-Turonian allochtonous limestone. The conglomeratic formation grades laterally into reef limestones containing Late Coniacian *Hippurites* fossils. Green mudstones, siltstones and thin turbiditic beds made of reworked reef limestone overlie the reef limestones (Sosson et al., 2010).

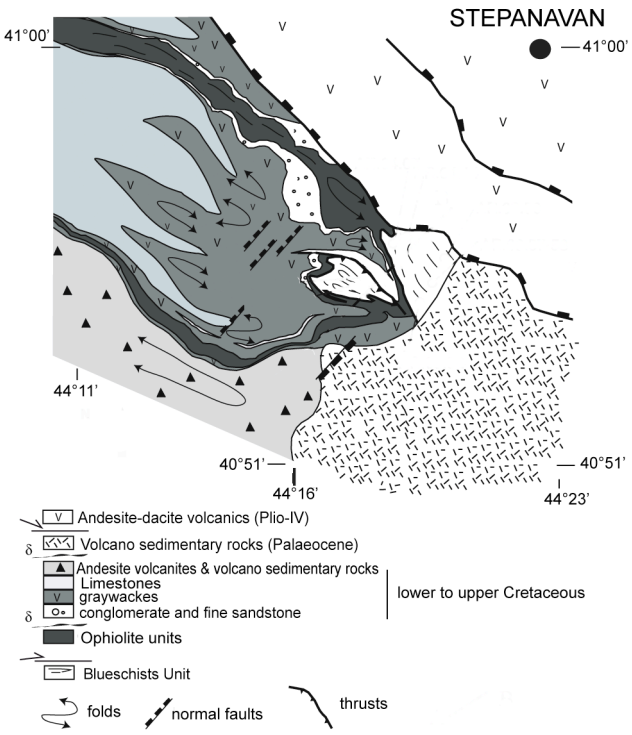

Fig. 3.4 – Geological map of the Stepanavan Blueschists Ophiolite complex. d; unconformity (Rolland et al., 2009, mod.).

The collision stage in the Lesser Caucasus belt of Armenia is described in Chapter I. According to stratigraphic and structural data from Sosson et al. (2010), the collision between the South Armenian Block and Eurasia started during the Palaeocene as shown by the development of a foreland basin in the southeastern part of the belt and by the folding/thrusting and uplift of the Sevan-Akera suture zone. Following this uplift and erosion phase during Early Eocene the north flank of the suture zone and the Eurasian margin subsided, resulting in deposition of Early Eocene detrital rocks and magmatism (Sosson et al., 2010; Galoyan et al., 2007). In summary, during Palaeocene to Late-Middle Eocene time southern Armenia was occupied by a flexural molassic basin abutting against the obducted ophiolite and related structures, which was then progressively

deformed and partially incorporated into the frontal part of the fold-and-thrust belt until the Miocene (Sosson et al., 2010).

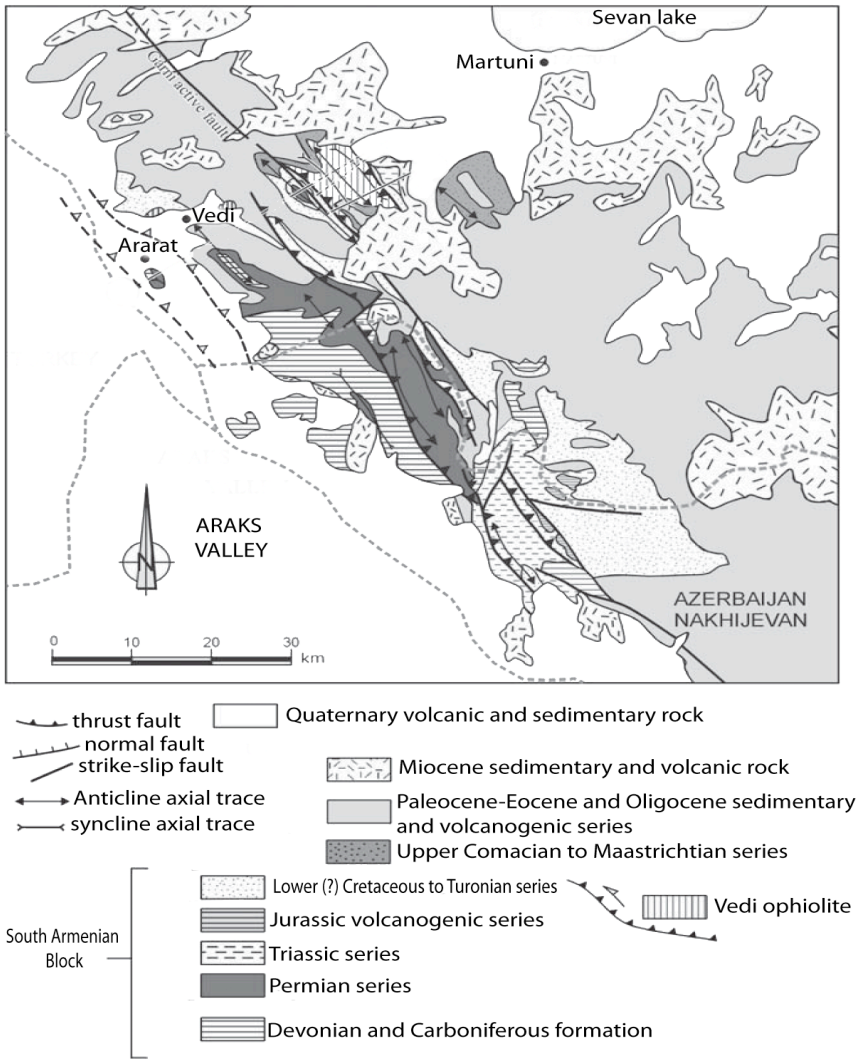

Fig. 3.5 – Structural map of the Vedi area (Sosson et al., 2010).

The Miocene epoch corresponds to a drastic transition in the deformation style of the belt. The stress field evolved, and shortening direction changed from NE-SW to NNW-SSE (Avagyan et al., 2005). Since then deformation has remained with similar features, which resulted in the opening of NW-SE elongated volcanic clusters in the main shortening direction and in a general uplift of the area (Karakhanian et al., 2004; Avagyan et al., 2005; Avagyan & Sosson, 2010).

3.3 SAMPLING AND ANALYSIS

The study area is located in northern Armenia (Fig. 3.1). We collected twelve samples from suitable rock types distributed over a wide area (Fig. 3.6). Two main geological provinces were sampled. (i) The northwestern termination of the Middle-Late Jurassic magmatic arc in northernmost Armenia close to the Georgian border. Such magmatic arc continues to the southeast in Azerbaijan wher additional samples were taken in the Fall of 2012 and are currently being prepared. (2) Scattered outcrops of the Precambrian basement complex of Panafrican affinity. Sampling was carried out in October 2011 in collaboration with Prof. Rafael Melkonyan and Dr. Ghazar Galoyan of the Institute of Geological Sciences of the Armenian Academy of Sciences. Procedure for sample preparation and analysis are described in Appendices A and B. Grains from seven samples were sent to irradiation, since in the other five no apatite grains were found.

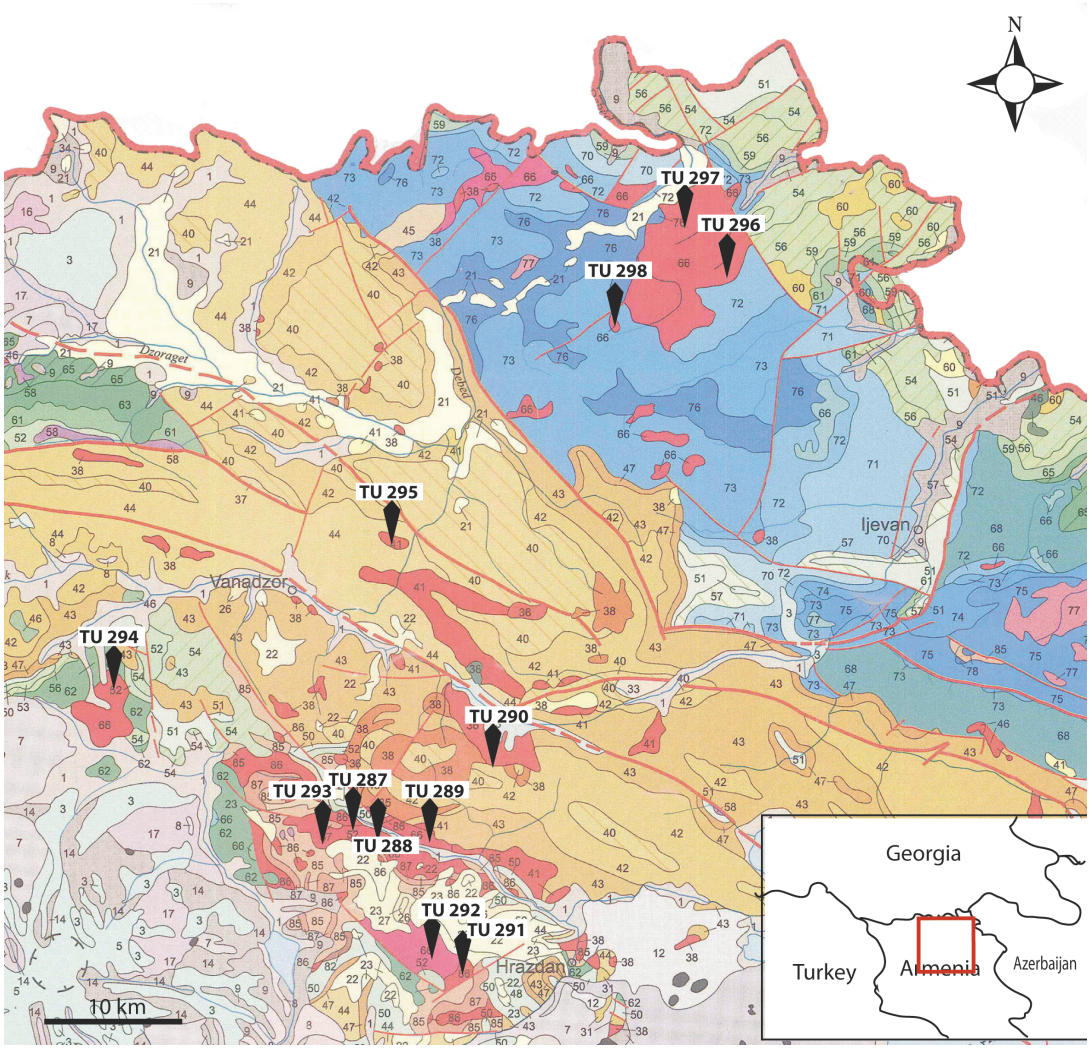

Fig. 3.6 – Geological map of northern Armenia with samples location and number. Explanation of units: 66, intrusive rocks (Jurassic): leucocratic granites, tonalites, quartz diorites and gabbrodiorites; 36, porhyric granites and granodiorites (Late Paleogene); 87, metamorphosed rocks, lower polimetamorphic gneiss-crystalline slate complex (Paleozoic); 86, intrusive rocks, gabbrodiorites, gneissic granites, tonalites (Paleozoic). (From Geological map of the Republic of Armenia, scale 1:500,000; Geological Agency, Ministry of Nature Protection of Armenia, 2005).

3.4 RESULTS

AFT ages range between ca. 17 (Burdigalian) and 12 Ma (Serravallian) (Fig. 3.7 and Tab. 3.2). They show a distinctive geographic pattern: the two older ages come from the northeastern portion of the study area (i.e. the Jurassic magmatic arc) whereas the three younger ages are from the southwestern portion of the study area, where a mixed array of Precambrian to Late Eocene intrusives crops

out. It is noteworthy that the two sample groups were taken from the two sides of the Sevan-Akera suture zone.

Modelling of fission-track data was performed on two samples with a single-age grain population and a relatively high number of measured track lengths. Fission-track lengths were measured only in two samples since the others had a small numbers of confined tracks (< 50). Data from to these two samples were modelled using the HeFty program (Ketcham et al., 2009; see Appendix A;). The time-temperature constraints for the modelling are the intrusion age (35 Ma for TU 290 and 145 Ma for TU 297) and its related temperature (500°).

Modelling of sample TU290 (from the southern sample group and with a cooling age of 16.8 Ma; Fig. 3.8) shows a rapid cooling between 19 and 17 Ma ca. Modelling of TU297 (from the northern sample group and with a cooling age of 11.9 Ma; Fig. 3.9) shows a fast cooling at ca. 13-10 Ma.

Table 3.1 – List of samples taken in northern Armenia.

SAMPLE	AGE	LITHOLOGY	ELEVATION (m)	COORDINATES
TU 287	LATE JURASSIC	TONALITE	2023	38T 045048 4498070
TU 288	? MIDDLE EOCENE	PORPHIRITIC DIKE	1956	38T 0457712 4498686
TU 289	LATE JURASSIC	TONALITE	1889	38T 0463117 4496675
TU 290	UPPER EOCENE	MONZONITE	1846	38T 0475087 4499519
TU 291	PRECAMBRIAN	ORTHOGNEISS	1788	38T 0469751 4480111
TU 292	LATE JURASSIC	TONALITE	1923	38T 0463243 4484734
TU 293	PRECAMBRIAN	GRANODIORITE	2214	38T 0450504 4495969
TU 294	LATE JURASSIC	TONALITE	2112	38T 0432349 4509637
TU 295	LATE EOCENE	GRANODIORITE	1297	38T 0463268 4520965
TU 296	LATE JURASSIC	TONALITE	646	38T 0486745 4558283
TU 297	LATE JURASSIC	GRANITE	665	38T 0484745 4558283
TU 298	MIDDLE JURASSIC	TONALITE	665	38T 0475695 4550861

Table 3.2 – Apatite fission-track data from northern Armenia

Sample number	Coordinates (UTM)	No. of crystals	Spontaneous		Induced		$P(\chi)^2_{\%}$	Dosimeter		Age (Ma) ± 1σ	Mean confined (μm)track lenght	St. dev	No. of tracks measured
			ρ_s	N_s	ρ_i	N_i		ρ_d	N_d				
TU289	38T 0463117 4496675	6	0.72	40	0.89	496	34.31	9.8	4798	13.4±7.2	-	-	-
TU290	38T 0475087 4499519	17	1.75	57	17.32	559	99.43	9.8	4798	16.8±2.5	14.50	0.70	55
TU291	38T 0469751 4480111	20	1.91	80	18.45	773	80.92	9.6	4798	16.7±2.1	12.70	1.02	10
TU292	38T 0463243 4484734	20	2.05	101	18.30	898	95.68	9.5	4798	17.9±2.1	13.45	1.40	12
TU295	38T 0463268 4520965	7	0.97	141	16.30	1165	38.56	9.8	4798	13.7±7.9	-	-	-
TU297	38T 0484745 4558283	21	1.53	59	18.83	722	98.77	9.7	4798	11.9±1.7	14.58	0.80	50
TU298	38T 0475695 4550861	20	2.26	179	16.83	1134	100	9.8	4798	12.4±1.1	-	-	-

Central ages calculated using dosimeter glass CN5 and ζ–CN5=336.4±5.33 (analyst IA) ρs: spontaneous track densities (x 105 cm-2) measured in internal mineral surfaces; Ns: total number of spontaneous tracks; ρi and ρd: induced and dosimeter track densities (x 106 cm-2) on external mica detectors (g=0.5); Ni and Nd: total numbers of tracks; P(χ2): probability of obtaining χ2-value for n degrees of freedom (where n=number of crystals-1); a probability >5% is indicative of an homogenous population. Samples with a probability <5% have been analyzed with the binomial peak-fitting method.

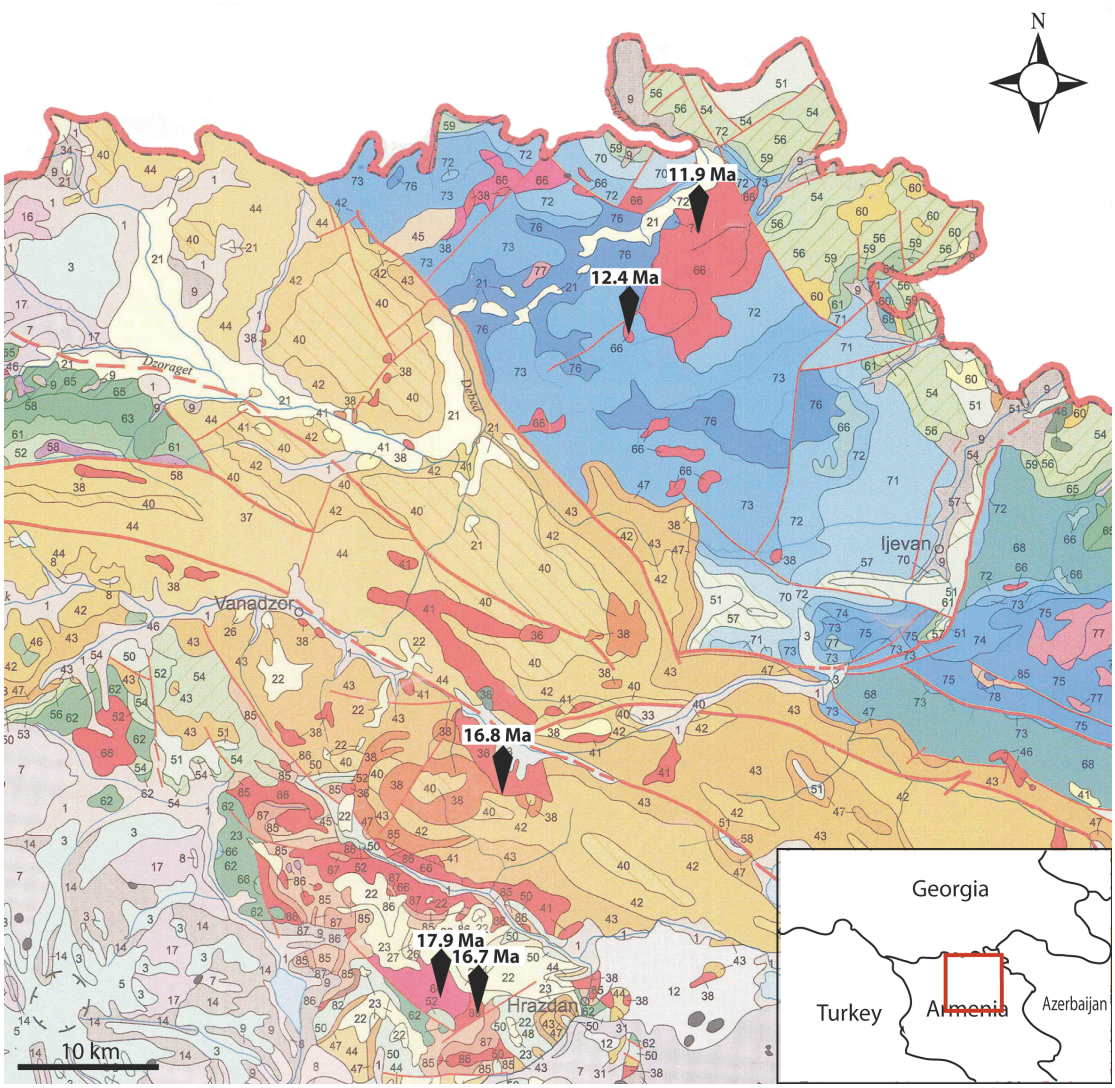

Fig. 3.7 – Geological map with apatite fission-track ages from northern Armenia. From Geological map of the Republic of Armenia, scale 1:500,000; Geological Agency, Ministry of Nature Protection of Armenia, 2005. Sample TU289 and TU295 – Table 3.2 are not shown because of the low statistical significance of their analytical results, $X^2 < 50\%$).

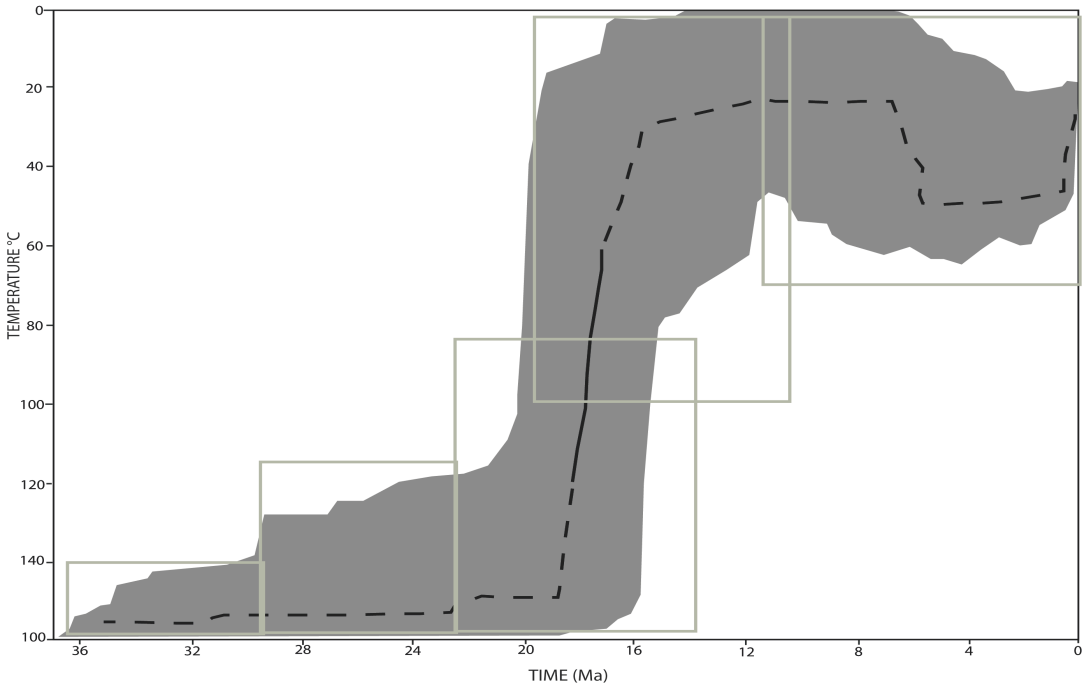

Fig. 3.8 – Time-temperature paths for sample TU290 (cooling age 16.8 ± 2.5 Ma). Model age: 16.7 Ma; measured age 16.8 Ma; age GOF 1.00; length GOF 0.98. GOF= goodness-of-fit, values give an indication about the fit between observed and predicted data (value close to 1 showing an high degree of agreement).

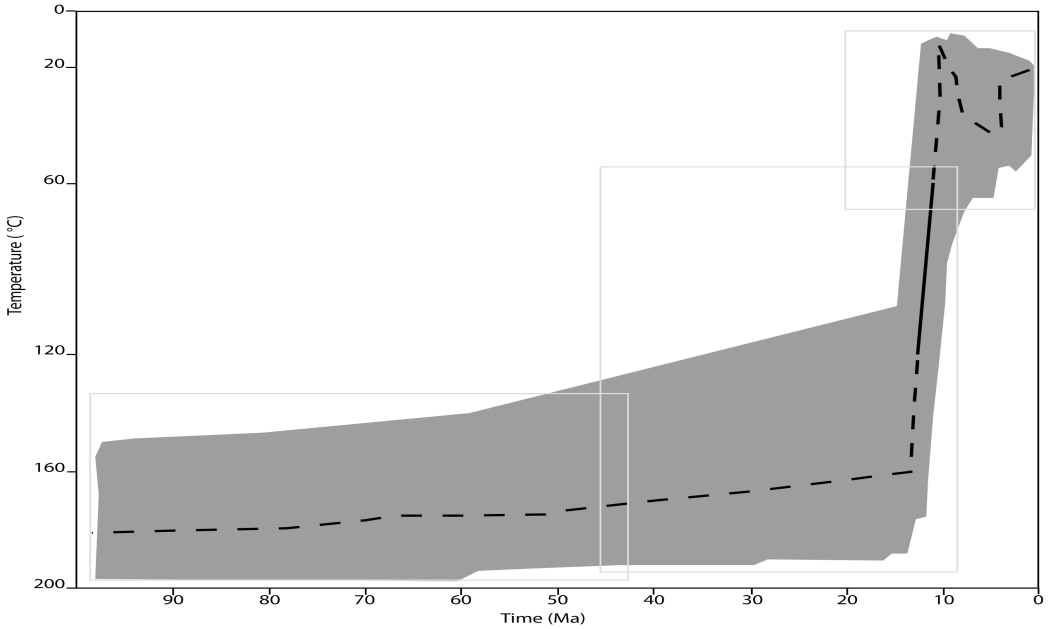

Fig. 3.9 – Time-temperature paths for sample TU297 (cooling age 11.9 ± 1.7 Ma). Model age: 11.8 Ma; measured age 11.7 Ma; age GOF 0.97; length GOF 0.83. GOF= goodness-of-fit, values give an indication about the fit between observed and predicted data (value close to 1 showing an high degree of agreement).

3.5 DISCUSSION AND CONCLUSIONS

AFT ages obtained from the samples collected in northern Armenia indicate Early-to-Middle-Miocene cooling, thus partially coeval to the peculiar and discrete episode of mid-Miocene cooling/exhumation documented for the Eastern Pontides (Chapter Two). We interpreted such episode as a possible far-field effect of the Arabia-Eurasia collision along the Bitlis suture to the south. It is tempting to extend such interpretation to the largely overlapping AFT ages obtained in Armenia, but the current scarcity of thermochronological data in the Lesser Caucasus of southern Armenia and Azerbaijan compared to the vastness and structural complexity of this geologic province makes the formulation of an overall interpretation premature.

The internal consistency of the dataset, with Early and Late Miocene AFT ages respectively south and north of the Sevan-Akera suture zone, is very promising. In the hope of obtaining a more robust dataset, sampling in central-western Azerbaijan along the strike of the Late Jurassic magmatic arc has been already accomplished and a new field season in southern Armenia and Nagorno-Karabagh is planned for the Summer of 2013. For the time being, as to potential interpretative tools of the two AFT age groups delineated so far, it should be noted that already Peive et al. in their classic "Tectonics of Europe and Adjacent Areas" (1982) pointed out that (i) the entire Jurassic magmatic arc of the Lesser Caucasus is generally thrust toward the SW onto the Sevan-Akera ophiolites and the terrains of the Armenian block, and that (ii) Late Miocene coarse-grained, syntectonic conglomerates are peculiar both of the Greater and Lesser Caucasus. We argue tentatively that mid-Miocene shortening and exhumation might have played an important role in the structural development of the Lesser Caucasus

(particularly along the reactivated Sevan-Akera suture) and in the closure of the Mediterranean-Paratethys-Indian Ocean gateway. Significant shortening in this region is also supported y the anomalously thick crust (see Fig.1.28).

Chapter Four

GENERAL DISCUSSION AND CONCLUSIONS

4.1 APATITE FISSION-TRACK AGES AND LARGE-SCALE DEFORMATION PATTERNS

Three interrelated processes are commonly used to described the tectonic-geomorphological evolution of orogens: *rock uplift*, *surface uplift*, and *erosion* (Reiners & Brandon, 2006). Understanding these terms is essential for a thorough assessment of the implications of fission-track data and low-temperature thermochronometry in general. As clarified by England & Molnar (1990), rock and surface uplift describe the vertical motion of rock or a portion of the Earth's surface relative to a datum, such as sea level. Erosion is the superficial removal of mass at a point in the landscape by both mechanical and chemical processes, and can be considered as the difference between rock uplift and surface uplift. Erosion is one type of the broader process of *denudation*, which, following Ring et al. (1999), is the removal of rock or soil by tectonic and/or surficial processes at a specified point at or under Earth's surface. The other types of denudation are tectonic normal faulting and ductile thinning. Another term that it frequently used in studying orogenic evolution is *exhumation*, which Ring et al. (1999) defined as the unroofing history of a rock, as caused by tectonic and/or surficial processes.

Cooling ages of low-temperature thermochronometers such as the fission-track system in apatite provide bounds on the possible thermal histories of rocks. Although cooling may be a result of several processes, over large scales and with support of complementary geologic constraints it is often interpreted as resulting from exhumation. In contractional orogens most exhumation is due to shortening-driven erosion rather than to normal faulting or ductile thinning. Episodes or varying rates of erosion may be attributable to a variety of causes,

but in contractional orogens most important variations in erosion rates in both space and time are reasonably associated with differences in topographic relief caused by rock uplift. Thus to the extent that erosion can be related to rock uplift, and rock uplift related to contractional deformation, cooling ages can be used to elucidate spatial-temporal patterns of deformation. To the extent that deformation can be related to surface uplift, cooling ages also provide clues to patterns of topographic evolution through time.

The fission-track system -applied to large study areas in conjunction with stratigraphic and structural analyses- can thus help elucidating broad deformational patterns and the structural evolution of continental collision zones. Our approach to the thermochronologic study of the foreland of the Arabia-Eurasia collision zone in Eastern Turkey, Georgia, and northern Armenia is based on the assumption that crustal shortening and thickening is arguably the most important mechanism for surface uplift and topographic development of collisional orogens. Nevertheless the link between patterns of rock and surface uplift on one hand and deformation/shortening on the other hand may be complicated by mantle processes, which may act to produce punctuated episodes of rock or surface elevation change. In the case of our study area, mantle-driven processes and dynamic topography clearly have had a role in the shaping of the present-day topography. The high-elevation Anatolian Plateau is underlain by upwelling asthenosphere but dynamic topography alone cannot explain our FT results, as the mostly Plio-Quaternary attainment of high elevations in the plateau has not exhumed the apatite partial annealing zone and therefore is not recorded by the fission-track thermochronometer.

Erosion plays a critical role in orogenic evolution in several ways (Reiners & Brandon, 2006). From a general viewpoint, it is a dynamic link between tectonic uplift and many other processes, including chemical weathering and long-term climate change, and sediment production, routing, and deposition. Erosion directly influences not only topographic decay, but also the growth of an orogen, by modulating the pattern and rates of surface uplift (Reiners & Brandon, 2006). Because erosion is also related to climate (e.g., precipitation), it provides an important feedback between climate and tectonics, but when the erosion owing to the climatic processes is slower than tectonics processes the mountainous topography is governated only by surface uplift (Reiners & Brandon, 2006).

4.2 THE MEDITERRANEAN-INDIAN OCEAN GATEWAY

The middle Miocene (ca. 19-14 Ma) closure of the gateway to the Indian Ocean had profound climate implications because it interrupted a direct marine connection between Africa and Eurasia forcing ocean currents to pass south of Africa. The northward migration of the African-Arabian plate and collision with the Eurasian plate progressively disconnected the proto-Mediterranean from the Indian Ocean during the Miocene (Fig. 4.1). The resulting closure of the Mediterranean-Paratethys-Indian Ocean gateway has been put forward to explain the dramatic climatic change that took place from Earth's last major warm episode 17-15 Ma (the Mid-Miocene Climate Optimum) to the much colder icehouse state and the development of a permanent East Antarctic ice cap as a consequence of circulation changes. The major climatic cooling step at ca. 13.8 Ma, the Mi3b oxygen isotope event, gave rise to a much enlarged ice volume, but

the age of this dramatic cooling step is in contrast with the available age constraints on the initial gateway closure at ~19 Ma. The latter age is mostly based on African-Eurasian mammal migration. Several distinct waves of mammal migration and marine biogeographic evolution in the Proto-Mediterranean and Indo-West Pacific region suggest intermittently short-lived marine connections - possibly related to sea-level rise during the Mid-Miocene Climate Optimum - until it was permanently closed at ~14 Ma. However, precise dating of any of these events is seriously hampered by the lack of well-dated mammal- or invertebrate-bearing sections. It should be noted that AFT ages (and other independent geological evidence) from the Bitlis collision zone point coherently to an episode of rapid exhumation at 18.0-13.4 Ma (Okay et al., 2010), in agreement with the closure of the Paratethys based on mammal migration paths. The AFT ages obtained in this dissertation for the easternmost Pontides point to an episode of fast cooling/exhumation between ca. 15.2 and 12.4 Ma, thus bracketing the major climatic cooling step at ca 13.8 Ma. The occurrence of climatically driven erosion/exhumation during this period cannot be totally excluded but several lines of evidence point to the contrary: (i) exhumation in the eastern Pontides is synchronous with exhumation in the Bitlis collision zone >200 km to the south (Okay et al., 2010); (ii) widespread angular unconformities indicate deformation along the easternmost Pontides and in the northern Anatolian Plateau.

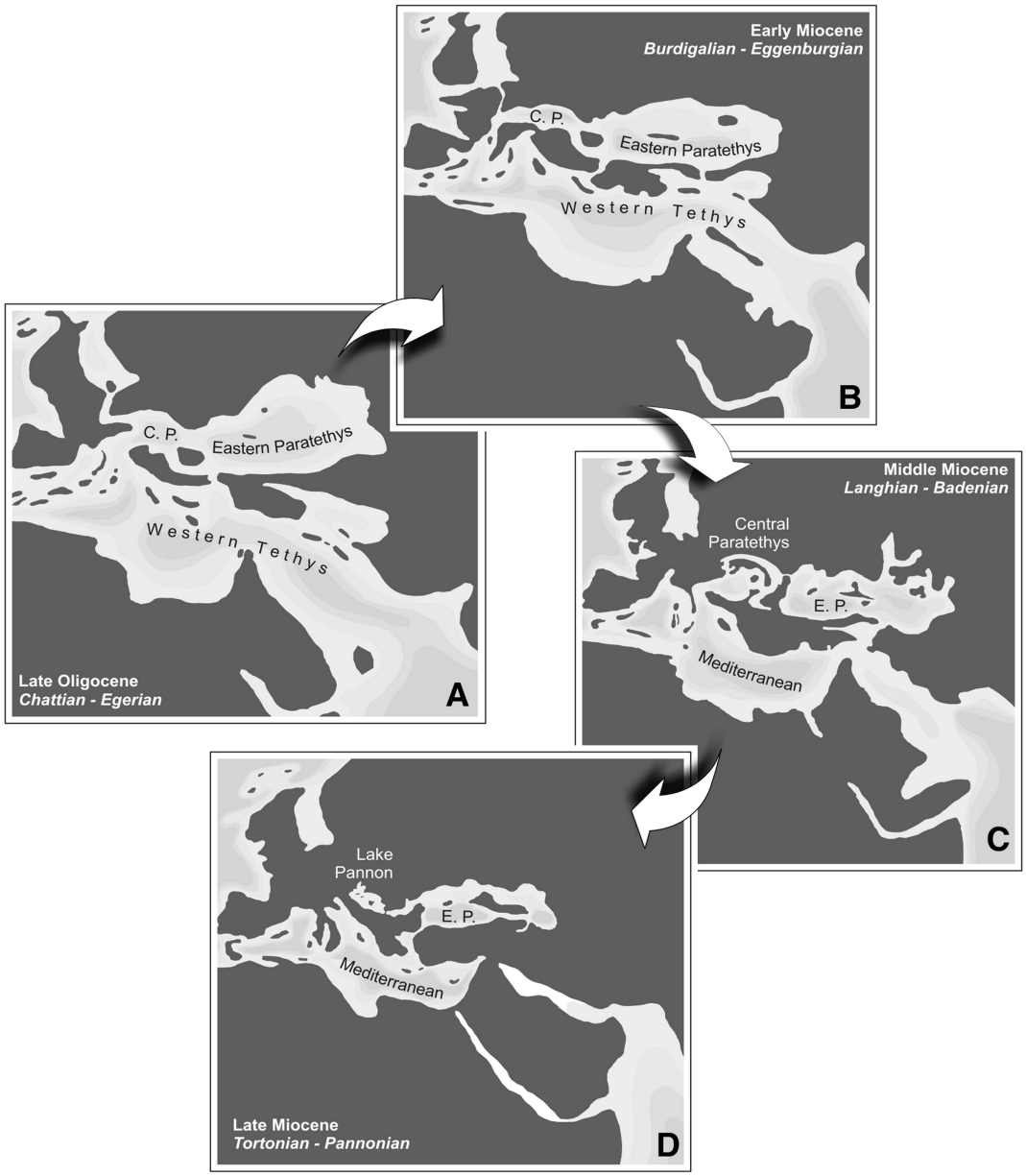

Fig. 4.1 - Palaeogeographic sketch-maps of the circum-Mediterranean area with focus on the Paratethys Seas (from Harzhauser & Piller, 2007). Note that a serious palinspastic model incorporating large-scale deformation for the entire area is still missing. [C.P. = Central Paratethys; E.P. = Eastern Paratethys]

4.3 FAR-FIELD TECTONIC EFFECTS OF THE ARABIA-EURASIA COLLISION

The collision between Arabia and Eurasia led to the development of (i) the Bitlis Zagros suture and associated orogenic belt, (ii) the formation of the North and East Anatolian Fault systems, (iii) the structural inversion of Caucasian basin(s), and (iv) a widespread deformation in what is now the Anatolian-Armenian-Iranian plateau. The latter effect has been the subject of much debate, with contrasting hypothesis linking the development of the plateau either to compressional stress transfer or to wholesome, mantle-driven uplift (i.e. an effect of dynamic topography). Widespread Plio-Quaternary volcanism across much of the plateau seems to underscore the importance of extensional tectonics during this time frame, as the ascent of such large quantities of magma would be hampered by compressional tectonics.

Despite the importance of the event, the timing of collision-related deformation is poorly known, with estimates ranging from Late Cretaceous (Hall, 1976; Berberian & King, 1981; Alavi, 1994), to Late Eocene-Oligocene (35-25 Ma; Jolivet & Faccenna, 200; Agard et al., 2005; Allen & Amstrong, 2008), to Miocene (Şengör et al., 1985; Dewey et al., 1986; Yılmaz, 1993; Robertson et al., 2007). The only low-temperature thermochronological data available for the Bitlis-Pütürge massif point to an episode of fast exhumation in the Middle Miocene (Okay et al., 2010). On the basis of available data, the working hypothesis evaluated in this dissertation is that the indentation of the Arabian Plate induced widespread tectonism, not only in in the Caucasus area but over a wide region potentially including the Anatolian-Iran Plateau, the Estern Pontides, and Transcaucasia. Within this general framework, this dissertation focused on selected aspects of the geological evolution of the Eastern Pontides, their

prosecution in the Lesser Caucasus of Georgia (Adjara-Trialeti zone) and north-western Armenia, and the Anatolian-Iranian plateau. This is a key area to better constrain the tectonic effects of the Arabia-Eurasia collision because mechanical coupling and indentation along this segment of the Bitlis-Zagros suture was maximum.

The application of the low-temperature thermochronological method based on apatite fission-track analysis, has produced significant constraints to the geological evolution of Anatolia and Transcaucasia following Arabia-Eurasia collision. The main *analytical* results of this dissertation can be summarized as follows.

1) Exhumation of the Cretaceous and Eocene granitoids along the Black Sea coast in the eastern Pontides region occurred in the Middle Miocene, mirroring the age of a maximum tectonic coupling between the Eurasia and Arabia plates along the 2,400 km long Bitlis-Zagros suture zone, some 200 km to the south. In fact, exhumation ages along the easternmost Pontides are virtually identical to those obtained by Okay et al. (2010) along the Bitlis segment of the suture. The mid-Miocene ages obtained along the easternmost Pontides are interpreted as a tectonic far-field effect of the Arabia-Eurasia collision. Such effects are concentrated along the Black Sea coast at the boundary between polydeformed continental lithosphere and pristine (and rheologically stronger) oceanic lithosphere of the Eastern Black Sea.
2) Exhumation in the Anatolian Plateau occurred in the Paleogene (with a cluster of ages in the Middle-Late Eocene). Such exhumation ages were the results of the deformation related to the closure of the Izmir-Ankara-

Erzincan ocean and the corrisponding collision between the Sakarya and Anatolide-Tauride terranes. The memory of this continental amalgamation has been retained by the AFT thermochronometer because limited exhumation during the creation of the Anatolian Plateau was insufficient to expose a new apatite parzial annealing zone.

3) Stress from the Bitlis collision zone was transmitted heterogeneously in the region of the Lesser Caucasus. The Adjara-Trialeti zone of western Georgia was structurally affected but exhumation was insufficient to expose a new apatite PAZ. Exhumation in northern Armenia is instead coeval with the Arabia-Eurasia collision and focused along preexisting structural discontinuities like the Paleogene Sevan-Akera suture zone, and was strong enough to expose to the surface a new PAZ.

From a wider, more *interpretative* perspective, comparision available data on present-day crustal dynamics and the thermochronological data presented in this paper provide a comparison between short- and long-term deformation patterns for the entire eastern Anatolian-Transcaucasian region and has some bearing on the timing of the overall westward "tectonic escape" of Anatolia. Two successive stages of Neogene deformation of the northwestern foreland of the Arabia-Eurasia collision zone, can be inferred (Fig.4.2). (1) During Early-Middle Miocene time, continental deformation was concentrated along the Arabia-Eurasia (Bitlis) collision zone but tectonic stresses related to the Arabia-Eurasia collision were transmitted over a wider area and focused along the coast of the eastern Black Sea and in the Greater Caucasus, inducing significant shortening and exhumation. The Black Sea (quasi)oceanic lithosphere is fundamentally stronger than the polydeformed continental lithosphere to the south and

therefore represented a “backstop” resisting deformation and deviating the impinging continental lithosphere (McClusky et al., 2000). Other small areas along kinematic block boundaries may have been affected. From this viewpoint, it is significant that a new set of Miocene AFT ages in northwestern Armenia was yielded by samples straddling the boundary between kinematic blocks proposed by Reilinger et al. (2006) based on the analysis of GPS motion vectors. This particular aspect is now under study in a follow-up of this dissertation in a cooperation program with foreign partners. (2) Since late Middle Miocene time the westward translation of Anatolia and the activation of the North and Eastern Anatolian Fault systems have reduced efficient northward stress transfer. In this new tectonic regime –still active today- most of the Arabia-Eurasia convergence has been accomodated by the westward motion of Anatolia whereas the eastern Pontides have been mechanically decoupled from the foreland of the Bitlis collision zone, as shown by the absence of significant seismicity in the area.

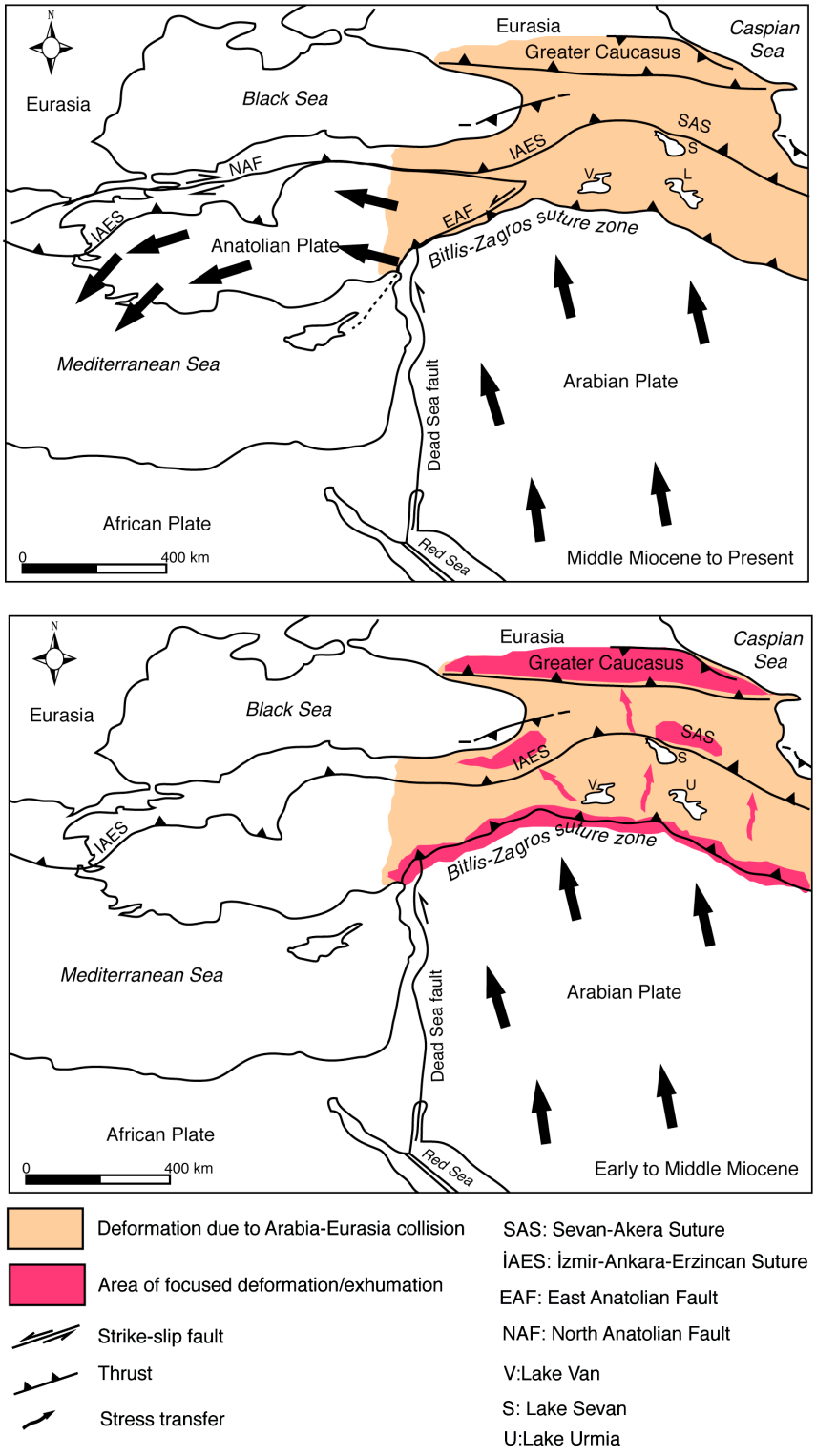

Fig. 4.2 - Stages of Neogene deformation patterns in the Eurasia foreland of the Bitlis-Zagros collision zone. The development and westward movement of the Anatolian Plate has decoupled to a large extend the collision zone from its northern foreland. Dark red indicates areas of focused deformation/exhumation, as determined by fission-track analysis. The plate velocity field is only schematically shown.

AFT data presented in this dissertation indicate widespread mid-Miocene deformation/exhumation possibly related to the indentation of Arabia. The geodetic and seismological data presented in Chapter Two show the present-day deformation pattern. One may argue that the transition between the two successive deformation stages outlined above may have occurred any time during the 15 Ma between the Middle Miocene and the present, but abundant independent stratigraphic and structural data clearly indicate that the North Anatolian Fault system was activated in the mid-Miocene (see, for a review, Şengör et al., 2005). Thus, the transition between shortening-dominated and strike-slip-dominated deformation occurred most likely in the Middle Miocene, shortly after maximum mechanical coupling between Arabia and Eurasia.

We do not tackle here the hotly debated topic of the cause for the Anatolian westward motion. A mounting body of evidence points to widespread extension in the Aegean region (particularly in its northern part) and in western Anatolia already in the Oligocene, possibly connected with progressive roll-back of the Aegean subduction zone, as the primary cause for Anatolian westward "escape" (see Doglioni et al., 2002, for a discussion). Nevertheless, the temporal coincidence in the Middle Miocene between the deformation acme along the Bitlis suture and the nucleation of the Northern and Eastern Anatolian Fault systems should not be underestimated. The AFT dataset presented here, if compared with the present-day GPS-derived plate motion vectors and overall seismicity, clearly indicates that a major change of tectonic regime occurred in the Middle Miocene, following maximum mechanical coupling between Arabia and Eurasia. This hypothesis takes into account most available geological,

geodetic, and geophysical data and will represent the basis for future research in the region.

REFERENCES CITED (Chapters I, III, and IV; Appendices A and B)

ADAMIA S.H. (1975) – *Plate tectonics and evolution of the Alpine System: discussion.* Geol. Soc. Am. Bull., **86**, 719-720.

ADAMIA S.H., BELOV A., KAKELIA M. & SHAVISHVILI I. (1987) – *Paleozoic tectonic development of the Caucasus and Turkey (Geotraverse C),* In: Fluegel H.W., Sassi F.P. & Grecula P. (eds.) Pre-Variscan and Variscan events in the Alpine-Mediterranean Mountain Belt, Mineralia Slovaca, Alfa Bratislava, 23-50.

ADAMIA S.H., CHABUKIANI A., CHKHOTUA T., SADRADZE N., ZAKARIA D. & ZAKARIADZE G. (2010) – *Geology of the Caucasus and adjacent areas, 1:250.000 scale geological map.* In: Christofides G., Kantinaris N., Kostopoulos D. & Chatzipetros A. (eds), Proceedings, XIX Congress of the Carpathian Balkan Geological Association, **99**, 1-9.

ADAMIA S.H., CHKHOTUA T., KAKELIA M., LORDKIPANIDZE M. & SHAVISHVILI I. (1981) – *Tectonics of the Caucasus and adjoining regions: implications for the evolution of the Tethys ocean.* J. Str. Geol., **3**, 437-447.

ADAMIA S.H., MUMLADZE T., SADRADZE N., TSERETELI E., TSERETELI N. & VARAZANASHVILI O. (2008) – *Late Cenozoic tectonics and geodynamics of Georgia (SW Caucasus).* Georgian Int. J. Sci. Tech., **1**, 77-107.

ADAMIA S.H., ZAKARIADZE G., CHKHOTUA T., SADRADZE N., TSERETELI N., CHABUKIANI A. & GVENTSADZE A. (2011) – *Geology of the Caucasus: a review*. Tur. J. Earth Sci., **20**, 489-544.

AGARD P., OMRANI J., JOLIVET L. & MOUTHEREAU F. (2005) – *Convergence history across Zagros (Iran): Constraints from collisional and earlier deformation*. Int. J. Earth Sci., **94**, 401-409.

AGHAMALYAN V.A. (2004) – *The Lesser Caucasus earth crust formation and evolution in the collision zone of Paleo-Tethys.* 5TH Int. Sym. on the Eastern Mediterranean Geology. Thessaloniki, Greece, 14-20 April 2004, 17-20.

AKINCI Ö.T. (1984) – *The Eastern Pontide volcano-sedimentary belt and associated massive sulphide deposits*. In: J.E. Dixon & A.H.F. Robertson (eds.). The Geological Evolution of the Eastern Mediterranean. Geol. Soc. Spec. Publ., **17**, 415-428.

ALAVI M. (1994) – *Tectonic of the Zagros orogenic belt of Iran – New data and interpretation*. Tectonophysics, **229**, 221-228.

ALBINO I., CAVAZZA W., ZATTIN M., OKAY A.I., ADAMIA S. & SADRADZE N. (2012) – *Apatite fission-track analysis of the tetonic effects of the Arabia-Eurasia collision*.

Abstract for "European Geosciences Union (EGU)" General Assembly, Wien 22-27 April 2012. P.1

ALBINO I., CAVAZZA W., ZATTIN M., OKAY A.I., ADAMIA S. & SADRADZE N. (2012) – *Apatite fission-track analysis of the tetonic effects of the Arabia-Eurasia collision*. Abstract for "Società Geologica Italiana (SGI)" Cosenza, 18-20 September 2012. pp. 1-3.

ALLEN M. & ARMSTRONG H. A. (2008)– *Arabia-Eurasia collision and the forcing of midCenozoic global cooling:* Paleogeography, Palaeoclimatology. Palaeocology, **265**, 52-58.

ALLEN M., JACKSON J. & WALKER R. (2004) –*Late Cenozoic reorganization of the Arabia-Eurasia collision and the comparison of short-term deformation rates*. Tectonic, **23**, 1-16.

ANDERSON D.L. (2005) – *Large igneous provinces, delamination, and fertile mantle.* Elements, **1**, 271-275.

ANDERSON D.L. (2007) – *The eclogite engine: chemical geodynamics as a Galileo thermometer.* In: Fouger G.R. & Jurdy D.M., eds. *Plates, plumes, and planetary processes.* Geol. Soc. Am. Sp. Publ., **430**, 47-64.

ARMIJO R., MEYER B., NAVARRO S., KING G. & BARKA A. (1999) – *Asimmetric slip partitioning in the Sea of Marmara pull-apart: a clue to propagation processes of the North Anatolian Fault?*. Terra Nova, **14**, 80-86.

ASLANYAN A.T. & SATIAN M.A. (1977) – *On the geological features of Transcaucasia ophiolitic zones.* Izvestia Academy of Sciences Armenia SSR, Nauki o Zemle, **4-5,** 13-26 (in Russian).

ASLANYAN A.T. & SATIAN M.A. (1982) – *Middle Cretaceous ophiolite zones of transcaucasus and tectonic reconstruction.* Ophioliti, **7,** 131 (abstract).

AVAGYAN A. & SOSSON M. (2005) – *Neogene to Quaternary stress field evolution in the Lesser Caucasus and adjacent regions using fault kinematics analysis and volcanic cluster data.* Geodinamica Acta**, 18,** 401-416.

AVAGYAN A. & SOSSON M. (2010) – *Recent tectonic stress evolution in the Lesser Caucasus and adjacent region.* In: Sosson M., Kaymakci N., Stephenson R.A., Bergerat F. & Starostenko V. (eds). *Sedimentary Basin Tectonics from the Black Sea and Caucasus to the Arabia Platform*. Geol. Soc. Lond Spec. Publ.**, 340,** 4393-408.

BARKA A., AKYÜZ S., ALTUNEL E., SUNAL G., ÇAKIR Z. (2000) – *The August 17, 1999 Izmit earthquake, M= 7.4, Eastern Marmara region, Turkey: study of surface rupture and slip distribution*. pp, 15-30.

BARKA A., AKYÜZ S., ALTUNEL E., SUNAL G., ÇAKIR Z. (2002) – *The surface rupture and slip distribution of the 17 August 1999 Izmit earthquake (M 7.4), North Anatolian Fault.* Bull. Seismol. Soc. Am**., 92,** 43-60.

BELLEMANS F., DE CORTE F. & VAN DEN HAUTE P. (1995) – *Composition of SRM and CN U-doped glasses: significance for their use as a thermal neutron fluence monitors in fission track dating.* Radiat. Meas, **24/2**, 153-160.

BERBERIAN M. & KING G. (1981) – *Toward a paleogeography and tectonic evolution of Iran.* Can. J. of Earth Sciences, **18**, 210-265.

BHANDARI N., BHAT S.G., LAL D., RAJAGOPALAN G., TAMHANE A.S.J. & VENKATAVARADAN V. (1971) – *Fission fragment tracks in apatite: recordable track length.* Earth Planet. Sci. Lett., **13**, 191-199.

BIGAZZI G. (1981) – *The problem of the decay constant λ_f of ^{238}U.* Nucl. Tracks, **5**, 35-44.

BIGAZZI G. & HADLER J.C. (1989) – *Errori di conteggio ed errori sistematici nella datazione con il metodo delle tracce di fissione.* Boll. Soc. Geol. It., **108**, 325-350.

BIRD P. (1979) – *Continental delamination and the Colorado Plateau.* J. Geophy. Res., **84**, 7561-7571.

BOZKURT E. (2001) – *Neotectonics of Turkey – a synthesis*. Geodinamica Acta, **14**, 3-30.

BOZTUĞ D., JONCHEERE R., WAGNER G.A. & YENĞIL Z. (2004) – *Slow Senonian and fast Palaeocene-Early Eocene uplift of the granitoids in the Central Eastern Pontides, Turkey: apatite fission track results*. Tectonophysics, **382**, 213-228.

BRANDON M.T. (1996) – *Probability density plot for fission-track grain-age samples.* Radiat. Meas., **26**, 663-676.

BURTNER R.L., NIGRINI A. & DONELICK R.A. (1994) – *Thermochronology of Lower Cretaceous source rocks in the Idaho-Wyoming thrust belt.* , Am. Ass. Petr. Geol. Bull., **78/10**, 1613-1636.

CALK L.C. & NAESER C.W. (1973) – *The thermal effects of a basalt intrusion on fission tracks in quartz monzonite*. J. Geol., **81**, 189-198.

CAVAZZA W., FEDERICI I., OKAY A.I. & ZATTIN M. (2012) – *Apatite fission-track thermochronology of the Western Pontides (NW Turkey)*. Geol. Mag., **149 (1)**, 133-140.

CAVAZZA W., OKAY A.I. & ZATTIN M. (2008) – *Rapid early-middle Miocene exhumation of the Kazdağ Massif*. Int. J. Earth Sci., **98**, 1935-1947.

CHADDERTON L.T. BIERSACK J.P. & KOUL S.L. (1988) – *Discontinuous fission tracks in crystalline detectors*. Nucl. Track. Radiat Meas., **15**, 31-40.

CHEN F., SIEBEL W., SATIR M., TERZIOĞLU N. & SAKA K. (2002) – *Geochronology of the Karadere basement (NW Turkey) and implications for the geological evolution of the Istanbul zone.* Int. J. Earth Sci, **91**, 469-481.

COPLEY A. & JACKSON J. (2006) – *Active tectonics of the Turkish-Iranian Plateau*. Tectonics, **25**, 1-19.

CROWLEY K.D., CAMERON M. & SCHAEFER R.L. (1991) – *Experimental studies of annealing of etched fission track in fluoroapatite*. Geoch. Cosm. Acta, **55**, 1449-1465.

CROWLEY K.D., NAESER C.W. & NAESER N.D. (1989) – *Fission-track analysis: theory and applications.* Geol. Soc. Am., **55**, 1449-1465.

COSENTINO D., SCHILDGEN T.F., CIPOLLARI P., FARANDA C., GLIOZZI E., HUÀCKOVA N., LUCIFORA S., STRECKER M.R. (2012) – *Late Miocene surface uplift of the southern margin of the Central Anatolian plateau, Central Taurides, Turkey.* Geol. Soc. Am. Bull, **124 (1-2)**, 133-145.

DANELIAN T., ASATRYAN G., SOSSON M., PERSON A., SAHAKYAN L. & GALOYAN G. (2008) – *Discovery of two distinct Middle Jurassic Radiolarian assemblages in the sedimentary cover of the Vedi ophioite (Lesser Caucasus, Armenia)*. Comptes, Rendus, serie Palevol, **7**, 324-334.

DANELIAN T., ASATRYAN G., SAHAKYAN L., GALOYAN G., SOSSON M. & AVAGYAN A. (2010) – *New and revised Radiolarian biochronology for the sedimentary cover of ophiolites in the Lesser Caucasus (Armenia).* In: Sosson M., Kaymkci N., Stephenson R.A., Bergerat F. & Starostenko V (eds). *Sedimentary Basin Tectonics from the Black Sea and Caucasus to the Arabian Platform.* Gel. Soc. Lon., Spec. Publ., **340**, 383-391.

DARTYGE E., DURAUD J.P. & MAURETTE M. (1978) – *Thermal annealing of iron tracks in muscovite, labradorite and olivine*. Nucl. Tracks Suppl., **1**, 395-399.

DARTYGE E., DURAUD J.P. & MAURETTE M. (1981) – *New model of nuclear particle tracks in dieletric minerals*. Nucl. Phys. Rev., **B23**, 5213-5229.

DE CORTE F., BELLEMANS F., VAN DEN HAUTE P., INGELBRECHT C & NICHOLL C. (1998) – *A new U doped glass certified by the European Commission for the calibration of fission-track dating.* In: Van Den Haute P. & De Corte F. (eds.). *Advances in fission-track geochronology*. Kluwer, Dordrecht, 67-78.

DEMETS C., GORDON R., ARGUS D. & STEIN S. (1990) – *Current plate motions*. Geophy. J. Int., **101**, 425-478.

DEWEY J.F., HEMPTON M.R., KIDD W.S.F., ŞAROĞLU F. & ŞENGÖR A.M.C (1986) – *Shortening of continental lithosphere: the neotectonics of Eastern Anatolia – a young collision zone.* In: Coward M.P. & Ries A.C. (eds). *Collision Tectonics.* Geol. Soc. of London. Spec. Publ., **97**, 3-36.

DILEK Y. (2006) – *Collision tectonics of the Mediterranean region: causes and consequences*. Geo. Soc. Am., **Special paper 409**, 1-13.

DILEK Y. & WHITNEY D.L. (2000) – *Cenozoic crustal evolution in central Anatolia: extension, magmatism and landscape development.* In: Proceedings of the Third International Conference on the geology of the Eastern Mediterranean, September 1998. Geol. Sur. Am. Dep., Nicosia, Cyprus, p. 183-192 **55**, 1449-1465.

DODSON M.H. (1973) – *Closure temperature in cooling geochronological and petrological systems*. Contrib.Mineral. Petr., **40**, 259-274.

DOGLIONI, C., AGOSTINI, S., CRESPI, M, INNOCENTI, F., MANETTI, P., RIGUZZI, F. AND SAVASÇIN, Y. (2002) – *On the extension in western Anatolia and the Aegean Sea.* In: Rosenbaun G. & Lister G.S. *Reconstruction of the evolution of the Alpine-Himalayan Orogen.* J. Virt. Ex., **8**, 161-176.

DONELICK R.A. (1997) – *Fact and fiction regarding apatite fission-track annealing kinetics*. On Track, **7/1**, 17-19.

ENGLAND P. & MOLNAR P. (1990) – *Surface uplift, uplift of rocks, and exhumation of rocks*. Geology, **18**, 1173-1177.

ERSHOV A.V. & NIKISHIN A. M. (2004) – *Recent geodynamics of the Caucasus-Arabia-East Africa region*. Geotectonics, **38 (2)**, 123-136.

FACCENNA C., BELLIER O., MORTINOD J., PIROMALLO C. & REGARD V. (2006) – *Slab detachment beneath eastern Anatolia: a possible cause for the formation of the North Anatolian fault*. Earth Plan. Sci. Lett., **242**, 85-97.

FEDERICI I., CAVAZZA W., OKAY A.I., BEYSSAC O., ZATTIN M., CORRADO S. & DELLISANTI F. (2010) – *Thermal evolution of the Permo-Triassic Karakaya subduction-accretion complex from the Biga Peninsula to the Tokat Massif (Anatolia):* Turkish. J. of Earth Sci., **13**, 201-213.

FLEISCHER R.L. & PRICE P.B. (1964) – *Glass dating by fission fragments tracks*. J. Geophys. Res., **69**, 331-339.

FLEISCHER R.L., PRICE P.B. & WALKER R.M. (1965) – *The ion explosion spike mechanism for formation of charged particle tracks*. J. Appl. Phys., **36**, 3645-3652.

FLEISCHER R.L., PRICE P.B., WALKER R.M. & HUBBARD E.L. (1967) – *Criterion for registration in dielectric track detectors*. Phys. Rev., **156**, 353-355.

FLEISCHER R.L., PRICE P.B. & WALKER R.M. (1975) – *Nuclear tracks in solids; Principles and applications*. University of California Press, Berkeley, 605 pp.

FORTE A., COWGILL E., BERNARDIN T., KREYLOS O. & HAMANN B. (2010) – *Late Cenozoic deformation of Kura fold-thrust belt, southern Greater Caucasus.* Geo. Soc. Am. Bull, **122**, 465-486.

GALBRAITH R.F. (1981) – *On statistical models for fission tracks counts.* Math. Geol. **13**, 471-478.

GALBRAITH R.F. (1984) – *On statistical estimation in fission-track dating.* Math. Geol. **16**, 653-669.

GALBRAITH R.F. & LASLETT G.M. (1985) – *Some remarks on statistical estimation in fission track dating.* Nucl. Tracks., **10**, 361-363.

GALBRAITH R.F. (1988) – *Graphical display of estimates having different standard errors.* Technometrics, **30**, 271-281.

GALBRAITH R.F. (1990) – *The radial plot: graphical assessment of spread in ages.* Nucl. Tracks Radiat. Meas., **17**, 207-214.

GALBRAITH R.F. & LASLETT G.M. (1992) – *Statistical models for mixed fission-track ages.* Nucl. Tracks. Radiat. Meas., **21**, 459-470.

GALBRAITH R.F. (1998) – *The trouble with probability density plots of fission-track ages.* Radiat. Meas., **29**, 421-435.

GALLAGHER K. (1995) – *Evolving temperature histories from apatite fission-track data.* Earth Plan. Sci. Lett., **136**, 125-131.

GALOYAN G., ROLLAND Y., SOSSON M., CORSINI M. & MELKONIAN R. (2007) – *Evidence for superposed MORB, oceanic plateau and volcanic arc series in the Lesser Caucasus (Stepanavan, Armenia)*. Comptes Rendus Geosciences, **339**, 482-492.

GLEADOW A.J.W. & LOVERING J.F. (1978) – *Thermal history of granitic rocks from Western Victoria: a fission-track dating study*. J. Geol. Soc. Austral., 2**5,** 323-340.

GLEADOW A.J.W. & DUDDY I.R. (1981) – *A natural long-term track annealing experiment for apatite*. Nucl. Tracks, **5,** 169-174.

GLEADOW A.J.W., DUDDY I.R., GREEN P.F. & LOVERING J.F. (1986) – *Confined fission track lengths in apatite: a diagnostic tool for thermal history analysis*. Contrib. Min. Pet., **94,** 405-415.

GÖK R., SANDVOL E., TÜRKELLI N., SEBER D. & BARAZANGI M. (2003) – *Sn attenuation in the Anatolian and Iranian plateau and surrounding regions.* Geo. Res. Lett., **30-24**, p. 8042.

GÖK R., PASYANOS M. & ZOR E. (2007) – *Lithospheric structure of the continent-continent collision zone: Eastern Turkey.* Geo. J. Int. , **169**, 1079-1088.

GÖK R., MELLORS R.J., SANDVOL E., PASYANOS M., HAUK T., YETIRMISHLI G., TEOMAN U., TURKELLI N., GODOLADZE T. & JAVAKISHVIRLI Z. (2009) – *Lithospheric velocity structure of the Anatolian Plateau-Caucasus-Caspian regions.* Lawrence Livermore National Laboratory, 11 p.

GREEN P.F. & DURRANI S. A. (1977) – *Annealing studies of tracks in crystals.* Nucl. Track Det., **1**, 33-39.

GREEN P.F. (1981) – *A new look at statistics in fission track dating*. Nucl. Track, **5**, 77-86.

GREEN P.F. (1985) – *Comparison of zeta calibration baselines for fission-track dating of apatite, zircon and sphene.* Chem. Geol. (Isot. Geosci. Sect.), **58**, 1-22.

GREEN P.F., DUDDY I.R., GLEADOW A.J.W., TINGATE P.R. & LASLETT G.M. (1985) – *Fission track annealing in apatite: Track length measurements and the form of the Arrhenius plot.* Nucl. Tracks, **10**, 323-328.

GREEN P.F., DUDDY I.R., GLEADOW A.J.W., TINGATE P.R. & LASLETT G.M. (1986) – *Thermal annealing of fission-track in apatite: 1.A qualitative description.* Chem. Geol. (Isot. Geosci. Sect.), **59**, 237-253.

GREEN P.F., DUDDY I.R., LASLETT G.M., HEGARTY K.A., GLEADOW A.J.W. & LOVERING J.F. (1989) – *Thermal annealing of fission-track in apatite: 4. Quantitative modelling techniques and extension to geological timescales.* Chem. Geol. (Isot. Geosci. Sect.), **79**, 155-182.

GÖĞÜŞ O.H. & PYSKLYWEC R.N. (2008) – *Mantle lithosphere delamination driving plateau uplift and synconvergent extension in the Eastern Anatolia.* Geology, **36 (9)**, 723-726.

GÜLEÇ N., HILTON D.R. & MUTLU H. (2002) – *Helium isotope variations in Turkey: relationship to tectonics, volcanism and recent seismic activities*. Chemical Geology, **187**, 129-142.

HADLER J.C., LATTES C.M.G., MARQUES A., MARQUES M.D.D., SERRA D.A.B & BIGAZZI G. (1981) – *Measurement of the spontaneous fission disintegration constant of ^{238}U*. Nucl. Tracks, **5,** 45-52.

HALL R. (1976) – *Ophiolite emplacement and the evolution of the Taurus suture zone, southeastern Turkey*. Geol. Soc. Am. Bull., **87**, 1078-1088.

HAMMERSCHMIDT K., WAGNER G.A. & WAGNER M. (1984) – *Radiometric dating on research drill core Urach III: a contribution to its geothermal history*. J. Geop., **54**, 97-105.

HARZHAUSER M. & PILLER W.E. (2007) – *Benchmark data of a changing sea-Palaeogeography, Palaeobiogeography and events in the Central Paratethys during the Miocene: Palaeogeography, Palaeoclimatology*. Palaeoecology, **253**, 8-31.

HOLDSWORTH R.E., BUTLER C.A. & ROBERTS A.M. (1997) – *The recognition of reactivation during continental deformation.* Jou. Geol. Soc. Lon., **154**, 73-78.

HURFORD A.J. & GREEN P.F. (1981) – *A reappraisal of neutron dosimetry and uranium-238 λ_f decay values in fission-track dating*. Nucl. Tracks, 53-61.

HURFORD A.J. & GREEN P.F. (1982) –*A users' guide to fission track dating calibration.* Earth Plan. Sci. Lett., **59**, 343-354.

HURFORD A.J. & GREEN P.F. (1983) – *The zeta age calibration of fission-track dating*. Is. Geo., **1**, 285-317.

HURFORD A.J., FITCH F.J. & CLARKE A. (1984) – *Resolution of the age structure of the detrital zircon populations of two Lower Cretaceous sandstones from the Weald of England by fission track dating*. Geol. Mag., **121**, 269-277

HURFORD A.J. (1990) – *Standardization of fission track dating calibration: recommendation by the Fission Track Working Group of the I.U.G.S. Subcommission and Geochronology .* Chem. Geol. (Isot. Geosci. Sect.), **80**, 171-178.

HURFORD A.J. (1998) – *Zeta: the ultimate solution of fission-track analysis calibration of just an interim measure?.* In: Van Den Haute P. & De Corte F. (eds.) – *Advances in fission-track geochronology.* Kluwer, Dordrecht, 19-32.

JACKSON J. & MCKENZIE D. (1988) – *The relationship between plate motions and seismic moment tensors, and the rates of active deformation in the Mediterranean and Middle East*. Geo. J.-R. Ast. Soc., **93**, 45-73.

JACKSON J. & AMBRESEYS N. (1997) – *Convergence between Eurasia and Arabia in Eastern Turkey and the Caucasus. Historical and Prehistorical Earthquakes in the Caucasus*. Kluwer Academic Publisher, 79-90.

JOLIVET L. & FACCENNA C. (2000) – *Mediterranean extension and the Africa-Eurasia collision*. Tectonics, **19**, 1095-1106.

JONCKHEERE R. (1997) – *Slightly longer tracks: heavy liquid separations and beware of the dreaded TININC's*. On Track, **7/2,** 8-9.

KADINSKY-CADE K., BARAZANGI M., OLIVER J. & ISACKS B. (1981) – *Lateral variations of high frequency seismic wave propagations at regional distances across the Turkish-Iranian plateau*. J. Geo. Res, **86,** 9377-9396.

KAYMAKCI N., ALDAMAZ E., LANGERIS C., SPELL T.L., GURER O.F., ZANETTI K.A. (2007) – *Late Miocene transcurrent tectonics in NW Turkey: evidence from paleomagnetism and ^{40}Ar-^{39}Ar dating of alkaline volcanic rocks* Geol. Mag., **144**, 379-392.

KARAKHANIAN A. & JRBASHYAN R. (2004) – *Active volcanoes and volcanic hazard in the Armenian Highland and adjacent areas.* Izvestia NAS of RA**, LVII,** 3-24.

KESKIN M., PEARCE J.A. & MITCHELL J.G. (1998) – *Volcano-stratigraphy amd geochemistry of collision-related volcanism on the Erzurum-Kars Plateau, North Eastern Turkey*. J. Volc. Geo. Res., **85**, 355-404.

KESKIN M. (2003) – *Magma generation by slab steepening and breakoff beneath a subduction-accretion complex: an alternative model for collision-related volcanism in Eastern Anatolia, Turkey*. Geo. Res. Lett., **30**, 1-4.

KETCHAM R.A. (2005) – *Forward and inverse modelling of low-temperature thermochronometry.* Rev. Min. & Geoch., **58**, 275-314.

KETCHAM R.A., DONELICK R.A., BALESTRIERI M.L. & ZATTIN M. (2009) – *Reproducibility of apatite fission-track length and thermal history reconstruction.* Earth Plan. Sci. Lett., **284**, 504-515.

KETIN I. (1948) – *Über die tektonisch-mechanischen Folgerungen aus den grossen anatolischen Erdbeben des letzten Dezenniums*. Geol. Rund., **36**, 77-83.

KHAIN V.E. (1975) – *Structure and main stages in the tectono-magmatic development of the Caucasus: an attempt at geodynamic interpretation*. A. J. Sci., **25-A**, 131-156.

KHAN H.A. & DURRANI S. A. (1972) – *Efficiency calibration of solid state nuclear track detectors*. Nucl. Instr. Meth, **98**, 229-236.

KNIPPER A.I. (1975) – *The oceanic crust in the structure of the Alpine folded Belt (South Europe, western part of Asia and Cuba)*. Transactions, **267,** Moscow "Nauca" (in Russian).

KOCYĞIT A., YILMAZ A., ADAMIA S. & KULOSHVILI S. (2001) – *Neotectonics of East Anatolian Plateau (Turkey) and Lesser Caucasus: implications for transition from thrusting to strike-slip faulting.* Geodinamica Acta, **14**, 177-195.

KONAK N. & HAKYEMEZ H.Y. (2001) – *Tectonic units of the easternmost part of the Pontides: stratigraphical and structural implications*. Proceedings of the 2nd Int. Symp. On the Petroleum Geology and Hydrocarbon potential of the Black Sea Area, pp. 93-103. Turk. Ass. Pet. Geo., Spec. Publ. 4.

KONAK N., OKAY A.I. & HAKYEMEZ Y (2009) – *Tectonics and stratigraphy of the Eastern Pontides.* Field Trip Guide Book, 2nd International Symposium Geology of Black Sea Region, pp. 113.

KOWALLIS B.J., HEATON J.S. & BRINGHURST K. (1986) – *Fission-track dating of volcanically derived sedimentary rocks.* Geology, **14**, 19-22.

LEI J. & ZHAO D. (2007) – *Teleseismic evidence for a break-off subducting slab under eastern Turkey.* Earth and Plan. Sci.Lett., **257**, 14-28.

LORDKIPANIDZE M., MELIKSETIAN B. & DJERBASHIAN R. (1988) – *Mesozoic-Cenozoic magmatic evolution of the Pontian-Crimean-Caucasian region*. Mém. Soc. Geo. Fr., **154**, 103-124.

MCCLUSKY S., BALASSANIAN S., BARKA A., DEMIR C. (2000) – *GPS constraints on plate kinematics and dynamics in the eastern Mediterranean and Caucasus.* J. Geophys. Res., **105**, 5695-5719.

MCKENZIE D.P. (1972) –*Active tectonics of the Mediterranean region.* Geophys. J. Astron. Soc., **30**, 85-109.

MILANOVSKI E.E. (1968) – *Neotectonics of the Caucasus*. Nedra, Moscow, p. 484 (in Russian).

MOORES E. M. & FAIRBRIDGE R.W. (1982) – *Encyclopedia of European and Asian Regional Geology*, pp.26-34.

NAESER C.W. & FAUL H. (1969) – *Fission track annealing in apatite and sphene*. J. Geophy. Res., **74,** 750-710.

NAESER C W., IZETT G.A. & OBRADOVICH J.D. (1980) – *Fission-track dating and K-Ar ages for natural glasses*. U.S. Geo. Surv. Bull., **1849,** 1-31.

NAESER C.W., MCKEE E.H., JOHNSON N.M. & MACFADDEN B.J. (1987) – *Confirmation of a late Oligocene-early Miocene age of Deseadan Salla beds of Bolivia*. J. Geol., **74,** 825-828.

OKAY A.I. (2008) – *Geology of Turkey: A Synopsis*. Anschnitt, **21 (1)**, 19-42.

OKAY A. I., İZVER T. & OKAN T (2001) –*Obduction, subduction and collision as reflected in the Upper Cretaceous – Lower Eocene sedimentary record of western Turkey.* Geol. Mag., **138 (2)**, 117-142.

OKAY A.I. & MOSTLER H. (1994) – *Carboniferous and Permian radiolarite blocks from the Karakaya Complex in northwest Turkey.* Tur. J. Earth Sci., **3**, 595-598.

OKAY A.I. & ŞAHINTÜRK Ö. (1997) – *Geology of the Eastern Pontides*. In: A. Robinson (eds.) *Regional and Petroleum Geology of the Black Sea and surrounding regions.* Ass. Petr. Geo., Memoir **68**, 291-311.

OKAY A.I., SATIR M., MALUSKI H., SIYAKO M., MONIE P., METZGER R. & AKYÜZ S. (1996) – *Paleo- and Neo-Tethyan events in the northwestern Turkey: geological and geochronological constrains*. In: A. Yin & M. Harrison (eds.). *Tectonics of Asia.* Cambridge University Press, 420-441.

OKAY A.I. & TÜYSÜZ O. (1999) –*Tethyan sutures of northern Turkey*. In: Duran B., Jolivet L., Horvàth F. & Séranne M. (eds). *The Mediterranean Basin: Tertiary Extention within the Alpine Orogen*. Geol. Soc. London, Spec. Publ., **156**, 475-515.

OKAY A.I., TÜYSÜZ O. & ŞINASI K. (2004) – *From transpression to transtension: changes in morphology and structure around a bend on the North Anatolian Fault in the Marmara region*. Tectonophysics, **391**, 259-282.

OKAY A.I., TÜYSÜZ O., SATIR M., ÖZAN-ALTINER S., ALTINE D., SHERLOCK S. & EREN R.H. (2006) – *Cretaceous and Triassic subduction-accretion, HP/LT metamorphism and continental growth in the Central Pontides, Turkey*. Geol. Soc. Am. Bull., **118**, 1247-1269.

OKAY A.I., ZATTIN M. & CAVAZZA W. (2010) – *Apatite fission-track data for the Miocene Arabia-Eurasia collision*. Geology, **38**, 35-38.

PEARCE J.A., BENDER J.F., DELONG S.E., KIDD W.S.F., LOW P.J., GUNER Y., ŞARAOĞLU F., YILMAZ Y., MOORBARTH S. & MITCHELL J.J. (1990) – *Genesis of collision volcanism in eastern Anatolia, Turkey*. J. Vol. Geo. Res., **44**, 189-229.

PEIVE A.V., KHAIN V.E., MOURATOV M.V. & DELANY F. (1982) – *Tectonics of Europe and Adjacent Areas*. Explanatory notes to the International Tectonic Map of Europe and Adjacent Areas, scale 1:2,500,000. Nauka Publishing House, Moscow, two volumes, 415+627 p.

PHILIP H., AVAGYAN A., KARAKHANIAN A., RITZ J-F. & REBAI S. (2001) – *Estimating slip rates and recurrence intervals for strong earthquakes along an intracontinental fault: example of the Pembak-Sevan-Sunik fault (Armenia)*. Tectonophysics, **343**, 205-232.

PODGOROSKY J., HEARN E., MCCLUSKY S., REILINGER R., TAYMAZ T., TAN O., PRILEPIN M., GUSEVA T. & NADARIYA M. (2007) – *Postseismic deformation following the 1991 Racha, Georgia earthquake.* Geophy. Res. Lett., **34**, 1-5.

REILINGER R., MCCLUSKY S. & SOUTER B. (1997) – *Preliminary estimates of plate convergence in the Caucasus collision zone from global positioning system measurements* . Geophy. Res. Lett., **24**, 1815-1818.

REILINGER R., MCCLUSKY S., VERNANT P., LAWRENCE S., ERGINTAV S., CAKMAK R., OZENER H., KADIROV F., GULIEV I., STEPANYAN R., NADARIYA M., HAHUBIA G., MAHMOUD S., SAKR K., ARRAJEHI A., PARADISSIS D., AL-AYDRUS A., PRILEPIN M., GUSEVA T., EVREN E., DMITROTSA A., FILIKOV S.V., GOMEZ F., AL-GHAZZI R. & KARAM G. (2006) –*GPS constrains on continental deformation in the Africa-Arabia-Eurasia continental collision zone and implications for the dynamics of plate interections*. J. Geophy. Res., **111**, 1-26.

REIMER G.M. & WAGNER G.A. (1971) – *Fission-track studies of alpine epidotes and garnets*. Ann. Soc. Geol. Bel., **94**, 127pp.

REINERS P.W. & BRANDON M.T. (2006) – *Using thermochronologic to understand orogenic erosion*. Ann. Rev. Earth Planet. Sci., **34**, 419-466.

RING U., BRANDON M.T., WILLET S.D. & LISTER G.S. (1999) – *Exhumation processes.* Geol. Soc. Lond. Spec. Publ. **154**, 1-27.

ROBERTS J.H., RUDDY F.H. & GOLD R. (1984) – *Optical efficiency for fission fragment track counting in muscovite solid state detectors*. Nucl. Tracks Radiat. Meas., **8**, 365-369.

ROBERTSON A.H.F., PARLAK O., RIZAOĞLU T., ÜNLÜGENÇ Ü., INAN N., TASLI K. & USTAÖMER T. (2007) – *Tectonic evolution of the South Tethyan ocean: evidence from the Eastern Taurus Mountains (Elaiğ* REGION, *SE Turkey*). In: Ries A.C. Butler R.W.H. & Graham R.H. (eds). *Deformation of continental crust*, Geol. Soc. Lon., Spec. Publ., **272**, 231-270.

ROBINSON A.G., BANKS C.J., RUTHERFORD M.M. & HIRST J.P.P. (1995) – *Stratigraphic and structural development of the Eastern Pontides, Turkey*. J. Geo. Soc. London, **152**, 861-872.

RODGERS A.J., NI J.F. & HEARN T.M. (1997) – *Propagation characteristics of short-period Sn and Lg in the Middle East.* Bull. Seismo. Soc. Am., **87 (2)**, 396-413.

ROLLAND Y., BILLO S., CORSINI M., SOSSON M. & GALOYAN G. (2007) – *Blueschists of the Amassia-Stepanavan Suture Zone (Armenia): linking Tethys subduction history from E-Turkey to W-Iran*. Int. J. Earth Sci., **98**, 533-550.

ROLLAND Y., GALOYAN G., BOSCH D., SOSSON M., CORSINI M., FORNARI M. & VÉRATI C. (2009) – *Jurassic back-arc and hot-spot related series in the Armenian ophiolites – implications for the obduction process*. Lithos, **112**, 163-187.

SAINTOT A., BRUNET M.F., YAKOVLEV F., SÉBRIER M., STEPHENSON R., ERSHOV A., CHALOT-PRAT F. & MCCANN T. (2006) – *The Mesozoic-Cenozoic tectonic evolution of the Greater Caucasus*. Geol. Soc. Lon. Mem., **32**, 277-289.

SANDVOL E., AL-DAMEGH K., COLVERT A., SEBER D., BARAZANGI M., MOHAMAD R., GÖK R., TURKELLI N. & GURBUZ C. (2001) – *Tomographic imaging of Lg and Sn propagation in the Middle East.* Pure & Applied Geophysics, **158**, 1121-1163.

ŞENGÖR A.M.C. & KIDD W. S. F. (1979) – *The post-collisional tectonics of the Turkish-Iranian Plateau and a comparison with Tibet .* Tectonophysics, **75**, 181-241.

ŞENGÖR A.M.C & YILMAZ Y (1981) – *Tethyan evolution of Turkey, a plate tectonic approach*. Tectonophysics, **75**, 181-241.

ŞENGÖR A.M.C., YILMAZ Y. & SUNGURLU O. (1984) – *Tectonics of the Mediterranean Cimmerides: nature and evolution of the western termination of Palaeo-Tethys*. In: Dixon J.E., Robertson A.H.F. (eds.), Geological Evolution of the Eastern Mediterranean. Geo. Soc. Lond. Spec. Publ., **17**, 77-112.

ŞENGÖR A.M.C , GÖRÜR N. & ŞAROĞLU F. (1985) – *Strike-slip faulting and related basin formation in zones of tectonic escape: Turkey as a case study*. In: Bibble K.D. & Christie-Blick N. (eds). *Strike-slip deformation, basin formation and sedimentation.* Soc. Ec. Pal. Min. Spec. Publ., **17**, 227-274.

ŞENGÖR A.M.C & YILMAZ A (2003) – *East Anatolian high plateau as a mantle-supported, North-South shortened domal structure*. Geophy. Res. Lett., **30 (24)**, 1-8.

ŞENGÖR A.M.C, TÜYSÜZ O., IMREN C., SAKINÇ M., EYDOĞAN H., GÖRÜR N., LE PICHON X & RANGIN C. (2005) – *The North Anatolian Fault: a new look*. Ann. Rev. Earth Planet. Sci., **33**, 37-112.

ŞENGÖR A.M.C., ÖZEREN M.S., KESKIN M., SAKINÇ M., ÖZBAKIR A.D. & KAYAN I. (2008) – *Eastern Turkish high plateau as a small Turkic-type orogen: implications for*

post-collisional crust-forming processes in Turkic-type orogens. Earth Sciences Reviews, **90**, 1-48.

SEYMEN I, AYDIN A. (1972) – *The Bingöl earthquake fault and its relation to the North Anatolian Fault Zone*. Bull. Miner. Res. Explor. Inst., **79**, 1-8.

SOSSON M., ROLLAND Y., MÜLLER C., DANELIAN T., MELKONYAN R., KEKELIA S., ADAMIA S., BABAZADEH V., KANGARLI T., AVAGYAN A., GALOYAN G. & MOSAR J. (2010) – *Subductions, obduction and collision in the Lesser Caucasus (Armenia, Azerbaijan, Georgia), new insights.* Geol. Soc. Lond. Spec. Publ., **340,** 329-352.

STEIGER R.H. & JÄGER E. (1977) – *Subcommission on geochronology: convention on the use of decay constants in geo-and cosmochronology*. Earth Planet. Sci. Lett, **36,** 359-362.

STEPHENSON R., MART Y., OKAY A.I., ROBERTSON A.H.F., SAINTOT A., STOVBA S. & KHRIACHTCHEYSKAYA O. (2004) – TRANSMED Transect VIII. In: Cavazza W., Roure F., Spakman W., Stampfli G.M. & Ziegler P. (eds). *The TRANSMED Atlas: The Mediterranean region from Crust to Mantle.* Springer Verlag. pp. 141 + CD-ROM.

SUNAL G., NATAL'IN B., SATIR M. & TORMAN E. (2006) –*Paleozoic magmatic events in the Strandja Massif, NW Turkey.* Geodinamica Acta, **19**, 283-300.

TOMBRELLO T.A. (1984a) – *The dimension of latent ion damage tracks*. Nucl. Instr. Meth, **B1**, 23-25.

TOMBRELLO T.A. (1984b) – *Track damage and erosion of insulators by ion-induced electronic processes*. Nucl. Instr. Meth, **B2**, 553-563.

USTAÖMER T. & ROBERTSON A.H.F (2005) – *Late Paleozoic marginal basin and subduction-accretion: the Paleotethyan Küre Complex, Central Pontides, northern Turkey.* J. Geo. Soc. Lon., **151,** 291-305.

UYSAL T.I., MULTU H., ALTUNEL E., KARABACAK V. & GOLDING S.D. (2006) – *Clay mineralogy and isotopic (K-Ar, $\delta^{18}O$, δD) constraints on the evolution of the North Anatolian Fault Zone, Turkey* . Earth Plan. Sci. Lett., **243,** 181-194.

VAN DEN HAUTE P., DE CORTE F., JONCKHEERE R & BELLEMANS F. (1998) – *The parameters that govern the accurancy of fission-track age determinations: a pre-appraisal*. In: Van Den Haute P. & De Corte F (eds.). *Advances in fission-track geochronology*. Kluwer, Dordrecht, 33-46.

WAGNER G. A. & REIMER G.M. (1972) – *Fission track tectonics: the tectonic interpretation of fission track apatite ages*. Trans. Amer. Nucl. Soc., **15**, 117-127.

WAGNER & VAN DEN HAUTE P. (1992) – *Fission-track dating*. Kluwer, Dordrecht, 286 pp.

WALL T. (1986) – *Use of an alternative neutron dosimetry standard for fission track dating.* Nucl. Tracks Rad. Meas. **12**, 887-890.

WATT S. & DURRANI S.A. (1985) – *Thermal stability of fission track in apatite and sphene: using confined track length measurement*. Nucl. Tracks., **10**, 349-357.

YADA K., TANJI T. & SUNAGAWA I. (1981) – *Application of lattice imagery to radiation damage investigation in natural zircon*. Phys. Chem. Minerals, **7**, 47-52.

YADA K., TANJI T. & SUNAGAWA I. (1987) – *Radiation induced lattice defects in natural zircon ($ZrSiO_4$) observed at atomic resolution*. Phys. Chem. Minerals, **14**, 197-204.

YIĞITBAŞ E & YILMAZ Y. (2004) – *New evidence and solution to the Maden complex controversy of the Southeast Anatolian orogenic belt (Turkey).* Geologische Rundschau, **85**, 250-263.

YILMAZ Y., ŞAROĞLU F. & GÜNER Y. (1987) – *Initiation of the neomagmatism in East Anatolia*, Tectonophysics, **134**, 177-199.

YILMAZ Y. (1990) – *Comparison of young volcanic associations of western and eastern Anatolia under compressional regime: a review*. J. Soc. Vol. Geo. Res., **44**, 69-87.

YILMAZ Y. (1993) – *New evidence and model on the evolution of the southeast Anatolian orogen*, Geol. Soc. Am. Bull., **105**, 251-271.

YILMAZ A., ADAMIA S., CHABUKIANI A., CHKHOTUA T., ERDOĞAN K., TUZCU S., KARABIYIKOĞLU M. (1999) – *Structural correlation of the southern Transcaucasus (Georgia)-Eastern Pontides (Turkey).* In: *Tectonics and magmatism in Turkey and surrounding area*, (Eds.) E.Bozkurt, J.A. Winchester & J.A.D Piper, Geol. Soc. London Spec. Publ., **173**, 171-182.

ZAKARIADZE G., DILEK Y., ADAMIA S.H., OBERHÄNSLI R., KARPENKO S., BAZYLEV B & SOLOV'EVA N. (2007) – *Geochemistry and geochronology of the Neoproterozoic Pan-African Transcaucasian Massif (Republic of Georgia) and implication for island-arc evolution of the late Precambrian Arabian-Numbian Shield*. Godwana Research, **11**, 97-108.

ZATTIN M., OKAY A.I., CAVAZZA W. (2005) – *Fission track evidence for late Oligocene and mid-Miocene activity along the North Anatolian Fault in south western Thrace*. Terra Nova, **17**, 95-101.

ZATTIN M., ANDREUCCI B., JANKOWSKI L., MAZZOLI S. & SZANIAWSKY R. (2011) – *Neogene exhumation in the Outer Western Carpathians*. Terra Nova, **23**, 283-291.

ZATTIN M., CAVAZZA W., OKAY A.I. FEDERICI I., FELLIN M.G., PIGNALOSA A. & REINERS P. (2010) – *A precursor of the North Anatolian Fault in the Marmara Sea region*. J. Asian Earth Sci., **39**, 97-108.

ZIMMERMAN R.A. & GAINES A.M. (1978) – *A new approach to the study of fission track dating*. U.S. Geological Survey Open File Report, **78-701**, 467-468.

ZOR E., SANDVOL E., GURBUZ C., TURKELLI N., SEBER D. & BARAZANGI M. (2003) – *The crustal structure of the East Anatolian Plateau from receiver functions.* Geo. Res. Lett., **30**, p. 8044.

Appendix A

FISSION-TRACK DATING METHOD

A.1 NUCLEAR FISSION

Nuclear fission is one of the several modes of disintegration which occur among heavy nuclides of atomic mass $\geq$230 and atomic number $\geq$90. These nuclides are isotopes of elements of actinide series (Th, Pa, U, Np, Pu, etc.), most of which also disintegrate by other processes such as a-decay. Between them, only 232Th and two isotopes of U (^{235}U and ^{238}U) occur in appreciable concentrations in natural substances. Nevertheless, most of the tracks are produced by ^{238}U, which in the most abundant isotope in the U series. Moreover, its half-life for the fission and the a-decay are relatively shorter, as displayed in table A.1.

	Relative abundance (compared to ^{235}U)	Total half-life (years)	Spontaneous fission half-life (years)
^{232}Th	4	1.40×10^{10}	1.0×10^{21}
^{235}U	7.25×10^{-3}	7.04×10^{8}	1.0×10^{19}
^{238}U	1	4.47×10^{9}	8.2×10^{15}

Table A.1 - Abundances and half-lives of three major naturally occurring nuclides suffering spontaneous fission.

Examples of fission reactions are:

^{235}U + n -- ^{236}U-- ^{93}Br + ^{141}La + 2n

^{235}Cf + n -- ^{108}Rb-- ^{93}Br + ^{140}Xe + 4n

Most of the fission reactions produce two fragments, which, as shown by the reported examples, can have different atomic masses (Fig. A.1). In some cases, the heavy fragments can have a mass twice the mass of the light fragments.

A.2 STRUCTURE OF THE FISSION-TRACK

When the heavy charged particle produced by a nuclear fission travels trough a crystal, it will produce a damage zone in the lattice (*latent fission-track*). The size of the track can be extremely variable, ranging from less of 1 mm to some mm according to the charge and the kinetic energy of the particle and to the damage solid. In most of cases, the track width is of some nm and it is not observable under a normal optical microscope. The only way to see the latent tracks is by using either transmission electron microscope (TEM) or some high-resolution electron microscopes (HRTEM; Yada et al., 1987). These observations give the possibility to see that the crystal lattice is completely destroyed in the track core, for a width of 5 nm or less, surrounded by less damaged zones, which may extended up to 10 nm. The images of Yada et al. (1981, 1987) show almost amorphous state of low density in the core of the track. The lattice planes appear to be strained at their intersection with the tracks whereas point defects are observed around the track ends.

X-ray scattering experiments carried out on mica and olivine (Dartyge et al., 1978, 1981) seem to indicate an intermittent or discontinuous character of the latent track. These experiments suggest the presence of two types of defects: *extended defects* and *point defects* (Fig. A.2). The extended defects, with a width of 15-40 Å, are zones of high density of point defects and are connected by low-density defects zones (gaps). The distance between two extended defects is about 200 Å (Dartyge et al., 1981). They have demonstrated that the track has essentially a continuous structure which can be described as a long uninterrupted cylinder with a Gaussian radial density variation

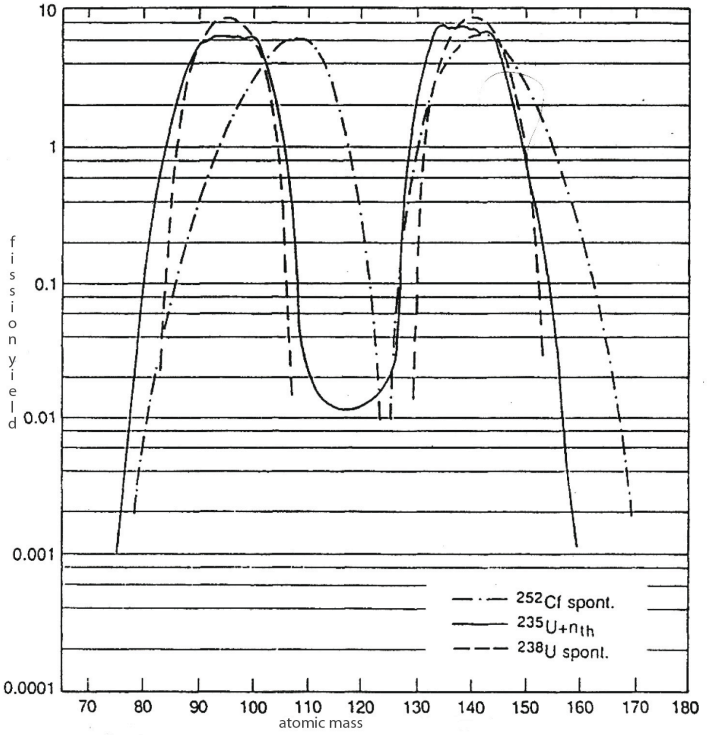

Fig. A.1 - Mass distribution curves of fission fragments for the thermal neutron induced fission of ^{235}U and for the spontaneous fission of ^{238}U and ^{252}Cf (After Wagner & Van den Haute, 1992).

.

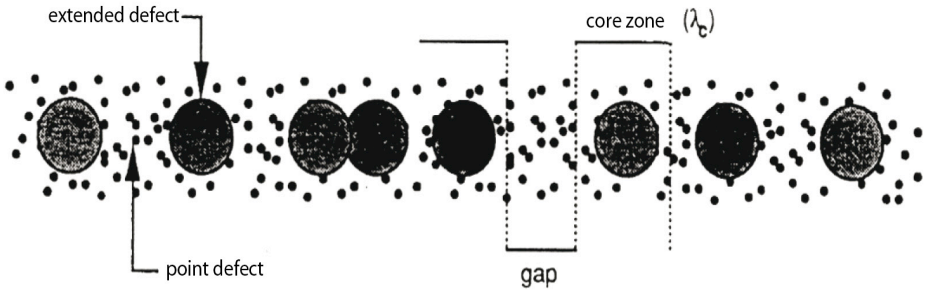

Fig. A.2 - Schematic structure of a charged particle track (Dartyge et al., 1981).

Whereas the discontinuous nature of the tracks has not yet been truly demonstrated, the normal optical observation on mica and apatite seem to indicate an irregular track etching behaviour, especially when a thermal treatment was applied before etching. During heating at low temperatures, only point defects are removed, leaving undamaged zones between extended defects. The whole problem is very important, above all after the recent increasing use of

the track-size measurements in order to retrieve information on the cooling history of the rocks.

A.3 TRACK FORMATION PROCESSES

Nuclear fission track is an exoenergetic process and occurs both spontaneously and artificially by bombardment with neutrons, protons or other particles. Each reaction produces a large amount of energy (210 MeV) in form of fission fragments, neutrons and g-rays. Part of this energy (about 170 MeV) is liberated in form of kinetic energy because of the Coulomb repulsion between the just formed nuclides. Part of remnant energy is transferred to the neutrons released during fission, which are capable of producing new fission of other heavy nuclei. The kinetic energy is about the same in two fragments which have, as a previously discussed, different masses. As the kinetic energy is proportional to the mass of the particle, it follows that the lighter fragment will be the fastest and it will travel for a longer distance before stopping. As a consequence, track centre will not coincide with the original position of the U atom.

Speed of produced fragments is 3-5% of the light speed but it is sufficient to exceed the orbital electrons speed. Hence some electrons are lost by the fission fragments which become positive ions. Interactions can be of two types: collision with the lattice then gradually stop the charged ions. These interactions can be of two types: collision with the lattice atoms or interactions with the host electrons. The elastic collision is very rare event, considering the reduced dimension of the *nucleo* compared with the atom one, but it prevails at low energy. At high energy, the second mechanism is more probable. High-ionized fragments, along their

pathway, can excite electrons to higher levels or cause their exit from the orbit as d-rays. The described process is the base of the so-called *ionization spike model*, proposed for the first time by Fleischer et al. (1965, 1967, 1975). It can be summarized into three steps (Fig. A.3):

- the charged particles induce ionization through electronic interactions in the lattice of the solid;
- the adjacent ions repulse each other into interstitial positions, leaving a series of vacancies along pathway;
- the local lattice stress is spread by elastic relaxation.

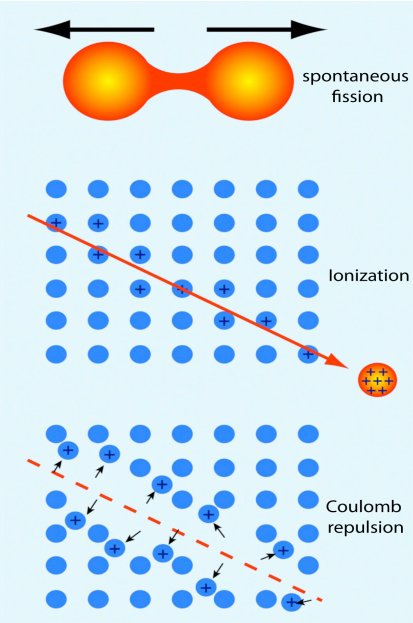

Fig. A.3 - The three stages of track formation according to the "ionization spike model" (redrawn after Fleischer et al., 1975).

A confirmation of this theory is offered by the fact that tracks are only formed in insulators and not conductors, where the lattice ions would be immediately neutralized, before action of the Coulomb repulsion. This theory, however, does

not account for possible discontinuities in the track structure, as previously described. In fact, if two different types of defect exist, then two different ionization processes have to be involved in track formation. A possible solution is the presence of sites along the particle pathway where electrons are tightly bound to the lattice atoms (Trombrello, 1984a, b). Chadderton et al. (1988) argue that the intermittent character of the tracks is a consequence of the discontinuities of the crystal lattice, especially in minerals with layered structure.

A.4 CHEMICAL ETCHING

A direct of the latent track is only possible with transmission electron microscope (TEM). In order to render the tracks visible under a normal optical microscope, several techniques have been developed. These are destructive methods which exploit the damage along the track as preferred site for removal of detector material by a chemical etching. In consequence, only tracks which intersect or are connected with the etched surface can be removed. Etching consist in a simple immersion of the crystal in an appropriate chemical reagent which is able to dissolve more efficiently sites at higher free energy, that is along the latent tracks.

Generally, etching rate along tracks (V_T) is higher than be general or bulk etching rate (V_G). As illustrated in Fig. A.4, track length after a time t will be (Fleischer et al., 1975):

$$l = (Vt - Vg)\, t \quad (1)$$

The angle q indicated in Fig. 4a will be given by:

$$\theta = \arcsin(Vt/Vg) \quad (2)$$

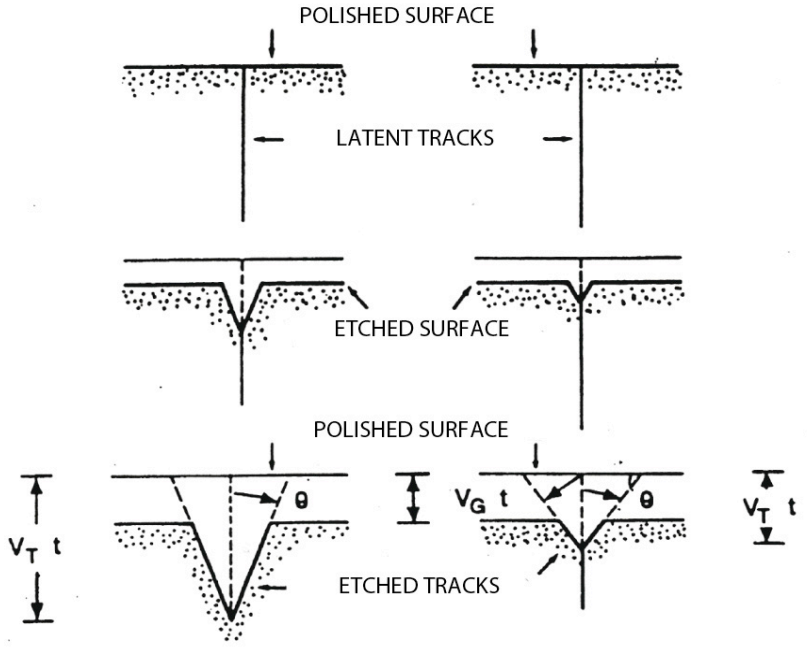

Fig. A.4 - Schematic illustration of the development of normally incident etched tracks when VT and VG are constant. Top: Unattached (latent) tracks. Middle: partially etched tracks. Bottom: left track fully etched. The track etch velocity (VT) for the track on the left is larger than that for the track on the right; as consequence, the track on the right has a larger cone angle (Crowley et al., 1991).

The ratio V_T/V_G is characteristic for each kind of mineral and etching reagent. V_T is usually much higher than V_G (by a factor 10 or more), which is very variable in relation to the crystallographic orientation of the etched surface. In apatite, the etching rate on the prismatic planes which contain the c-axis is much lower than etching rate on the basal face. The angle q can range between 1° and 5°, but it is much higher in glasses.

In order to be effectively revealed by etchant, a track has to intersect the crystal surface at an angle that exceeds a minimum value. This is defined as the

critical angle θ_C and it is equal to (Fleischer et al., 1964):

$$VgT = VtT \sin\theta c \quad (3)$$

$$\theta c = arcsin(Vt/Vg) = \theta \quad (4)$$

During etching process, not all the tracks are revealed, but a small number is destroyed by removing of superficial part of the crystal. An etching efficiency h is so defined as:

$$\eta = 1 - \sin\theta \quad (5)$$

In glass or amorphous solids, etching efficiency range between 0.10 and 0.70 (Fleischer et al., 1975), whereas it is usually higher in the crystals (varying according to the etched plane). For example, for the muscovite values between 0.92 and 0.99 have been observed (Khan & Durrani, 1972; Wall, 1986; Roberts et al., 1984), and this is one of the reason because of it is used as external detector.

Therefore, in crystal etching, a characteristic feature is the etching rate, which can vary with crystallographic orientation of the etched surface. This is also the responsible of the shape of the etch pits. Obviously, if the track is not parallel to the surface, its shape will be influenced by the crystallographic properties of the planes along which it is developed. Apatite is the mineral where variation of shape of etch pits is better observable. In fact, on the apatite, it has been also demonstrated that there is a reduction of length of tracks oriented parallel to the c-axis, showing an anisotropy given by the etching direction (Green et al., 1986).

More clearly, V_G is higher along direction parallel to c-axis and this causes a widening of the tracks perpendicular to the c-axis by a factor 3. Therefore it is much easier to identify the typical "knife-blade" shape of tracks oriented at high angle with the c-axis, whereas the tracks parallel to it are much more thinner. In these tracks it is more difficult to observe discontinuities in the etching process and this fact suggest a higher stability of tracks with this orientation. Heating experiments on crystals has shown a strong anisotropy in the track lengths, which are appreciably longer for orientations of less of 45° with the c-axes (Green et al., 1986).

The etching process can be summarized into three steps:

- tracks are under a observable limit;
- fast increasing of the visible tracks (underetching phase), above all of those intersecting the crystal surface;
- much slower increasing, with relevation of confined tracks (overetching phase).

Visible tracks considered for track-length investigation can be divided into two groups. The first one is given by tracks which directly intersect the crystal surface and which are also counted for age determinations. The second one is represented by the confined tracks which are entirely localized in the interior of the crystal but which are revealed by etchant because they intersect another track, a cleavage or a fracture that emerge at the crystal surface. These tracks are also called with the acronyms TINT (Tracks IN Tracks) and TINCLE (Tracks IN CLEavage) (Fig. 5.A); Bhandari et al., 1971).

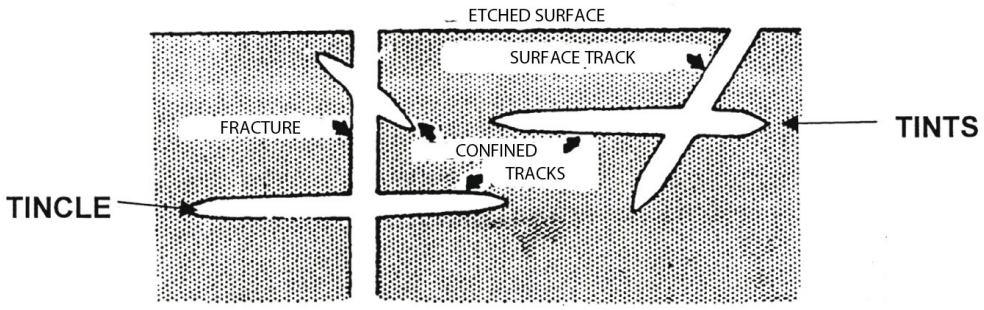

Fig. A.5 - Schematic cross-section illustrating the revelation of fission-tracks by chemical etching. Only latent tracks in communication with the surface exposed to the etchant are revealed. These include tracks-in-tracks (TINTS) and tracks-in-cleavage (TINCLES) (Crowley et al., 1989).

The acronym TININC has been proposed for tracks which intersect an inclusion (Jonckheere, 1997). Beside the crystallographic orientation of the mineral, it is obviously very import the chemical etchant. In fact, on the same face, shape and diameters of the etch pits can vary according to different etching anisotropy of different reagent solutions. Generally, it is better to use etchants which isotropically reveal the tracks and with the highest possible efficiency.

A.5 PRINCIPLES OF THE DATING METHOD

Fission-track dating is very similar to the other isotopic dating methods based on the decay of an unstable parent to a stable daughter atom. The age is function of the proportion between the abundance of the new stable isotope and the parent unstable atom. In fission-track dating methodology, these two quantities, otherwise measurable only with expensive spettrometer techniques, are substituted by the number of observable tracks and the amount of uranium present in the sample.

The radioactive decay is a statistically random process, constant during the time. The probability that any specific nucleus of a given isotope will decay

within a specific time period is given by the decay constant l. The total number of radioactive decays per unit of time is given by l x N, where N is the total number of nuclei from the radioactive isotope present.

The rate of the radioactive process can be expressed as:

$$-\frac{dN}{dT} = \lambda \cdot N \quad (6)$$

This quantity is negative because the total number of nuclei decreases with time.

Integration for the initial conditions $N = N_0$ (atoms at the time $t = t_0$) gives:

$$N_0 = Ne^{(\lambda t)} \quad (7)$$

N_0 can not be directly measured but it can be expressed as function either of the number of daughter nuclides (D) and of the parent isotopes remaining at present (N) which can be directly determined.

$$D = N_0 - N \quad (8)$$

Substition of eq. (8) into eq. (7) gives:

$$D = Ne^{(\lambda t)} - N \quad (9)$$

Solving for t gives:

$$t = \frac{1}{\lambda} \cdot log\left(\frac{D}{N} + 1\right) \quad (10)$$

In fission-track methodology, D is given by the revealed tracks, produced by the decay of ^{238}U, which not only decays by spontaneous fission but also by α-emission and the decay constant for spontaneous fission:

$$\lambda_d = \lambda_\alpha + \lambda_f \quad (11)$$

The total number of decays due to spontaneous fission is proportional by the ratio l_f/l_d to the total number of decays of ^{238}U. Hence, the number of spontaneous tracks N_s that will have accumulated (per unit of volume) is given by:

$$N_s = \frac{\lambda_f}{\lambda_d} \cdot {}^{238}N\left(e^{\lambda dt} - 1\right) \quad (12)$$

where ^{238}N is the number of atoms of ^{238}U still present. As the decay constant for the spontaneous fission is several orders of magnitude lower than the constant for a-decay, it can be stated that $\lambda_d = \lambda_\alpha$. Equation (10) can be rewritten as:

$$t = \frac{1}{\alpha} \cdot \log\left[\left(\frac{\lambda_\alpha}{\lambda_f}\right) \cdot \left(\frac{N_s}{^{238}N}\right) + 1\right] \quad (13)$$

The quantity of U still present in the crystal (^{238}N) can be easily determined by irradiation of sample with thermal neutrons in a nuclear reactor. Irradiation induce the artificial fission of ^{235}U and the total number of fission is given by:

$$N_i = {}^{235}N \cdot \sigma \cdot \phi \quad (14)$$

where f is the neutron fluence (neutrons/cm^2), ^{235}N is the atomic density of the isotope ^{235}U and s represents the cross-section, that is the probability for an atom of ^{235}U to absorbed a thermal neutron. Because the relative abundances of the uranium isotopes are practically constant in nature, also ^{235}U/^{238}U is constant ad it is called I. Hence:

$$N_i = {}^{235}N \cdot I \cdot \sigma \cdot \phi \quad (15)$$

Combination of eq. (13) and (15) gives:

$$t = \frac{1}{\lambda_i} \log \left[\left(\frac{\lambda_\alpha}{\lambda_f} \right) \left(\frac{N_s}{N_i} \right) \cdot I \cdot \sigma \cdot \phi + 1 \right] \quad (16)$$

which is the fundamental age equation for the fission-track method. Therefore, the age determination is based on measurements of the neutron fluence and of N_s and N_i, expressed as number of tracks per unit volume. In practice, because we observe a surface, N_s and N_i can be considered as densities (r_s and r_i), which can be measured at the microscope as number of tracks per known area. These densities are function of the type and the duration of the etching process and of the observation conditions and can be expressed as:

$$\rho_s = g_s \cdot N_s \cdot R_s \cdot \eta_s \cdot f(t) \cdot q_s \quad (17)$$

$$\rho_i = g_i \cdot N_i \cdot R_i \cdot \eta_i \cdot f(t) \cdot q_i \quad (18)$$

where:

$g_{s,i}$ = the geometric factor

$R_{s,i}$ = the average length of a track after the etching process

$\eta_{s,i}$ = the etching efficiency factor

$f(t)_{s,i}$ = the etch time factor

$q_{s,i}$ = the observation factor

The geometric factor g is, by definition, constant and it is = 1 for internal or = 0.5 for external crystal surfaces. In the same material, R_s and R_i are practically equal (Bhandari et al., 1981), whereas η, f(t) and q depend upon the techniques that are used for revelation and observation of tracks. Combining eq. (17), (18) and (16) we obtain:

$$t = \frac{1}{\lambda_t}\log\left[\left(\frac{\lambda_t}{\lambda_f}\right)\left(\frac{\rho_s}{\rho_i}\right)\cdot Q\cdot G\cdot I\cdot\sigma\cdot\phi+1\right] \quad (19)$$

where: $G = \frac{g_i}{g_s}$ and $Q = \frac{\eta_i f(t)_i q_i}{\eta_s f(t)_s q_s}$

If the etching and observation conditions are the same for spontaneous and induced tracks, Q assumes a value = 1. The values of λ_a and I have been fixed by the *IUGS Subcommission on Geochronology* (Steiger & Jäger, 1977) in 1.55125 x 10^{-10} a^{-1} and 7.2527 x 10^{-3} respectively. Non general agreement has been yet reached about the parameters λ_f and σ, as discussed in the following paragraphs.

A.6 THE COSTANT DECAY FOR THE SPONTANEOUS FISSION

More than 40 determination of the decay constant λ_f have been carried out till now (a complete list can be found in Bigazzi, 1981). Results can be grouped into two values, which differ each other by about 20%: $6.9 \times 10^{-17} a^{-1}$ and 8.5×10^{-17} a^1. The lower value has been measured with experiments on the fission-track production and with analyses of minerals and glasses of known age. The higher value has been obtained by measurements with rotating bubble chambers, ionization chambers (Hadler et al., 1981) and radiochemical analyses. It is important to note that nearly all the determination of the constant through fission-track experiments and age determinations are based on a presumed perfect knowledge of the irradiation conditions and, therefore, of the quantity of irradiated uranium. According to Bigazzi & Hadler (1989), the difference between the two values is due probably to systematic errors typical of the experimental procedures. Two main approaches have been developed for age determination in fission-track dating. The first one (*absolute approach*) is based on the physical calibrations, through a determination of the fluence and of the decay costant λ_f. The second one (*zeta approach*) avoids determinations of physical constant through a calibration with geological standards of known age.

A.7 THE NEUTRON DOSIMETRY

Two methodologies have been developed for the determination of the neutron fluence. The first one is based on the measurement of the γ-activity, which is proportional to the fluence, through metallic monitors, (Au, Cu, and Co) whereas the second one is based on track counting on standards and glasses.

In a nuclear reactor, the total fluence (φ) is given by the sum of three components: fast neutrons (φ_f), epithermal neutrons (φ_{epi}) and thermal neutrons (φ_{th}). The fast neutrons are high energy particles (0.5-10 MeV), produced by the fission of the isotope ^{235}U in the fuel of the reactor, and their kinetic energy is lowered by "moderators" (usually graphite or water). Thermal neutrons are obtained if their energy ranges between 0 and 0.25 eV whereas epithermal neutrons are obtained if their energy is comprised between 0.1 eV and 0.5 MeV. fission of ^{235}U contained in the sample can be induced both by the thermal neutrons and by the epithermal neutrons. Since the cross-section for the epithermal neutrons is about half of the cross-section of thermal neutron, the ratio $\varphi_{th}/\varphi_{epi}$ should be < 50 to have less than 1% o tracks produced by epithermal neutrons. The γ-activity is based on the assumption of a good thermalization of the reactor, which can be checked by the so-called "Cd ratio". The cadmium can absorve most of the neutrons with an energy of less than 0.5 eV. If a monitor is irradiated by Cd, its activity can be induced only by epithermal neutrons with an energy > 0.5 eV, whereas activity in a uncovered monitor can be induced both by thermal and epithermal neutrons. The Cd ratio (CR) is defined as the ratio between the activity induced in a uncovered monitor and the activity induced in a monitor surrounded by Cd, and it can be experimentally determined. A good reactor should have CR which are > 3 for an Au monitor, > 48 for a Cu monitor and > 24 for a Co monitor (Hurford, 1990).

Determination of the metallic monitor activity is not possible for most of the fission-track geochronologist because it requires an easy access to the reactor facility and a strict collaboration with the reactor scientists. To solve this problem, the National Bureau of standards (NBS) produced a series of glass

wafers (SRM961-964) of different uranium concentration that were irradiated in the NBS reactor with a thermal fluence monitored by Au and Cu foils. The neutron fluence can be determined by measurements of the induced tracks on non-irradiated standard glasses (ρ) and on the NBS wafers (ρ_{NBS}) according to the equation:

$$\phi = \frac{\rho_{NBS} \cdot \rho}{\rho_{NBS}} \quad (20)$$

The NBS standards have been criticized because: 1) there is a systematic difference between calibration with Au and Cu foils; 2) a considerable content of Th and B, which give fission-tracks undistinguishable from those produced by uranium, is present; 3) the ratio $^{238}U/^{235}U$ is not the same present in nature; 4) the uranium is not homogenously distributed (Bigazzi & Hadler, 1989). Since some years, a new series of standard glasses have been produced (CN1-6 and IRMM-540; De Corte et al., 1998).

A.7.1 The age standard approach

To solve the problem of determinations of neutron fluence and decay costant λ_f, Fleischer et al., (1975) proposed to irradiate an age standard (with the age determined from a comparative analysis) together with the samples. The unknown age of the sample can be calculated by a comparative analysis between the track density in the sample and the track density in the standard. The equation (19) can be rewritten using a Z factor (Hurford & Green, 1982, 1983) that replaces the parameters λ_f, ϕ, σ and I (which have the same values in the standard and in the sample):

$$t = \frac{1}{\lambda_a} \log\left[1 + Z \cdot \lambda_a \cdot \frac{\rho_s}{\rho_i}\right] \quad (21)$$

where Z is derived from the standard age through the equation:

$$Z = \frac{\left[e^{\lambda_a \sigma_{STD}} - 1\right]}{\lambda_a \left|\frac{\rho_s}{\rho_i}\right|} \quad (22)$$

The track densities for the standard and the sample have to be determined for a same irradiation and with the same conditions of chemical etching and microscopical observation.

An alternative approach provides that a glass dosimeter with an homogeneous distribution of U is calibrated with a series of standards (Hurford & Green, 1981). Different dosimeter (series SRM and CN), with different uranium contents, have been produced. Once the so-called ζ-factor has been precisely evaluated, the sample ages are calculated measuring the track density on the glass monitor or in its external detector (ρ_d). The eq. (19) can be written as:

$$t = \frac{1}{\lambda_a} \log\left[1 + \zeta \cdot \lambda_a \cdot \frac{\rho_s}{\rho_i} \cdot \rho_d\right] \quad (23)$$

where the ζ-factor is determined with the equation:

$$\zeta = \frac{\left[e^{\lambda_a \sigma_{STD}} - 1\right]}{\lambda_a \left|\frac{\rho_i}{\rho_s}\right| \cdot \rho_d} \quad (24)$$

The calibration of ζ-factor has to be repeated for more than 5 analyses, preferably using more than one standard, each of them included in different irradiation (Hurford, 1990). The obtained values are specific to each scientist, because the counting procedure can be different in each person, and the mineral phase (Green, 1985). Results obtained from 13 different analysts who have used the same microscope, the same standards and the same counting approach, are reported in Fig.6a. Variation of the mean value aries from factors such as small differences in the size cut-off point for acceptance a track, the crystal selection criteria and the precision of locating and induced image on the detector (Hurford, 1998).

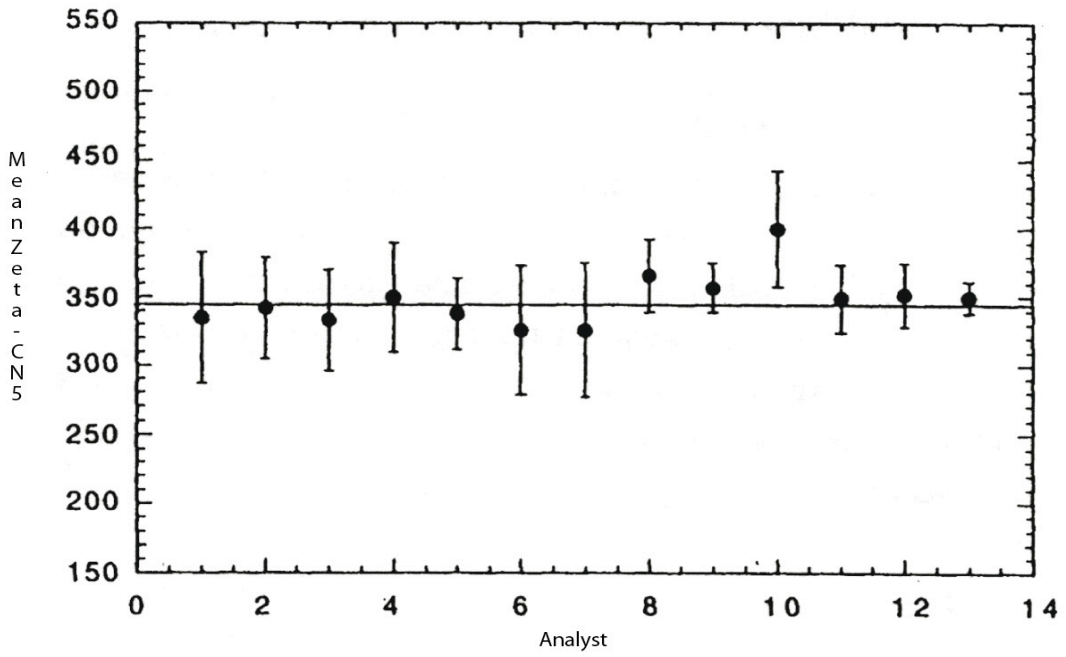

Fig. A.6 - Comparison of mean zeta values measured by 13 analysts on the same Fish Canyon Tuff and Durango apatite standards. Each mean value represents >15 determinations; error bars ± 1s (Hurford, 1984).

The age standards should have the following requisites (Hurford & Green, 1983):

- the sample should come from a very well-documented horizon, readily accessible and which contains reasonable amounts of the standard;

- sample should be homogeneous in age (the mineral separate should consist of a single age population);
- the independent K/Ar and Rb/Sr ages should be unambiguous and compatible with the known stratigraphy;
- the fission-track age must relate to the independent age and neither to the age of an inherited component nor to an overprinting event or post-formational slow cooling

The ideal standards should come from sub-volcanic rocks rapidly cooled and which were not affected by heating events. The current standard are listed in Table A.2.

According to Bigazzi & Hadler (1989), the use of age standards can led to systematic errors because the reference age has been obtained with different techniques and, often, it cannot be comparable with a fission-track age. Moreover, the length of spontaneous tracks is 5-10% shorter than the length of the induced tracks (Gleadow et al., 1986) and this suggest the existence of a significant post-formational annealing.

Table A.2 - Reference samples used as age standards in fission-track dating

Mineral	Geological specification	Region	Age (Ma)	Dating method
zircon	Bishop Tuff	California	0.7324 ± 0.024	$^{40}Ar/^{39}Ar$ (sanidine)
glass	Moldavite	Southern Boemia	15.21 ± 0.15	K-Ar
zircon	Buluk Tuff from the Bakata Fm.	Bakata Valley, Kenya	16.4 ± 0.2	K-Ar
apatite, zircon	Fish Canyon Tuff	Colorado	27.8 ± 0.2	$^{40}Ar/^{39}Ar$ (biotite)
zircon	Tardree rhyolite	Northern Ireland	58.7 ± 1.1	K-Ar and $^{40}Ar/^{39}Ar$ (sanidine)
apatite	Durango apatite ore body in Carpintero volcanic group	Cerro de Mercado, Mexico	31.4 ± 0.6	K-Ar
apatite, zircon, sphene	Mount Dromedary intrusive complex	New South Wales, Australia	98.8 ± 0.6	Rb-Sr (biotite)

A. 8 DATING METHODS

A.8.1 Population method

Two splits of the mineral separate are used to determine the fossil and induced track densities. Two different procedures can be chosen. In the first alternative (*population subtraction method*; Naser et al., 1980), the grains for induced tracks are irradiated, polished and etched. In this way, both induced and spontaneous tracks are revealed. The quantity of fossil tracks can be determined in the non-irradiated second aliquot of the sample. In the second alternative (*population method s.s*), the spontaneous tracks are completely annealed before the aliquot is irradiated. After irradiation, only induced tracks will thus be seen, whereas spontaneous tracks can be counted in the other aliquot. The first method is used

especially for glasses analysis because irradiation can strongly alter the etching characteristic. About the counting procedure, a unitary area that can be contained in all the crystals is chosen and more than fifty grains are then analysed.

An important limit of this procedure is the assumption that all the examined minerals have the same uranium content and that no strong internal compositional zonations are present. Moreover, the population method may become totally inappropriate dealing with sedimentary samples, especially when they are not affected by a total post-depositional annealing, because different crystal populations, with very different ages, can be present.

A.8.2 External detector method (EDM)

In the external detector method, single crystals are dated and, thus, it has immediately applied for zircon analysis, where strong variations in the uranium content are common. The mineral grains are mounted in epoxy resin (apatite) or teflon foils (zircon), polished and etched. In a second time, the mount is covered with an external detector (usually a piece of low uranium muscovite) where, after irradiation, induced tracks can be revealed by another chemical etching. The grain mount and the detector are then affixed to a microscope slide and counted. Fossil tracks are counted in the crystals, whereas induced tracks are counted in the correspondent image of the crystal in the external detector. A part of the crystal is usually chosen, avoiding zonations and rims, where tracks coming from close grains can be present (Gallegher, 1995). The EDM is currently used for all the minerals, but it must be used with caution for dating crystals (above all apatites) with defects and dislocations. It is the ideal method to date

sedimentary rocks can be very useful for dating tephras, where detrital grains (which commonly occur) can be easily recognized and eliminated from the analysis. It cannot be used for dating glass, because glass and the material used for the external detector have very different etching efficiencies.

A.9 THE ANNEALING OF FISSION-TRACKS

A.9.1 Laboratory experiments

In principle, several geological parameters such as ionizing radiation, plastic deformation, pressure and temperature, can influence the stability of latent fission tracks in solids. In some experimental studies on minerals and glasses, Fleischer et al. (1965) exposed samples to irradiations, high hydrostatic pressure up to 80 KB, shear stress and heating. Result is that temperature is by far the most dominant parameter that influences the stability of fission-tracks. A simple heating experiment can easily show a decreasing of the number of tracks and a reduction of their length. This process is known as *annealing*.

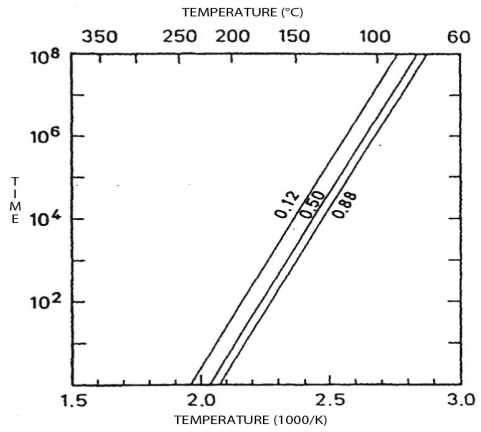

Fig. A.7 - Arrhenius diagram with parallel lines of equal degrees of track density reduction during annealing in monocompositional apatite, Sljudjanka, Siberia (Wagner & Reimer, 1972).

The annealing experiments consist in the measurements of tracks lengths and densities of samples exposed to different heating steps at different temperatures. Data are traditionally presented in the so-called Arrhenius diagrams, in which the logarithmic annealing time is plotted against the inverse absolute temperature. The annealing degree is expressed by the parameters density r and length *l*, normalized to pre-heating conditions (r_0 and l_0). All points with equal track-density reduction r/r_0 form straight lines (Fig. A.7; Naeser & Faul, 1969; Wagner & Reimers, 1972; Hammerschmidt et al., 1984; Green et al., 1985). This means that the same annealing level can be reached with a short exposure to high temperatures or, on the contrary, a long exposure to low temperature.

Since the fragments produced by fission events causes highest ionization at the beginning of their paths, the density of defects along a fission-track decreases from the central part towards both of its ends. During the annealing process, reduction of lengths begins from the ends, as demonstrated by Green et al. (1986) with experiments carried out on the Durango standard apatite. At high degrees of annealing, the tracks become broken by unetchable gaps into separate segments. This fact is in according to the hypothesis of the presence of discontinuities in the track structure. In fact, an increase of temperature causes the removal of the puntiform defects and different segments of the track cannot be etched anymore (Gleadow et al., 1981).

As show in Fig. A.8 the reduction of the ratio l/l_0 from values of about 0.65 to the total erasion of the track occurs in a very narrow temperature range (about 10°C). If the reduction of lengths is plotted against the reduction of areal density ρ/ρ_0 (Fig. A.9), it can be noted that below the value $l/l_0 = 0.65$, the ratio ρ/ρ_0

rapidly decreases to zero. Green et al 1989, suggests that this is due to an easier detection of the long tracks in respect of the short tracks, which, of consequence, are under-estimated at high degrees of annealing.

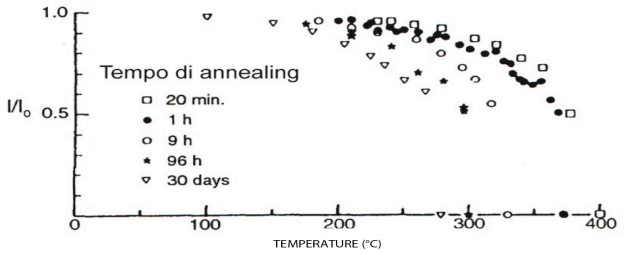

Fig. A.8 - Isochronal annealing data for five annealing times in a experimental study (Green et al., 1986)

In addition to temperature, there are other factors which may influence the annealing rate of fission-tracks. Annealing is not an isotropic process into the crystal. In apatite, fission-tracks parallel to the c-axis are more resistant against annealing than tracks perpendicular to the c-axis, and this anisotropy increases as the annealing proceeds (Green & Durrani, 1977).

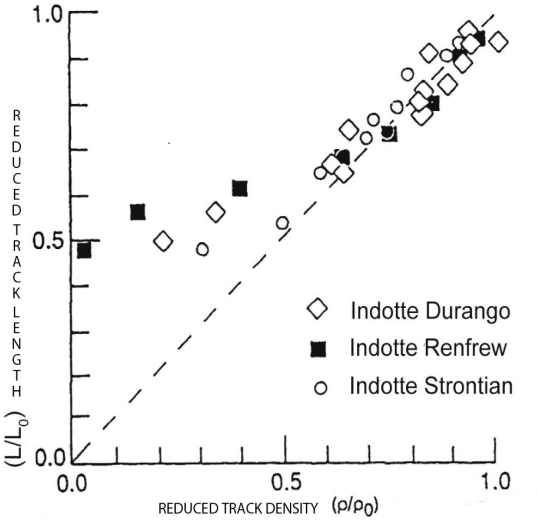

Fig. A.9 - Relationship between reduction of confined track length (l/l_0) and reduction of track density (ρ/ρ_0) for induced tracks in three mono-compositional apatites (Green et al., 1986).

The fission-track annealing rate also depends on the crystal chemical composition. The apatite composition $Ca_{10}(PO_4)_6(F,OH,Cl)_2$ can be modify by other elements, such as REE, Sr etc.; in nature, the fluoroapatites are predominant (Naeser et al., 1987). All the experimental studies demonstrate the Cl-rich apatites are more resistent to annealing (Fig. 10a; Gleadow & Duddy, 1981; Green et al., 1986). According to Green et al., (1986), Cl is the only element capable to strongly influence the annealing kinetics and all the fission-track studies should include microchemical analyses on the dated crystals. Also the experiments carried out by Crowley et al. (1991) demonstrate a substantially identical resistance to annealing for fluoroapatites and apatites rich in Sr and REE, while Donelick (1997) argue that also different contents of OH, Mn and Fe can be important. An alternative procedure to the microchemical analysis is given by the recent observation of the existence of a strong correlation between the diameter of tracks parallel to the c-axis and the Cl and F content (Burtner et al., 1994; Donelick, 1997). Apatites with tracks with diameters less than 1.75 mm are less resistant to annealing and can be considered as typical fluoroapatites.

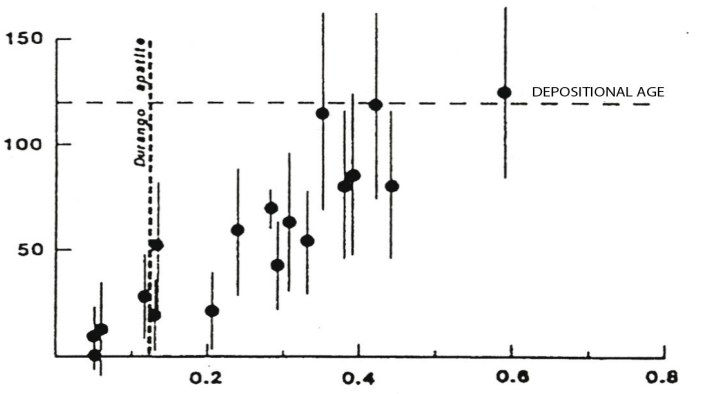

Fig. A.10 - Relationship between apparent fission-track age and the chlorine content in individual apatite grain from an Otway Group sandstone bore-hole sample (2585 m deep at 92°C). The composition of Durango apatite is shown for reference (Green et al., 1986).

A.9.2 Track annealing under natural conditions

The ideal geological conditions to test the laboratory models are offered by deep bore-holes, especially where the tectonic evolution and the thermal histories are well known. The more detailed studies have been carried out on samples coming from several drill holes in the Otway sedimentary basin (southern Victoria, Australia) which contains 3-4 thick fluviatile sediments of volcano-clastic origin (Gleadow & Duddy, 1981; Green et al., 1989).

From fission-track dating of zircon and sphene, it has been inferred that most of this early Cretaceous volcanogenic detritus was derived from contemporaneous volcanism. Therefore, tracks observable on the apatite grains are all formed after his volcanic event. Stratigraphic data suggest that the sediments reached the maximum burial depth (3.5 km in the deepest well) in the Early Oligocene and, since then, no important uplift events occurred. Diagram of Fig. 11a shows that the ratio ρ/ρ_0 begin to decrease at about 60°C and reach the value of 0.5 at 95°C. All the tracks are completely erased at about 125°C. Also fission-tracks value of 0.5 at 95°C. All the tracks are completely erased at about 125°C. Also fission-tracks length decreases systematically with increasing temperature.

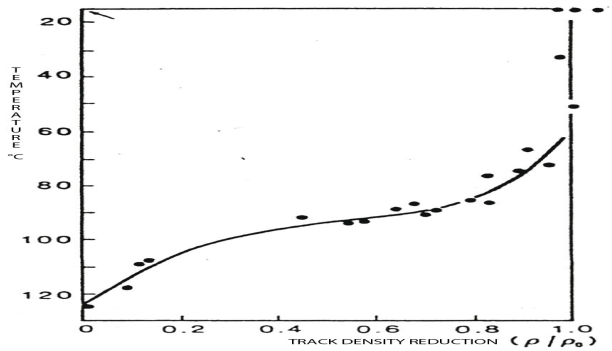

Fig. A.11 - Reduction of the fossil fission-track density r/r_0 with down-hole temperature in drill-hole samples from the Otway Group sandstone (Gleadow & Duddy, 1981)

Comparison of these data with the extrapolation of laboratory annealing data give an excellent agreement, even if the temperature range over which partial annealing should occur is wider in the laboratory experiments. This implies that the time factor is more important in the laboratory experiments. Some systematic differences can be found in lengths measured in sample subjected to temperatures > 70°C. Moreover, in samples collected at temperatures of 95°C, dating of single crystals yields an age range between 0 and 120 Ma. Since analyses have been carried out on a population of different crystals and not on a single apatite, Green et al. (1985) suggested that the amount of annealing is not identical in different grains subject to the same temperature, but is controlled by their chemical composition. It should be also taken in account that the measurements of track densities is dependent upon individual track identification criteria, which vary from person to person, rendering comparison of different studies difficult (Green et al., 1986). More precise are fission-track length measurements, which represent a more fundamental parameter in annealing studies.

Some studies on the annealing temperatures have been carried out also on outcropping rocks, even if with a very minor precision and with contrasting results. Calk & Naeser (1973) and Gleadow & Lovering (1978) put in evidence the variations of apatite fission-track ages around magmatic intrusions. Wagner & Reimer (1972) and Hurford (1989) used independent dating techniques (Rb/Sr and K/Ar) and data obtained with fission-track dating in order to study exhumation in the Central Alps and to define the closure temperatures.

A.9.3 The Partial Annealing Zone (PAZ)

Both the experimental data and the analyses on natural conditions have shown that the annealing is a gradual process. The temperature range in which reduction of lengths occurs is known as *Partial Annealing Zone* (PAZ; Wagner & Van den Haute, 1992). According to this concept, temperatures of any geological setting are divided into three zones in respect to fission-track annealing:

- *total annealing zone*, in which the latent tracks are immediately erased after any fission event;
- *partial annealing zone*, where the ratio r/r_0 increases from 0 to 1 with the decrease of temperature;
- *stability zone*, where tracks are stable (this is not completely true as mentioned in chapter).

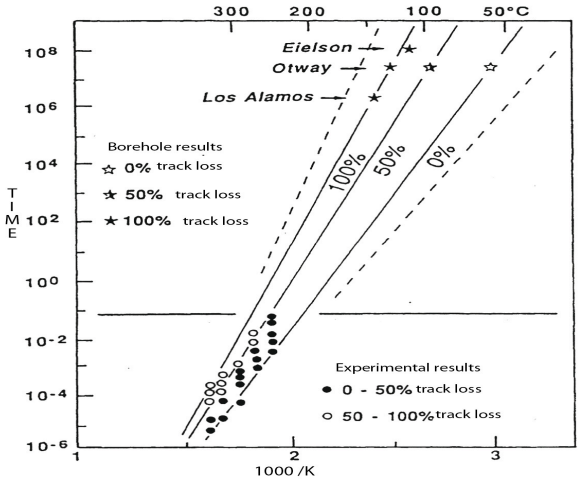

Fig. A.12 - Comparison between the geologically observed track-retention temperatures at the drill-holes Otway basin, Eielson and Los Alamos, and the extrapolated laboratory predictions (Gleadow & Duddy, 1981).

As it is possible to see in the Arrhenius diagram (Fig. A.7), temperatures at which annealing actually occurs depends on the rate of the geological process

and the PAZ temperature range cannot univocally defined. For apatite, temperatures between 140 and 120°C are cited for the bottom whereas 70 to 40 °C for the top of the PAZ. More precisely, Gleadow & Duddy (1981), on the basis of data obtained from samples from drill holes in the Otway basin, suggest a PAZ between 145 and 180 °C for heating events 1 Ma long, and between 110 and 45°C for events 1 Ga long (Fig. A.12).

A.9.4 The closure temperature

Since the tracks are used as a dating methodology, the cooling range in the PAZ have to be necessarily "simplified" in a single temperature value, to which the age has to be referred, defined by Dodson (1973) as the *closure temperature*. This concept can be better illustrated by the diagrams in Fig. A.13. The fission-track age is given by the intercept of the linear portion of the track accumulation curve with the time axis. The projection of this age on the temperature curve gives the closure temperature. These diagrams show also that the closure temperature depends from the cooling rate.

Wagner & Reimer (1972) suggest that the closure temperature correspond to the temperature at which 50% of the tracks are retained. In conclusion, the best assessments of the closure temperatures are: 130$\pm$10°C, 110$\pm$10°C and 85$\pm$15°C for cooling rates of 100°C/Ma, 1°C/Ma and 0.01°C/Ma respectively (Naeser & Faul, 1969; Watt & Durrani, 1985; Zimmermann & Gaines, 1978).

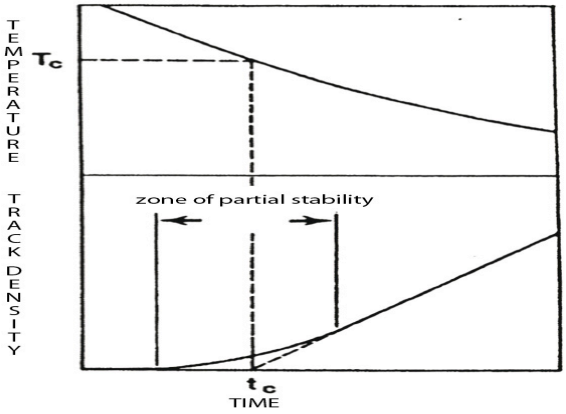

Fig. A.13 - Graphical representation of closure temperature (TC) and apparent age (tc) in a cooling isotopic system. The top part of the diagram represents the temperature history of the system; the bottom part of the diagram shows the accumulation of fission-track as a function of time (Crowley et al., 1991).

A.9.5 The annealing and the fission-track lengths

According to Gleadow et al. (1986), measurements of the length of induced tracks is 16.3±0.9 mm. In reality, the length of the tracks revealed by chemical etching is significantly less than the travel through the crystal of the charged fission fragments, which can be in theory calculated. The difference between these two lengths in called *range deficit* (Fleischer et al., 1975) and it depends from the mineral phase. For the apatite, the theoric length is of 21.1 mm whereas in the mica it is much closer to the length measurable with a normal microscope (Van den Haute et al., 1998). It is important to note that Donelick et al., (1997) demonstrated that the length of induced tracks is longer when the chemical etching is carried out a few days after the irradiation.

In a general way, the fossil tracks are shorter than the latent tracks of about 15-20% (Gleadow & Duddy, 1981), even in apatites not affected by annealing. As already mentioned, as soon the temperature exceed 60°C, tracks begin to reduce

and the rate of shortening will proceed according to duration and intensity of the heating event. Because of this, fission-track length measurements in apatite are extensively used as a diagnostic tool for thermal history analysis. Gleadow et al., (1986) demonstrated that apatite in volcanic and related rocks that cool rapidly and remain at temperatures < 45°C have a narrow, symmetric track length distribution, with mean track length of 14-15 mm and standard deviation of about $\pm$ 1 mm (Fig. A.14). This distribution is known as "indisturbed volcanic type" and it is a requirement for the standard apatites used for calibration in the dating procedure (Green, 1985).

When this kind of distribution is observed, the fission-track ages is the same of the age of formation of the rock because no annealing events affected the apatites. This is not completely true, as demonstrated by diagram in Fig. A.14 which shows a slight shortening of the tracks of about 1-1.5 mm (Green et al., 1985). These observations suggest that shortening might be expected to be found in all apatites even to low temperatures of the order of 20-50°C and this fact can led to systematic errors in the z calibration (Bigazzi & Handler, 1989; Jonckheere, 1997). It should be also note that shortening of track is very fast at the beginning of the heating event and this is probably due to the high instability of the ends of the tracks (Green & Durrani, 1977).

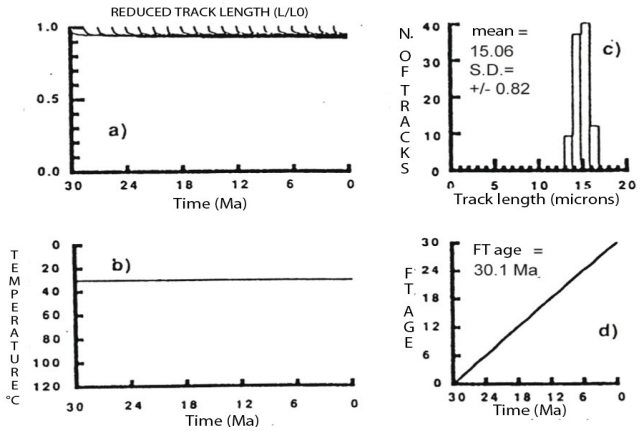

Fig. A.14 - Modelling of the length distribution (a, c) of fossil fission-track and the fission-track age (d) of apatite for a thermal history consisting of residence at 30°C for 30 Ma. The tracks produced at all times undergo a rapid decrease in length initially, after which practically no further shortening occurs (Green et al., 1989).

For a slow and uniform cooling pattern, the distribution becomes negatively skewed, with a mean length of 12-13 mm and a standard deviation of $\pm$ 1-2 mm (Fig. A.15). Gleadow et al., (1986) have termed this distribution as "undisturbed basement-type" distribution and it is characteristic of all the rocks subjected by a constant decrease of temperature. In this case, the fission-track age slowly increases during the first phases of cooling and then more rapidly and linearly with the decrease of temperature. Fore more complex thermal histories, which imply different heating and cooling events, a variety of distributions (simply called of "mixed type") can be obtained. In the diagrams of Fig. A.16, data concerning a thermal history of a rock heated to 85°C and then cooled to ambient temperature are represented. In the first heating step there is the shortening of tracks; during the cooling phase, all tracks become "frozen" at the length to which they were shortened at the thermal maximum and new tracks of 14-15 mm are added. This results in a bimodal distribution, which can be different depending on the duration of the heating event and the maximum temperature

reached. As regards the fission-track ages, these will be as younger as the maximum temperature reached. If the heating event exceed the temperature of 125°C, all the pre-existing tracks are erased and only the thermal history below this temperature can be detected by fission-track analysis (Fig. A.16).

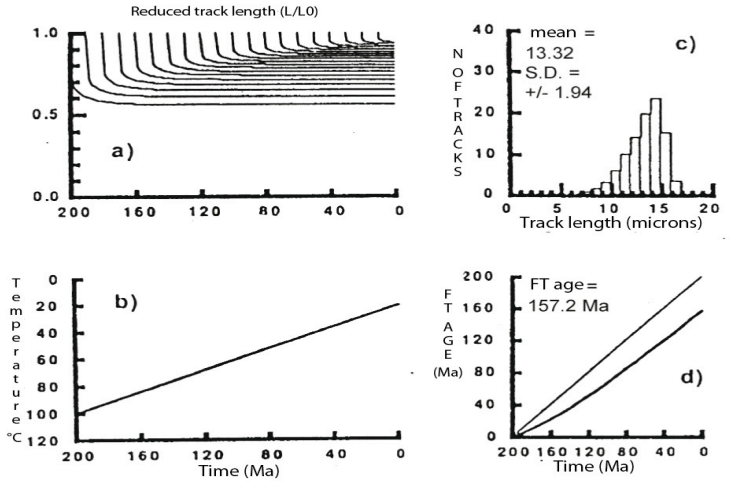

Fig. A.15 - Similar diagrams to Fig. 14a, for a thermal history consisting of linear cooling from 100°C to 20°C over 200 Ma (Green et al., 1989).

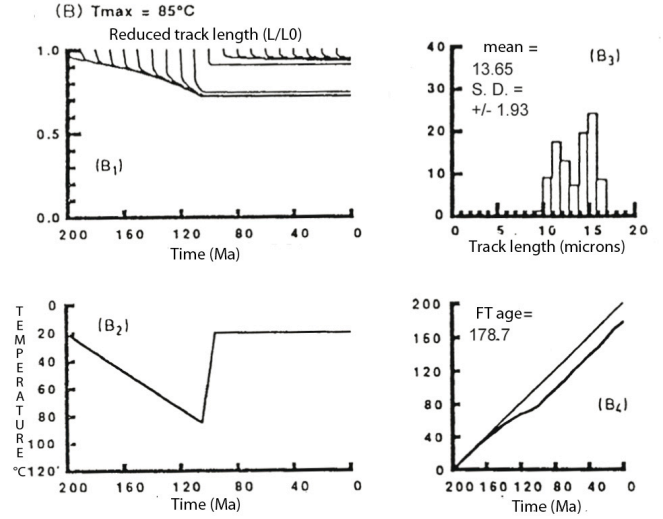

Fig. A.16 - Similar diagrams to Fig. 14a and 15a illustrating the effect of high temperature followed by cooling. Tracks formed during the heating phase are progressively shortened, to a length determined by the maximum temperature. In this case (maximum temperature of 85°C), the two generations of tracks are clearly resolved in the bimodal distribution of track lengths (Green et al., 1989).

A.10 SAMPLE PROCESSING AND ANALYTICAL PROCEDURES

A.10. 1 Separation of apatite and zircon

Sample are first washed and dried, then split and crushed using a jaw crusher and a disc mill to obtain sand-grain fragments. The heavy mineral fraction that includes both apatite and zircon grains is then separated using Gemeni shaking table. The minerals that have magnetic characteristic, including biotite, magnetite, muscovite, pyroxenes andamphiboles are removed using a Frantz magnetic separator. Its slope can be fixed at 12° and the strength of the electric current at 0.5 – 1.0 A but different conditions can be applied according to the quantity of magnetic minerals. To separate any remaining quartzo-feldspathic minerals, the < 250 μm fraction of heavy mineral separates is passed through different heavy liquids. For this step Tetrabromoethano (density 2.96 g/cm^3) is used. Apatite (density 3.1-3.35 g/cm^3) is then separated from zircon (density 4.6-4.7 g/cm^3) using the liquid methylene iodide (density 3.3 g/cm^3). The minerals are finally washed with acetone and dried.

A.10.2 Mounting in the epoxy resin and polishing

A mixture of resin and hardener (the parts depending from the specific product used) is prepared just before the mounting procedure. Each sample number is then engraved on microscope slides, previously cleaned with acetone. The slide (with the engraved number on the bottom of the glass) is put on a hot plane (also the temperature depends from the resin used) and some drops of the resin are put in the in the middle of the glass. The resin is carefully mixed to eliminate possible bubbles of air. The mineral concentrate can then be mixed with the

resin on an area of about 1 x 1.5 cm. To facilitate these operation, the area can be drawn on a piece of tin foil put above the glass and the mixing and distribution of grains can be done under a microscope at low magnifications. The ideal mounting consists in a single layer of crystals not too close each other. The resin is cured leaving the mounting on the hot plane for some minutes.

The apatite mounts are first hand-ground using wet grinding paper and then polished using a Buhler machine, using a 1 μm alumina slurry on a polishing cloth for about 10 min at 200 r.p.m. The process is separated until sufficient internal cross-sections of apatite crystals are achieved. To remove any remaining polishing scratches, the mounts are polished using 0.3 μm alumina slurry on a felt polishing cloth.

A.10.3 Chemical etching of apatites

The single mounts are put in HNO_3 5 M for 20 seconds and the immediately washed for some minutes (any residual of nitric acid can be eliminated leaving for an hour or more the mounts in simple water). At ambient temperature of 20°C is assumed.

A.10. 4 Preparation for the irradiation

The glasses are cut according the dimensions of the mounts. A corner of the obtained glass is slightly rounded. The surface of the mount is then carefully cleaned with acetone.

A piece of muscovite is split along the cleavage, to obtain a layer about 1 mm-thick. The mica can be cut according the dimension of the mount. It is important that the surface of the muscovite which will be in contact with the mount is perfectly clean and without grazes. On its external side the sample number is engraved with a diamond pen and the corner corresponding to the rounded corner in the mount is cut. Samples, dosimeters and standards are then put in the older as schematized in Fig. A.17. The samples are then irradiated with thermal neutrons in the DR3 reactor at the Radiation Centre of the Oregon State University with a nominal neutron fluence of 9 x 1015 n cm^{-2}. The standard glass CN5 was used as a dosimeter to measure the neutron fluence.

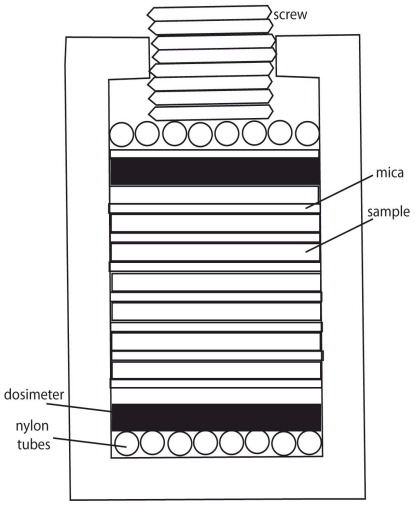

Fig. A.17 – Holder for irradiation and position of sample, mica and dosimeters.

A.10.5 Procedures after irradiation and chemical etching of mica

The tin containing the older is open and the radioactivity level is measured. The holder is put in a special container and left there until the radioactivity decreases down to 10 times the natural level (about 100 μR/h or 10 μS/h).

The muscovites are put in a PVC container with HF 40% for 40 minutes. It is possible etch more mica in the same container but, for an uniform etching, is better to distribute them into different containers. The foils are then washed with distilled water for some hours. An ambient temperature of 20°C is assumed.

A.10.6 The microscope analysis

AFT ages are measured and calculated using the external-detector (EDM) (Fig A.18) and the zeta-calibration methods (Hurford & Green, 1983). Zeta-calibration is performed following the procedure recommended by Hurford (1990). Neutron fluences is measured counting neutron-induced tracks in the Corning glass dosimeter CN-5 (Uranium concentration: 2.17± 0.62 ppm, 235U atom %: 0.720; Hurford, 1990; Bellemans et al. 1995). Age standard used are Durango and Fish Canyon apatites (IUGS age standards). The mean value obtained (336.34 ± 16.24) is in a good agreement with values obtained by other analyst working with similar techniques and criteria (Hurford, 1998).

The analyses were subject to the $\chi 2$ test (Gailbraith, 1981) to detect whether the data sets were normally or overall dispersed. A probability of less than 5% denotes a mixed distribution.

According to EDM, the spontaneous (ρ_s) and the induced (ρ_i) tracks densities are calculated on the mount and the mica respectively. Counting of tracks has been carried out using a microscope Zeiss Axioscope, equipped with motorized stage, transmitted and reflected lights and at a total magnification of x1250 (ocular X10 + additional lens Optovar X1.25 + objective X100). Before counting, the stage is calibrated to automatically pass from the apatite to the corresponding image on the mica. Where possible, at least twenty crystals with the proper characteristics (section parallel to the c axis; no fractures or inclusion, no zoning) are selected. The recognition of the proper section is facilitated by the reflected light since the etch pit are all parallel. The number of selected crystal can increase in specific case (low density of tracks, provenance studies etc.)

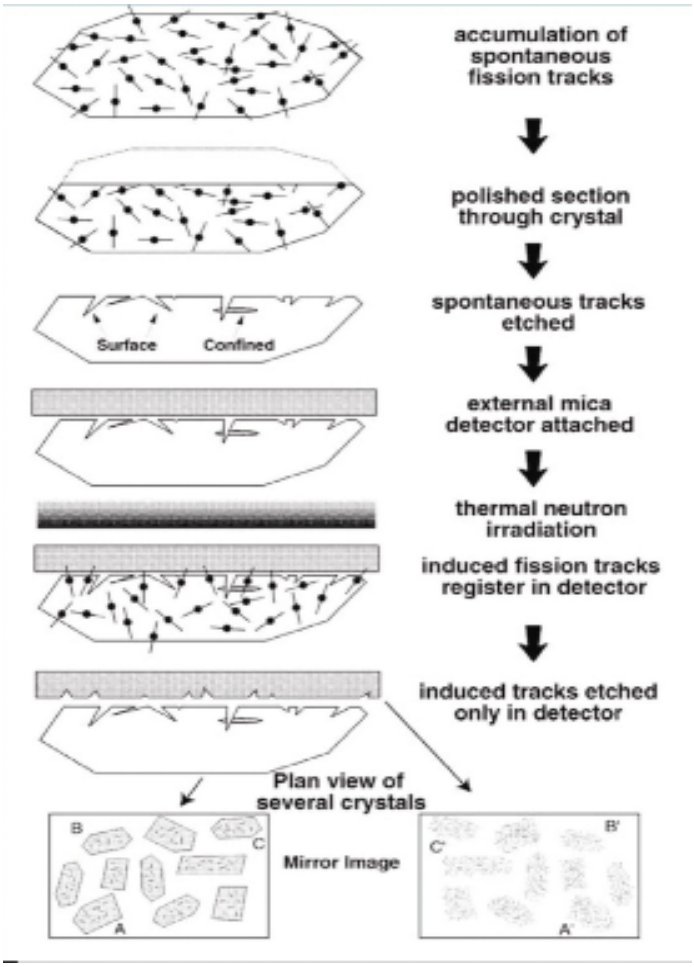

Fig. A.18 - External detector method (EDM), (Gallagher et al., 1998)

Track lengths are measured using digitizing table connected to a computer. A led is fixed to a cursor and its light is projected on the slide across a drawing tube. The led is used to determine the coordinates of the ends of the tracks; the computer then automatically calculates the length. Only the horizontal confined tracks on the section parallel to the c-axis can be measured, about 50 tracks should be measured to have a statistical significant distribution.

A.10.7 Modeling

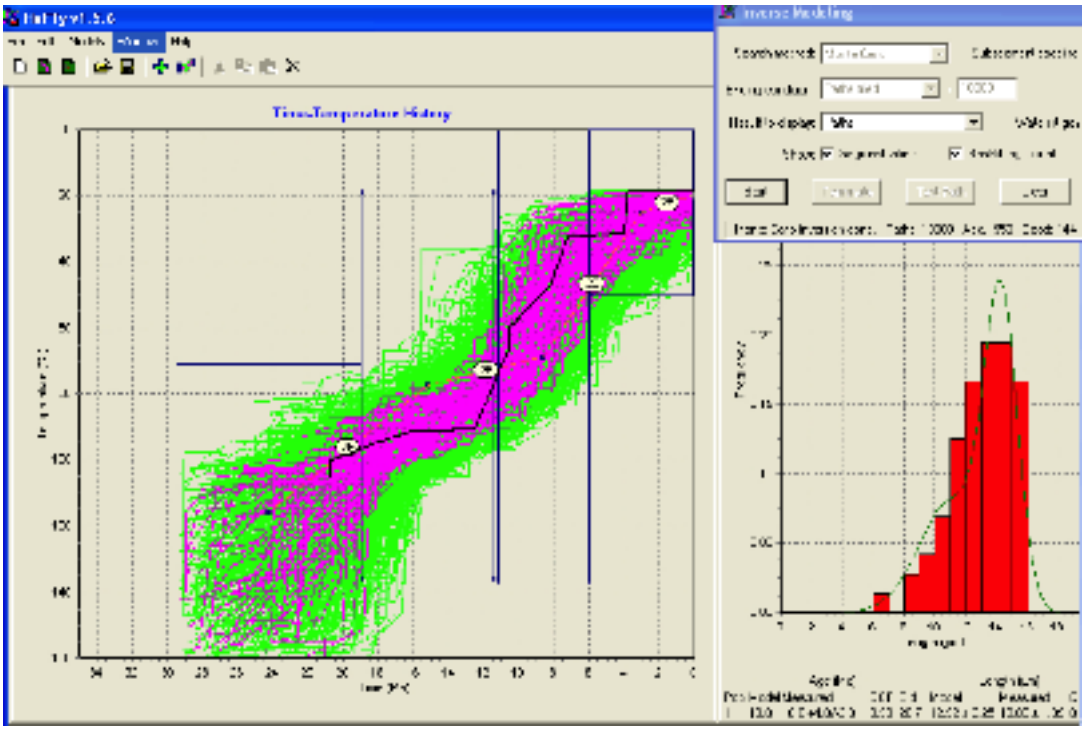

Fig. A.19 – Example of inverse modelling of track length using Hefty software.

Inverse modeling of track length data is performed using HefTy software (Ketcham, 2005). The software generates the possible T-t paths using a constrained Monte Carlo scheme that allows the user to specify regions of time-temperature space through which each path must pass, and the complexity of the paths pass certain statistical criteria, accepting some as having "good" or "acceptable" fit to the data and rejecting the rest (Ketcham et al., 2009). The criteria for a "good" fit in HeFTy are: Mean (GOF= goodness-of-fit) = 0.5, Min (GOF= goodness-of-fit) = 1/(N + 1), where N is the number of statistical tests used (Ketcham et al., 2009). GOF values give an indication about the fit between observed and predicted data (value close to 1 showing an high degree of agreement). In Fig. A.19 the modelling of sample TU 290 is reported as example.

Appendix B

STATISTICS OF FISSION-TRACK DATING

B.1 THE POISSON DISTRIBUTION

Many natural phenomena can be considered as single events in space and time. If the distribution of their occurrence is governed by chance alone, the statistical frequency distribution that better describe it is the Poisson distribution. To apply it, the following requisites have to be fulfilled:

- the probability that a single event happens in a very short time (or in a very small space) is proportional to the duration of the interval;
- the probability that different events happen in the same interval is near to zero;
- the probability that a single event happens in a selected interval is independent from the probability in a close interval.

The equation which expresses the probability to have a Poisson distribution is:

$$f(x) = \frac{\mu^x}{x!} e^{-\mu} \quad (1)$$

where x is the number of events and m is the average rate of the processes in a unit interval. A typical example of a process which can be described by the Poisson statistic is the a-decay. If the parent nuclide is homogeneously distributed throughout the volume of the solid, the number of decay events that will be registered after a certain time per unit of volume, will also vary randomly. As in the Poisson statistic the mean is equal to the variance and the standard deviation is equal to the square root of variance itself, it is quite simple to calculate an age and standard error from the observed fission-track data.

B.2 ERROR ANALYSIS IN THE EXTERNAL DETECTOR METHOD

In the external detector method, in any given grain the same area of the grain that is counted for spontaneous tracks must be exactly located and counted in the external detector for the induced tracks (Gailbraith, 1984; Gailbraith & Laslett, 1985). Hence, in each grain a single ratio ρ_s/ρ_i and a single age will be obtained. The error calculation for a single age is based on the equation:

$$\sigma_a = \sqrt{(\alpha^2 + \beta^2 + \gamma^2 + \delta^2)} \quad (2)$$

where:

σ_a = standard error of the age;

a = standard error of spontaneous tracks count;

b = standard error of induced tracks count;

g = standard error of the count for the neutron dose determination;

d =standard error of zeta factor;

If the Poisson statistic is applied to estimate the error of all terms in eq. (2), the standard deviation is equal to the square root of the number of counted tracks. The terms can be calculated as follows:

$$\alpha = \frac{\sqrt{N_s}}{N_s} \quad (3)$$

$$\beta = \frac{\sqrt{N_i}}{N_i} \quad (4)$$

$$\delta = \frac{\sigma_\zeta}{\zeta} \quad (5)$$

where N_s, N_i and N_d are respectively represents the total number of spontaneous, induced and neutron dosimetry counted tracks. In practice, the percentage of error due to the zeta factor is quite low (1-1.5% for 1s) and can be neglected (Wagner & Van den Haute, 1992). The error value calculated from the eq. (2) must be multiplied by the age to obtain the error in years. The probability that the age falls within the range covered by the given error (1s) is of about 68%. Sometimes fission-track ages are reported with double error (2s) and in this case the probability is of about 95%.

The Poisson distribution can be influenced by different factors such as an imperfect contact between the crystal and the detector, an inexact identification of the counting areas, a partial etching, a different chemical compositions of apatites, a presence of crystals with different thermal histories (very common in sedimentary rocks non totally annealed; a discussion of these factors can be found in Green, 1981). Ideally, all the determined ages should form part of a Poisson distribution. Gailbraith (1981) suggested the use of the chi quare test (c^2) to determine whether the data conform to a Poisson distribution or not. The calculation is based on the following formula:

$$\chi^2 = \Sigma_j \left| \frac{\left(N_{sj} + \aleph_{sj}\right)^2}{\aleph_{sj}} + \frac{\left(N_{ij} - \aleph_{ij}\right)^2}{\aleph_{ij}} \right| \quad (7)$$

where N_{sj} and N_{ij} are the expected counts of spontaneous and induced tracks in

the j_{th} grain where:

$$\aleph_{sj} = \frac{n_s + (N_{sj} + N_{ij})}{n_s + n_i} \quad (8)$$

$$\aleph_{ij} = \frac{n_i + (N_{sj} + N_{ij})}{n_s + n_i} \quad (9)$$

n_s and n_i are the fossil and induced tracks counted in the n grains. If the sample fails the test (that is there is less than 5% probability of finding the calculated χ^2 value), data are not consistent with a Poisson distribution. This fact does not mean that the age determination is not accurate, as it is easily possible to see in studies on sedimentary rocks or tuff levels in sedimentary sequences, where it is possible to find together zircons of the volcanic level and inherited grains (Bigazzi & Handler, 1989). In such cases, different approaches for age calculation have been developed. Green (1981) proposed to calculate the age using the mean of each single ratio ρ_s/ρ_i:

mean $(\rho_s / \rho_i) = \sum_{i=1}^{n} \frac{(\rho_s/\rho_i)}{n}$ with n = number of crystals) (10)

$$\sigma(\rho_s / \rho_i) = \sqrt{\frac{\left\{\sum_{i=1}^{n} (\rho_s / \rho_i)_i^2 - \left[\sum_{i=1}^{n} (\rho_s / \rho_i)_i\right]^2\right\}}{n(n-1)}} \quad (11)$$

This method is similar to the conventional analysis but the resulting error is usually greater. The more important defect of this procedure is that it gives the same weight to all the crystals, without taking in account the number of counted

tracks. Galbraith & Laslett (1992) has developed a procedure which uses an iterative algorithm that calculate a weighted modal age (the so-called *central age*) and the corresponding standard error (see also Galbraith & Laslett, 1992). In this case, the standard deviation is known as "age dispersion" or "relative error" and it is expressed as a percentage. A value higher than 20% indicates that the data doesn't follow a Poisson distribution.

B.3 GRAPHICAL METHODS

When data fail the chi-square test or have a high dispersion, can be useful to visualize the calculated single grain ages. These ages can be plotted on a histogram or, better, through the *probability density distribution plot* (Hurford et al., 1984; Kowallis et al., 1986; Brandon, 1996). The probability density distribution is approximate by a curve given by the equation:

$$f(A) = \sum_{i=1}^{n} \frac{exp - [(A - \bar{A})^2 / 2s_i^2]}{\sqrt{2\pi s_i}} \quad (12)$$

where:

A= age

$\bar{A}$= mean age for the ith crystal

s_i= standard error for the *i*th crystal

The curve gives the possibility to calculate a more probable age (*peak age*). When a sample pass the chi-square test, the central and the peak ages have more o less the same values. Naeser et al. (1987) have demonstrated that this method can give a qualitative spectrum of different grain population and the peaks are

particularly well defined for the youngest populations. A limit is the fact that the uncertainties related to single grain ages and the variations between these ages cannot be separated. The shape of the histogram or of the curve can be strongly influenced by the single errors, masking the variations between different ages. Quantitative considerations can be done by using an improved version of this statistical approach, developed by Brandon (1996).

A completely different approach has been developed by Gailbraith (1988; 1990), who introduces a *radial plot* that enables a good visual judgment of the homogeneity of a set of ages and an estimation of the single errors. The single age (z) and their standard error s are plotted as points whose coordinates are:

$$x = \frac{1}{\sigma} \quad (13)$$

$$y = \frac{(z - z_0)}{\sigma} \quad (z_0 \text{ represents the central age}) \quad (14)$$

The ages are generally transformed following a log- or -arcsin-scale. The main characteristics of this method are:

- each single point represents a crystal; the age can be read on the intersection between the line linking the origin with the point and the arc;
- the x coordinate represents the precision of the age which increases towards the arc;
- the error $\pm 2\sigma$, represented by the bar on the origin, is easily detected superimposing the bar on the selected point, without alteration of its dimensions.

In Fig. B.1 it is possible to see a comparison between these two different graphical representations. In this case, both the methods give the possibility to discriminate quite easily two main age groups. The radial plot clearly shows that the older age group is better defined because of a lower analytical error. This is not detected by the curve in the probability density plot, which overestimate the young group of ages. A discussion of limitations and advantages of radial and probability density plots can be found in Gailbraith (1998).

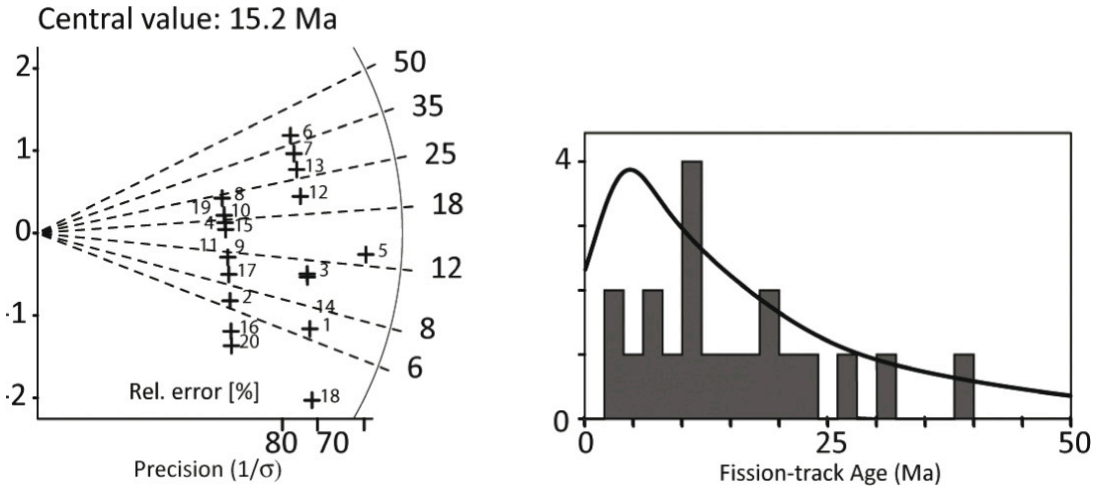

Fig. B.1 – Comparison between the probability density distribution plot and the radial plot for a generic sample.